FUNCTIONALLY GRADED SILICON NITRIDE (Si_3N_4) PRODUCTION FOR BIOMEDICAL APPLICATIONS

OGAN TANIL ORHUN

SEPTEMBER 2022

ÇANKAYA UNIVERSITY

GRADUATE SCHOOL OF NATURAL AND APPLIED SCIENCES

DEPARTMENT OF MATERIALS SCIENCE AND ENGINEERING

MASTER'S THESIS IN

MICRO AND NANOTECHNOLOGY

FUNCTIONALLY GRADED SILICON NITRIDE (Si_3N_4) PRODUCTION FOR BIOMEDICAL APPLICATIONS

OGAN TANIL ORHUN

SEPTEMBER 2022

ABSTRACT

FUNCTIONALLY GRADED SILICON NITRIDE (Si_3N_4) PRODUCTION FOR BIOMEDICAL APPLICATIONS

ORHUN, Ogan Tanıl

Master of Science in Micro and Nanotechnology

Supervisor: Assist. Prof. Dr. Şeniz Reyhan KUŞHAN AKIN

Co-Supervisor: Assoc. Dr. Gülsüm TOPATEŞ

September 2022, 131 pages

This thesis focuses on the bio-properties and gradual production of Si_3N_4 material. The produced samples were differentiated in three stages from the most dense region to the less dense region. The samples, which are designed to be obtained with this structure, have been engineered at high density to meet the novel mechanical properties in the base part and low density by creating a pore in order to increase the cell penetration in the surface part. In the middle layer, it is aimed to have a smooth transition zone, so that the harmony between the two different layers is high. This FGM microstructure plays an important role as it carries both the high biocompatibility of Si_3N_4 and its mechanical strength on a single bulk material. Studies on Si_3N_4 show that it is a very important material candidate in implant applications as well as many different uses.

The samples were prepared by using pure α-Si_3N_4 powder, Y_2O_3 as sintering additive and carbimide and semolina as pore-forming materials and were shaped using uniaxial press.

Samples were sintered at different temperatures GPS furnace. Phase characterization by XRD analysis was performed for each layer of the grading composition. By SEM analysis, the layers forming the FGM and the inner surface of the pores in the porous designed layers were examined and the desired gradual transition between layers was observed.

The bioactivity of the obtained samples was evaluated in terms of hydroxyapatite formation in SBF and the antibacterial resistance was examined by the agar well diffusion method.

Keywords: Si_3N_4, FGM, Biomaterials, Sintering, Pore Forming and Porosity

ÖZ

BİYOMEDİKAL UYGULAMALAR İÇİN FONKSİYONEL OLARAK DERECELENDİRİLMİŞ SİLİKON NİTRÜR (Si_3N_4) ÜRETİMİ

ORHUN, Ogan Tanıl
Mikro ve Nanoteknoloji Yüksek Lisans

Danışman: Dr. Şeniz Reyhan KUŞHAN AKIN
Ortak Danışman: Doç Dr. Gülsüm TOPATEŞ
Eylül 2022, 131 sayfa

Bu tez, Si_3N_4 malzemelerinin biyo özelliklerine ve kademeli olarak üretimine odaklanmıştır. Üretilen numuneler, çok yoğun bölgeden az yoğun bölgeye üç kademeli olarak farklılaştırılmıştır. Bu yapı şekli ile elde edilmesi tasarlanılan numuneler taban kısmında yüksek mekanik özellikleri karşılaması için yüksek yoğunluk ve yüzey kısmında cell penetrationı arttırabilmek adına gözenek oluşturularak düşük yoğunlukta elde edilmiştir. Orta katmanda ise smooth transition bölgesi bulundurularak iki farklı katman arasındaki uyumun yüksek olması hedeflenmiştir. Bu FDM mikroyapı tasarımı , hem Si_3N_4 ün yüksek biouyumluluğunu, hemde mekanik mukavemetini tek bir bulk malzeme üzerinde taşıması sebebi ile önem taşımaktadıt. Si_3N_4 üzerinde yapılan çalışmalar neticesinde birçok farklı kullanım amacının yanı sıra implant uygulamalarında da çok önemli bir malzeme adayı olduğunu göstermektedir .

Numuneler, saf alfa Si_3N_4 tozunun, sinterleme ilavesi olarak Y_2O_3 ve gözenek yapıcı malzeme olarak da carbimid ve irmik kullanılmasıyla hazırlanmış, eksenel presle şekillendirilmiştir. Numuneler GPS fırını kullanılarak farklı sıcaklıklarda sinterlenmiştir. Derecelendirme bileşiminin her katmanı için XRD analizi ile faz karakterizasyonu yapılmıştır.

SEM analizi ile FGM'yi oluşturan katmanlar ve gözenekli tasarlanmış katmanlardaki gözeneklerin iç yüzeyi incelenmiş ve katmanlar arasında istenen kademeli geçiş gözlemlenmiştir.
Elde edilen örneklerin biyoaktivitesi, SBF'de hidroksiapatit oluşumu açısından değerlendirilmiş ve antibakteriyel direnç, agar difüzyon yöntemi ile incelenmiştir.

Anahtar Kelimeler: Si_3N_4, FDM, Biomalzemeler, Sinterleme, Gözenek oluşturma, Gözeneklilik

ACKNOWLEDGEMENT

Special thanks to my supervisor Assist. Prof. Dr. Şeniz Reyhan KUŞHAN AKIN for the excellent guidance and providing me with an excellent atmosphere to conduct this research. Moreover, special thanks to my co-supervisor Assoc. Dr. Gülsüm TOPATEŞ for the guidance with her academical studies. My special gratitude also goes to the rest of the thesis committee Prof. Dr. Ziya Esen, Assoc. Dr. Ali ÇELİK for the encouragement and insightful comments. We would like to thank TÜBİTAK for their support with the project numbered 120N266.

Endless thanks, respect and love to my mom, wife and my family who have given tremendous effort in me coming to this very day with unconditional strength I feel behind me. Moreover, special thanks to my baby who is growing now, bottom-up in her mother's womb for the make my life energy high.

TABLE OF CONTENT

STATEMENT OF NONPLAGIARISM .....**Error! Bookmark not defined.**

ABSTRACT iv

ÖZ..... vi

ACKNOWLEDGEMENT viii

TABLE OF CONTENT ix

LIST OF TABLES xii

LIST OF FIGURES xiii

CHAPTER I 1

INTRODUCTION 1

1.1 SILICON NITRIDE (Si_3N_4) 1

1.1.1 Properties of Silicon Nitride (Si_3N_4) 2

1.1.2 Sintering 8

1.1.3 Porous Silicon Nitride (Si_3N_4) 18

1.1.4 Application areas of Silicon Nitride.....19

1.2 FUNCTIONALLY GRADED MATERIALS (FGM).....23

1.2.1 Bulk Production 27

1.2.2 Surface Coating Production.....45

1.3 STUDIES ABOUT THE SILICON NITRIDE FGM 52

1.4 AIM OF THIS STUDY.....55

CHAPTER II 57

EXPERIMENTAL PROCEDURE 57

2.1 POWDER PREPARATION 57

2.1.1 Raw Materials 59

2.1.2 Ball Mill 60

2.1.3 Evaparator 61

2.1.4 Screening 62

2.1.5 Turbula Mixing 63

2.1.6 Green Body Preparation 64

2.2 FGM GREEN BODY PREPARATION 65

2.2.1 Pressing 66

2.2.2 Cold Isostatic Pressing 67

2.2.3 Pore Forming Agent Burn Out 68

2.3 SINTERING 69

2.3.1 Gas Pressure Sintering (GPS) 69

2.3.2 Spark Plasma Sintering (SPS) 71

2.3.3 Density and open porosity measurements 72

2.4 PHASE CHARACTERİSATION BY X-RAY DIFFRACTION (XRD) 73

2.5 SCANNING ELECTRON MICROSCOPY (SEM) 74

2.6 BIOACTIVITY TEST - SIMULATED BODY FLUID (SPS) PREPARATION 75

2.7 ANTIBACTERIAL TEST 78

CHAPTER III 80

RESULTS AND DISCUSSIONS 80

3.1 DENSITY AND OPEN POROSITY 85

3.2 XRD ANALYSIS 86

3.3 SEM ANALYSIS 89

3.4 ANTIBACTERIAL TEST RESULTS 93

3.5 SBF ANALYSIS 94

CHAPTER IV 98

CONCLUSION 98

REFERENCES 100

LIST OF TABLES

Table 1: Density, Hardness, Bending Strength, Elastic Modulus, Porosity, Thermal Expansion and Thermal Conductivity difference with HP, RBSN, Pressureless Si_3N_4 and SSN..... 2
Table 2: Steps of Powder Metallurgy 29
Table 3: Liquic State Processes Table 30
Table 4: Properties of Raw Materials 59
Table 5: Green body composition table 64
Table 6: Table of FGM content 65
Table 7: Si_3N_4 samples and their codes sintered via GPS.....69
Table 8: The mixture of Simulated Body Fluid (SBF) 75
Table 9: Diameter of some pore forming agents 82
Table 10: Bulk density and open porosity of the samples.....85
Table 11: XRD samples 86

LIST OF FIGURES

Figure 1: a.) Densities of S_3N_4, SiC, Alumina, Cermet, Zirconia, Steel, Cemented Carbide. b.) flexural strength c.) Young's Modulus of Elasticity d.) Flexual Strength vs. Temperature 4
Figure 2: a.) Thermal Expansion b.) Thermal Conductivity c.) Thermal Conductivity d.) Heat Shock Resistance 5
Figure 3: Chemical Durability 7
Figure 4: Crystal Structure of Si_3N_4 a.) α-Si_3N_4 b.) β-Si_3N_4 c.) γ-Si_3N_4 7
Figure 5: Molded vs Sintered Body. 9
Figure 6: Reaction Bonding Sintering Furnace 11
Figure 7: Hot Pressing b.) HPSN Rods (Moustafa, Daoush, Ibrahim, & Neubaur, 2011) 12
Figure 8: Plessureless Sintering Furnace and pressureless sintered Si_3N_4 ceramic balls by powder injection molding 13
Figure 9: Gas Pressure Sintering (GPS) 15
Figure 10: a.) Load components into the furnace. b.) Load furnace into pressure vessel. Raise pressure and temperature simultaneously, and hold.c.) Cool, release gas (clean and recycle) and remove furnace from pressure vessel. Remove components from furnace 15
Figure 11: Shcematicaly drawing of Microwave Sintering Furnace 16
Figure 12: Schematicaly drawing of Spark Plasma Sintering (SPS) 18
Figure 13: Sections from XRD microtomography of bone (64 vol% pores)—(A), air-sintered Si_3N_4 (65 vol% pores)—(B), SRBSN (73 vol% pores)—(C) 19
Figure 14: (Silicon carbide bearing ceramic products: Stanford Advanced Materials), (Silicon nitride bearing rollers: Stanford Advanced Materials) (Silicon nitride electrical insulator, Si_3N_4 2020) 20
Figure 15: (3M™ Silicon Nitride Telemetry Tooling), (3M™ Silicon Nitride Wear Plate) 20

Figure 16: Si_3N_4 biomedical applications 22

Figure 17: Prothesis applications of Si_3N_4 22
Figure 18: Transition areas of Si substrate, TinON, TiO_2, Si_3N_4 and SiO_2 The bright field cross-sectional transmission electron microscopy (TEM) micrograph of the multilayer absorber and the corresponding electron diffraction pattern 24
Figure 19: Schematical drawing of Tooth anatomy (Tooth Anatomy images) b.) Section view of seashell 25
Figure 20: Difference of FGM Production.....27
Figure 21: Scheamatic gradient drawings by density, shape, orientation and dimention.....28
Figure 22: Gas Pressure Inflitration.....31
Figure 23: Pressure Die Infiltration 32
Figure 24: Squeeze Casting.....33
Figure 25: Stir Casting 34
Figure 26: Compocasting. 35
Figure 27: Centrifugal Casting. 36
Figure 28: Slip Casting 37
Figure 29: Tape Casting. 38
Figure 30: FGM samples produced with different support geometries produced by the Additive Manufacturing method.....39
Figure 31: 3D printed products.....40
Figure 32: a.) Powder Bed Schematic drawing b.) 3D printed truck parts 41
Figure 33: Directed Energy Deposition 42
Figure 34: Binder Jetting device and applications.....43
Figure 35: Sheet Lamination 44
Figure 36: Physical Vapor Deposition PVD 45
Figure 37: Electron Beam-PVD 46
Figure 38: Sputtering Based- PVD 47
Figure 39: Plasma Spray Based – PVD (PS -PVD).....48
Figure 40: Chemical Vapour Deposition (CVD).....49
Figure 41: Thermal Spraying 50
Figure 42: Surface Treatments, Gas nitriding, Carburizing. 51
Figure 43: SEM images of Si_3N_4 powders. 58
Figure 44: Planetary ball milling device and the Si_3N_4 jar with slurry inside. 60

Figure 45: Rotary evaporator equipment. 61
Figure 46: Screening. 62
Figure 47: Turbula Mixer. 63
Figure 48: Si_3N_4 samples mixed with pore-forming materials and placed in plastic containers, prior to turbula mixing. 63
Figure 49: Schematic drawing of FGM - Si_3N_4 65
Figure 50: a.) Uniaxial Press b.) Si_3N_4 pressed samples.....66
Figure 51: Cold Isostatic Press (CIP).....67
Figure 52: Muffle Furnace. 68
Figure 53: Gas Pressure Sintering (GPS) Furnace 70
Figure 54: Spark Plasma Sintering (SPS) Furnace 71
Figure 55: Archimedes principle [118]. 72
Figure 56: XRD device 73
Figure 57: Scanning Electron Microscopy (SEM) 74
Figure 58: pH meter.....76
Figure 59 : Samples waiting in water at 37 ^oC. 76
Figure 60: Ultrasonic cleaner, used for keeping the water hence the samples, at a constant temperature 77
Figure 61: a.) Vacuum Etuv b.) Samples 1Y/92, 1Y1C/92 and 1Y2C/92 78
Figure 62: Staphylococcus aureus bacteria 79
Figure 63: SEM images of Sintered Si_3N_4 sample - 1Y /92. 80
Figure 64: Samples containing semolina dispersed after the burn out process. 83
Figure 65: Temperatur vs Time graph taken from SPS during sintering of 1Y sample 84
Figure 66: a.) 1Y1C/92 b.) 1Y2C/92 c.) 1Y1C/83 d.) 1Y2C/83.....87
Figure 67: a.) 1Y /92 b.) 2Y /92 88
Figure 68: SEM images of FGM samples.....89
Figure 69: SEM magnituded images of Si_3N_4 samples 91
Figure 70: SEM Images of FGM samples produced by stacking the tape casted layers 92
Figure 71: Control and 1Y /92, 1Y1C /92 and 1Y2C /92 samples S.Aureus bacterias. 93

Figure 72: a.) Secondary electron image of sample 1Y after immersion in SBF for 28 days and (b) EDX spectum of a point analysis. b.), SEI (with different magnifications) and EDX results of sample 2Y. 94
Figure 73: (a) and (b) SEI of sample 2Y with different magnifications after immersion in SBF for 28 days and (b) EDX inspection field of the area given in (b) 95
Figure 74: SEI of samples after immersion in SBF for 28 days (a) Sample 1Y /92 (b) Sample 1Y1C /92 and (c) Sample 1Y2C /92. (d) is the EDX inspection field of the area given in (c) 97
Figure 75: SEI of samples after immersion in SBF for 28 days (a) Sample 1Y /92 (b) Sample 2Y /92.....97

LIST OF SYMBOLS AND ABBREVIATIONS

SYMBOLS

α	: Alpha
β	: Beta
γ	: Gamma
^{o}C	: Centigrade Degree
m	: Meter
cm	: Centimeter
μm	: Micrometer
nm	: Nanometer

ABBREVIATIONS

SAED	: Selected Area Diffraction
TEM	: Transmission Electron Microscope
RBSN	: Reaction Bonded Silicon Nitride
MPa	: Megapascal
GPa	: Gigapascal
Si	: Silicon
Ar	: Argon
N	: Nitrogen
SN	: Silicon Nitride

HF	: Hydrofluoric Acid
RB	: Reaction Bonding
HP	: Hot Pressing
HPSN	: Hot Pressing Silicon Nitride
GPS	: Gas Pressure Sintering
SPS	: Spark Plasma Sintering
FAST	: Field Assisted Sintering
HIP	: Hot Isostatic Pressing
GHz	: Gigahertz
MHz	: Megahertz
RF	: Radio Frequency
SAM	: Stanford Advanced Materials
FGM	: Functionally Graded Materials
KMM	: Knowledge-based Multifunctional Materials
SC	: Squeeze Casting
SL	: Semisolid – Liquid
SS	: Semisolid – Semisolid
AM	: Additive Manufacturing
CAD	: Computer Aided Designing
FDM	: Fused Deposed Modelling
DMLS	: Direct Metal Laser Sintering
SHS	: Selective Heat Sintering
SLM	: Selective Laser Melting
SLS	: Selective Laser Sintering

PBF	: Powder Bed Fusion
EBM	: Electron Beam Melting
DED	: Directed Energy Deposition
PP	: Plaster-Based 3D Printing
PBIH	: Powder Bed and Inkjet Head 3D Printing
PVD	: Physical Vapor Deposition
EB – PVD	: Electron Beam - Physical Vapor Deposition
PS – PVD	: Plasma Spraying - Physical Vapor Deposition
CVD	: Chemical Vapor Deposition
FGMMC	: Functionally Graded Metal Matrix Composites
SEM	: Scanning Electronic Microscope
XRD	: X-Ray Diffraction
CIP	: Cold Isostatic Pressing
EDX	: Energy Dispersive X-Ray
HAp	: Hydroxyapatite
SBF	: Simulated Body Fluid
METU	: Middle East Technical University
RPM	: Revolutions Per Minute

CHAPTER I
INTRODUCTION

1.1 SILICON NITRIDE (Si_3N_4)

Silicon Nitride is a very important structural ceramic for the scientific world, with the studies carried out from the past to the present and its expected/anticipated contributions to our lives from today to the future.

The basis of the magnificent properties of silicon nitride, which will be described throughout this thesis, lies in the covalent bonding of silicon and nitrogen atoms. The first academic study about the synthetically developed silicon nitride by H. Sainte - Claire Devil and Wohler was in 1857 with the following words: Nitrogen silicon is perfectly white, amorphous, infusible and unalterable at the highest temperatures, and not oxidizable even when heated in air. Acids and alkalis in solution have no effect on it, only fluoric acid gradually converts it into fluorosilicic ammonium. Smelting hydrated potash, it develops a large quantity of ammonia, changing into siliceous potash [1].

In 1955, silicon nitride started to be produced commercially for the first time by J. F. Collins and W. Gerby [2]. Examining the minerals found in a meteor rock structure, Lee and Russell in 1995 obtained the result that α-Si_3N_4 and β-Si_3N_4 occur naturally when they looked at the SAED pattern and TEM images [3].

The results obtained in the studies on reaction bonded silicon nitride (RBSN), which started in the 1950's, were markedly accelerated in the 1960's by the need for materials with good high temperature properties and thermal shock resistance in heat engines, industrial energy convention, metal working and defence industry [4].

The most important feature that makes Si_3N_4 preferred is that it preserves its mechanical and chemical properties even at high temperatures Si_3N_4 has many competitive properties such as high mechanical strength, wear resistance, high decomposition temperature, oxidation resistance, good chemical durability, low coefficient of friction, high corrosion and abrasion resistance, excellent thermal shock properties and biocompatibility [5]

1.1.1 Properties of Silicon Nitride (Si_3N_4)

1.1.1.1 Physical and Mechanical Properties of Silicon Nitride

Physical properties are the observable, measurable or perceptible basic properties that make the substances distinguishable from each other. These properties are independent of the chemical properties of the substance. Physical properties can be listed as follows; colour, transparency, odour, taste, quantity, size, flexibility, expansion, hardness, brittleness, workability, viscosity, density, specific heat, melting point, boiling point, freezing point and conductivity.

Si_3N_4 is usually dark in colour depending on the densification and additive conditions. They exhibit superior properties in terms of mechanical properties; high strength, high fracture toughness, high hardness, superior impact resistance, high wear resistance, creep and fatigue resistance and these superior properties are stable even at high temperatures [5-6]. In addition to these properties, they also have good thermal shock resistance, high temperature resistance, high thermal shock resistance, low thermal expansion coefficient [7].

The article published by Wei Chen et al. gives information about the physical and mechanical properties of Si_3N_4 composite ceramics produced by different production methods and is shared in Table 1 [8].

Table 1: Density, Hardness, Bending Strength, Elastic Modulus, Porosity, Thermal Expansion and Thermal Conductivity difference with HP, RBSN, Pressureless Si_3N_4 and SSN [8].

Material Type	Hot Pressing Si_3N_4	Reaction Sintering Si_3N_4	Pressure less Sintering Si_3N_4	Post Sintering Si_3N_4
Density / $g.cm^{-3}$	3.2 - 3.4	2.7 - 2.8	3.2 - 3.26	3.2 - 3.3
Hardness / HRA	92 - 93	83 - 85	91 - 92	90 - 92
Bending Strength / MPa	900 - 1200	250 - 400	600 - 800	600 - 670
Elastic Modulus / GPa	300 - 320	160 - 200	290 - 320	271 - 286
Apparent Porosity	< 0.1	10 - 20	0.01	< 0.2
Coefficient of thermal expansion / x^{-10}	2.60	3.2	3.4	3.55 -3.6
Thermal conductivity / $W.m^{-1}K^{-1}$	30	17	20 - 25	..

The explanations given in bullets below are based on figure 1 and figure 2.

- Si_3N_4, which has close results with SiC in the density graph, gives a denser structure than its competitors such as alumina and zirconia.
- As seen in the flexural strength graph, Si_3N_4 has higher strength than quartz, alumina, silicon carbide.
- Looking at the young modulus graphite, it shows 300 GPa strength and is higher than zirconia and stainless steel. Alumina and SiC attract attention with their high strength.
- Flexural Strength vs. in temperature graph, it is observed that zirconia has high strength up to 200°C. Despite this, the decrease observed in zirconia after 600°C reached the same strength level as Si_3N_4 and this decrease continued. Depending on the additives contained in Si_3N_4, which has managed to maintain its strength up to 1400°C.
- In the thermal expansion graphic, Si_3N_4 shows how assertive it is in this regard with 0.3% expansion at 800°C by giving better results than all its other competitors.
- It remained in a limited range of 12-30 W/(m.K) in the thermal conductivity graph. The conductivity, which showed a rapid decrease up to 400°C, continued almost constant until 1000°C was reached.
- In the heat shock resistance graph, Si_3N_4 samples, which present a very promising graph, show that it is resistant to all other competitors with a loss of only 100 MPa by quenching with water.

Below are the graphics prepared by the Kyocera Company from the data obtained as a result of the tests carried out for Si_3N_4 products [9].

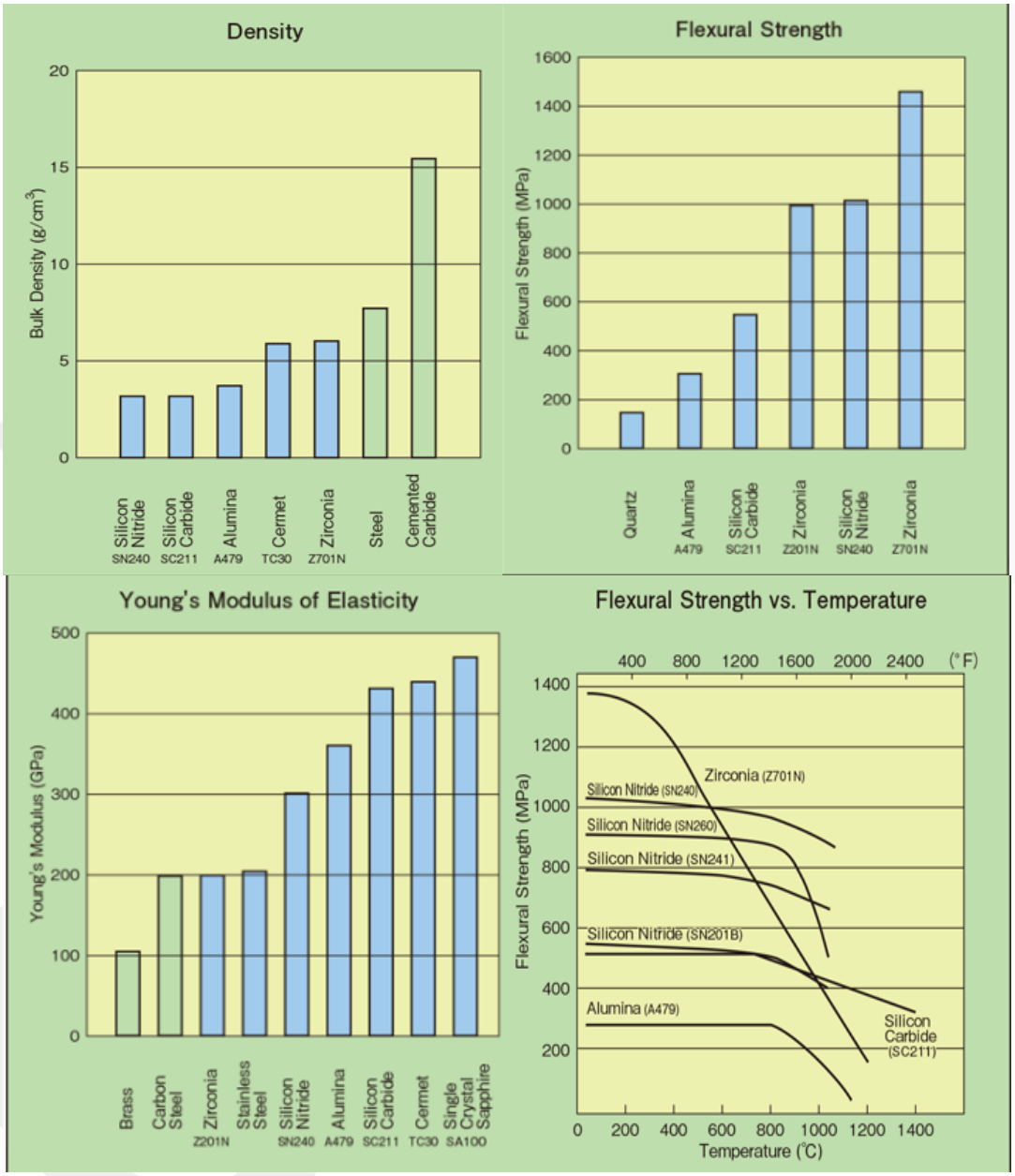

Figure 1: a.) Densities of S_3N_4, SiC, Alumina, Cermet, Zirconia, Steel, Cemented Carbide. b.) flexural strength c.) Young's Modulus of Elasticity d.) Flexual Strength vs. Temperature [9].

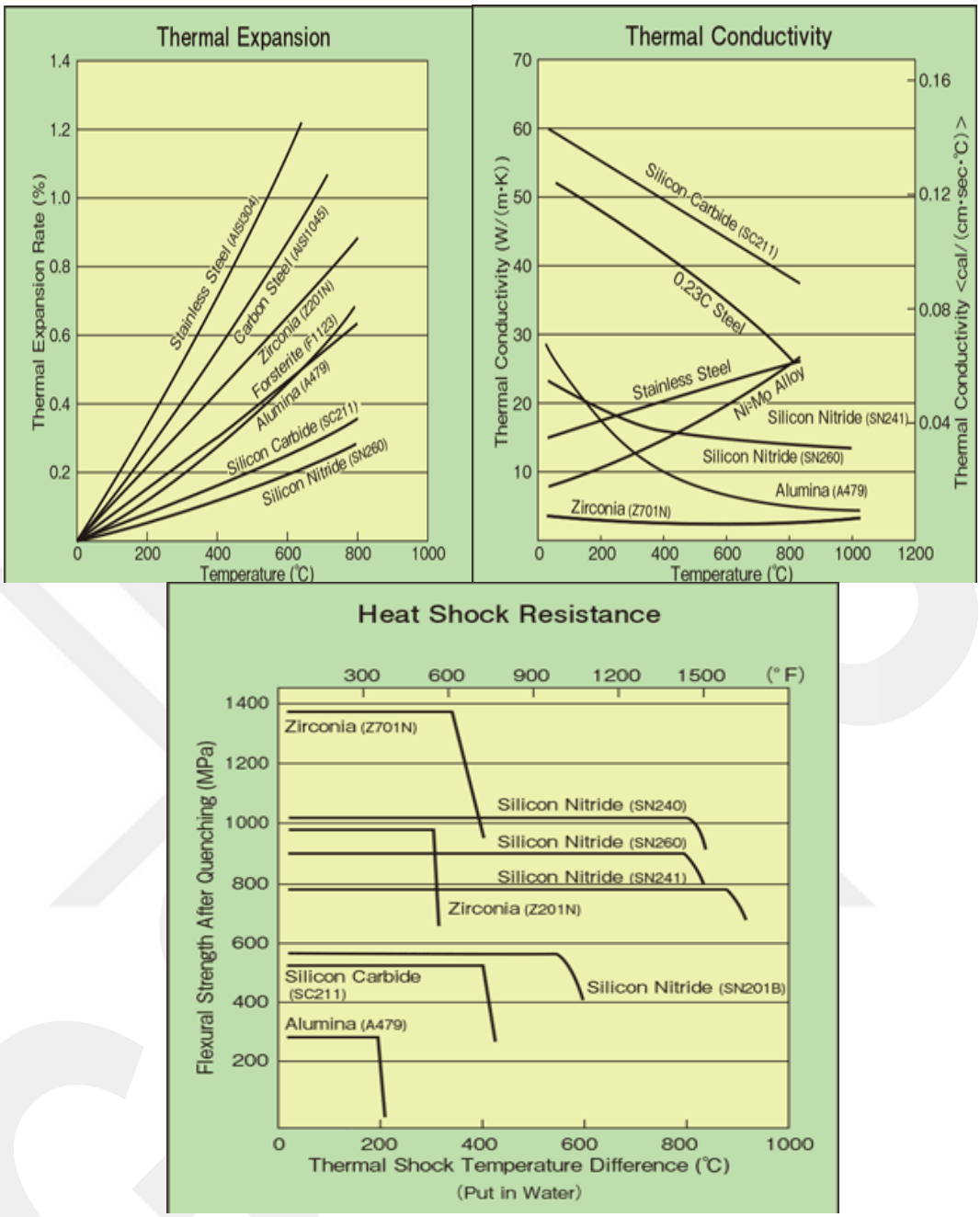

Figure 2: a.) Thermal Expansion b.) Thermal Conductivity c.) Thermal Conductivity d.) Heat Shock Resistance [9].

1.1.1.2 Chemical Properties of Silicon Nitride

Chemical properties are formed as a result of the chemical identity of a substance after or during a reaction. Chemical properties: It occurs as a result of changes in the internal structure of matter, at the molecular or atomic level. The main chemical properties are as follows; toxicity, oxidation, ignition, heat of combustion, enthalpy of formation, chemical stability and radioactivity.

- Si_3N_4 is a chemical compound of the elements Si and N_2.
- Si_3N_4 is the most thermodynamically stable of the silicon nitrides [10].
- In addition to its superior physical properties, good chemical resistance and good oxidation resistance [11].
- In terms of acid and alkali corrosion resistance it does not react with other inorganic acids, even hydrofluoric acid (HF). Under high temperature which shows strong anti-corrosion and anti-oxidation properties [12].
- It cannot be sintered via solid state sintering because they have very low diffusion coefficient also solid-state sintering starting above 1800^{o}C but dissolution observing at higher temperatures.
- In addition to different additives, Y_2O_3 to be examined within the scope of this thesis, the sintering process becomes easier. The presence of additive supports the formation of a third liquid phase.

Si_3N_4 in the graphs below taken from Kyocera Company; their resistance to HNO_3, H_2SO_4 and NaOH solutions is shown in terms of weight lost by erosion [9].

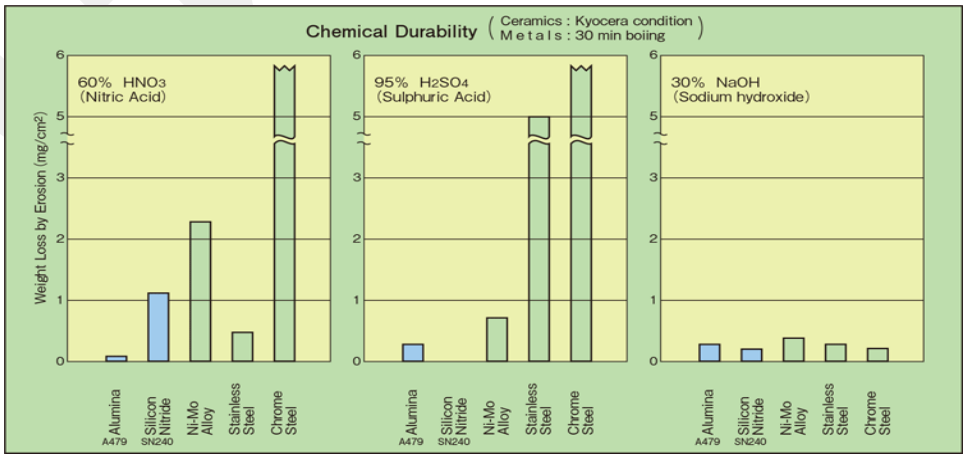

Figure 3: Chemical Durability [9].

1.1.1.3 Crystal Structure properties of Silicon Nitride

There is one Si in the center of Si_3N_4 and four N atoms attached to it. The bond between them has a tetrahedral structure. Three tetrahedral N bonds with Si_3N_4 at the corners where it is found. Si_3N_4 has 3 known crystal structures.

The first of these is α-Si_3N_4. It is geometrically hexagonal in shape. In α-Si_3N_4, the Si-N layers are arranged as ABCD ABCD .... The unit cage cell of the α-phase consists of 4-Si_3N_4, designated as $Si_{12}N_{16}$.

Another phase belonging to Si_3N_4 is β-Si_3N_4. It is formed by tetrahedral-bonded Si atoms showing a trigonal structure and hexagonal form, which arrangement is AB AB.... Liquid phase is needed for the formation of the more common β-form. This subject is discussed in detail in the sintering section.

Another phase of Si_3N_4 is γ-Si_3N_4. α-Si_3N_4 and β-Si_3N_4 while can be synthesized at normal pressures, the phase needs a high temperature and high pressure. It is the octahedral structure formed by the N atom bonding with two silicon atoms and the spinal formed by the bonding of four nitrogen and one Si atoms with the tetrahedral. This structure makes it harder than α and β-Si_3N_4.

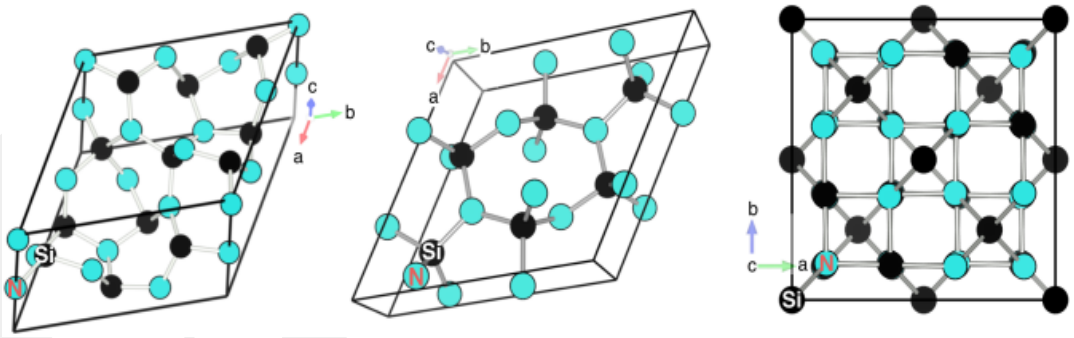

Figure 4: Crystal Structure of Si_3N_4 a.) α-Si_3N_4 b.) β-Si_3N_4 c.) γ-Si_3N_4 [13].

1.1.2 Sintering

The sintering process is the process of condensing and solidifying the structure with voids as a result of heating a ceramic, metal or mixed powder with thermal energy. Condensation and generally grain growth are observed during this process. The condensation process can be done by pressure, electric current, microwave energy and spark plasma methods. The sintering process is formed by solid state sintering or liquid phase sintering mechanisms. The temperature, below the melting temperature of the material is reached, liquid phases begin to form in the structure and liquid phase sintering and shrinkage occurs in the condensed material without deteriorating the designed shape.

Temperature and time are the most important inputs of the sintering process. The pores in the structure decrease with the method called, mass transport depending on the temperature increase and condensation occurs due to the binding of the particles of the reduced surface area. The condensation process occurs more rapidly at higher temperatures.

Diffusion occurs with the effect of temperature during sintering. Grain boundary growth occurs at the contact points of the clusters. The drag force of the sintering is decreasing of area of the solid-gas interface and decreasing of the surface energy on the connection surface.

The mass transport mechanism occurs in two ways. One is surface transport and the other is mass transport. Neither shrinkage nor densification is obtained during surface transport. In mass transport, shrinkage or densification can be achieved.

Sintering consists of stages. The structures called necks are obtained with the atomic diffusion that occurs between the clusters at the beginning. The increase in the surface area per unit volume, the size of the clusters reduces the driving force more, thus increasing the surface energy in the solid-gas interface. This step occurs while mass transport kinetics are taking place. Step 1 is considered complete when the neck radius reaches 0.5 times the radius of the cluster.

In the second stage, mass transport is carried out towards the necks and the pores in between begin to form a network. The pores settle at the grain boundaries of the necking mechanism and the necking regions are separated from each other and closed pores are obtained. After the pores become spherical, the necks begin to grow on top of each other. The formation of globalization, diffusion continues from the surface. The porosities disappear, grain boundaries, volumetric diffusion, grain growth and precipitation are observed at this stage. The pores in the grain boundaries disappear, while there is no difference in the pores in the bulk.

In the final stage of sintering, the pores are reduced to sizes that are too small to be seen with the naked eye due to the decreasing surface area, the surface energy is at its lowest, so this stage is slower than the other stages. The voids close and take their spherical shape, blocking both themselves and the grain boundaries. The sintering occurs while grain coarsening increases at this stage.

The decrease, shrinkage and even disappearance of the pores due to necking by diffusion and mass transport, which occur in the sintering mechanism, are shown in the figure below.

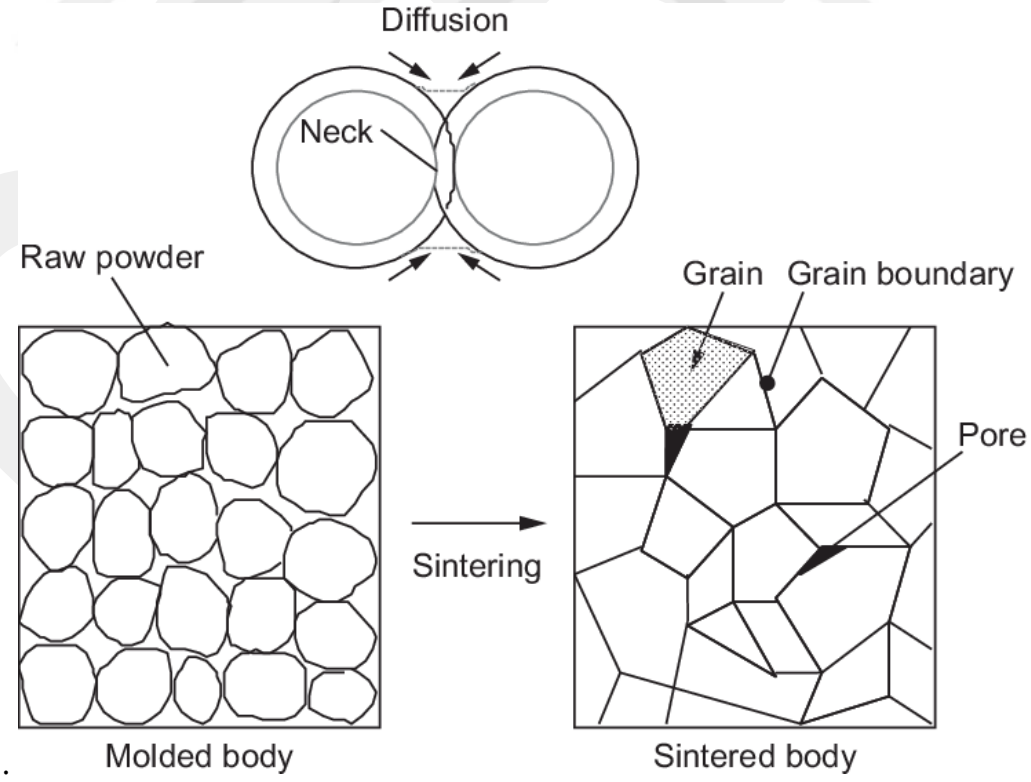

Figure 5: Molded vs Sintered Body [14].

Pure Si_3N_4 materials are difficult to manufacture completely dense by solid state sintering. In Si_3N_4, which has a high covalent structure, it is very slow during mass transfer by solid state diffusion. For this reason, which cannot be densified easily. Above 1800°C if no extra gas pressure is applied, it can decompose into Si and N_2 gas. Therefore, if additive or advanced technological sintering methods are not used, sintering process is not performed at above this degree.

Consequently, solid state sintering is not performed in Si_3N_4 production. Si_3N_4 can only be produced by liquid phase sintering. During liquid phase sintering, a liquid phase is present simultaneously with solid powder aggregates at the sintering temperature. In general, the liquid phase increases the bond formation between particles during sintering. Its most important advantage is which contribution to the sintering to the sintering mechanism. The capillary attraction forces created by the liquid phase pull the particles towards each other and form a rapid condensation without any external pressure.

The formation of the liquid phase during sintering is also important for the formation of the β-form. Alpha-Beta conversion begins to occur above 1400°C. The presence of the liquid phase reduces the activation energy and causes the dissolution and precipitation processes to occur. The bonds between Si and N need to be broken and rebuilt at this stage. In the absence of the liquid phase, the activation energy of the system is higher and the temperature must be increased up to 2200°C for α-β conversion to occur.

During liquid state sintering, some additives are used to obtain the eutectic liquid phase with the SiO_2 layer that exists on Si_3N_4 grains. Some additives are used to form the eutectic liquid phase with the SiO_2 layer on the Si_3N_4 grains. These additives increase the rate of conversion from the α-Si_3N_4 form to the β-Si_3N_4 form. Y_2O_3, Al_2O_3, CaO, MgO etc. are some examples for the sintering additives [15]. In this thesis, Y_2O_3 which is the one of the most commonly used ones was selected as an additive to achieve liquid phase sintering of Si_3N_4. The properties and quantities of the materials to be used are explained in more detail in the experiments section.

1.1.2.1 Reaction Bonding

Reaction bonding method (RB) is one of the most widely used Si_3N4 production methods since the 1970's. As a result of Si_3N_4 sintering, ~10-20 wt. % porosity is formed. This porosity decreases the mechanical properties. The SNRB method, on the other hand is based on the principle of sintering the samples after carbothermal reduction and nitriding. In the SNRB method; after silicon green bodies are vacuumed and cleaned of residues in order not to cause undesirable reactions, N_2 gas is given to the environment. This process is carried out in an atmosphere-controlled oven at 1200-1450°C in approximately 2 hours. After the process is completed, even if they have complex shapes, the size of the green bodies does not change, but on the contrary, sintering occurs. Both α and β polymorphs are seen in Si_3N_4 samples produced by this method. Generally, the porosity is in the range of ~12-15 wt. % and can go up to 20 wt. %. Although the pore diameters are at the submicron level in the final product, depending on the pore network in the microstructure, pores with a diameter of over 50 µm can also occur. The flexural strength is observed in the range of 150-350 MPa in the final product, while it can be sintered again after sintering at high temperatures, so that high strengths such as 500 MPa can be achieved. In case of low number of grain boundary phases, there will be no difference in mechanical properties in high temperature applications. In the second sintering, a decrease will occur in the aforementioned 12-15 wt. % pore rates. If this process is done above 1650°C, all α-Si_3N_4 in the structure will undergo full transformation and will form β-S_3N_4. Kuşhan Akın, Ş. R. [16].

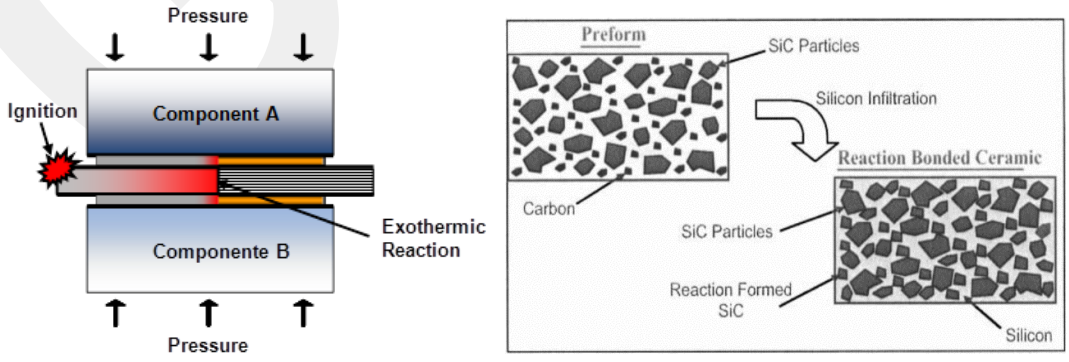

Figure 6: Reaction Bonding Sintering Furnace [17].

1.1.2.2 Hot Pressing

Hot pressing method is a heat treatment and sintering process carried out at high temperatures in order to create solid-phase diffusion below the melting temperature by mixing the powders to be sintered and placing them in a graphite mold.

Si_3N_4, SiC, Al_2O_3, B_4C etc. which need additives for liquid phase sintering hot pressing. It is a method in which temperature, pressure and sintering processes can be applied simultaneously in a single operation for the sintering of oxide and carbide materials with smooth internal structure can be produced with high density and low cost.

The applied force is coaxial, but the force is distributed from the center to the edges due to the friction on the surfaces of the powder molds. Besides that, the process is slow and the mold system is due to the difficulty of temperature control.

Si_3N_4 produced by this method are defined as HPSN which started to be developed in the 60's and 70's in order to produce some features of S_3N_4 and cannot be obtained with RBSN applications.

In the figure 7, there is the HPSN produced by pressing the HP method in a graphite mold at 1800°C and 40 MPa pressure. MgO is used as an additive. HPSN's are used in the production of non-complex structures where mold forming control can be done more easily.

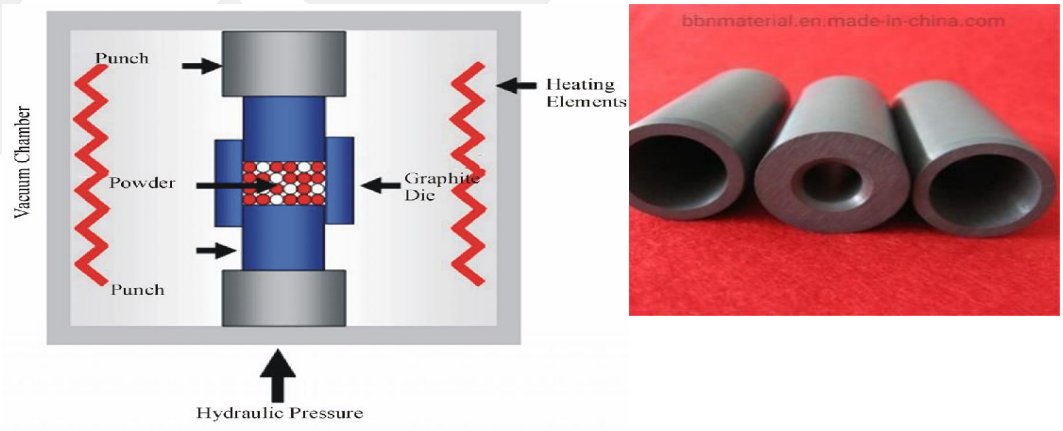

Figure 7: Hot Pressing b.) HPSN Rods (Moustafa, Daoush, Ibrahim, & Neubaur, 2011) [18].

1.1.2.3 Pressureless Sintering

Pressureless sintering technique is another sintering technique applied for sintering dense ceramic materials with complex shapes. Unlike other methods, it can be used to produce ceramic powders with a composition designed at low pressures such as 0.1 MPa and at high temperatures. Sintering additives similar to those used in other sintering methods are used in this technique as well for densification. In order for sintering to occur, the surface energy must be minimized. In this respect, it differs from the HP method. For this reason, it is known that while the condensation is observed more in the surface regions, the inner regions may not be concentrated at the desired level. Therefore, this method should not be used in productions with complex shapes. Since gas pressure is not applied in this sintering technique, it is inconvenient to apply high temperatures as it may cause decomposition [19].

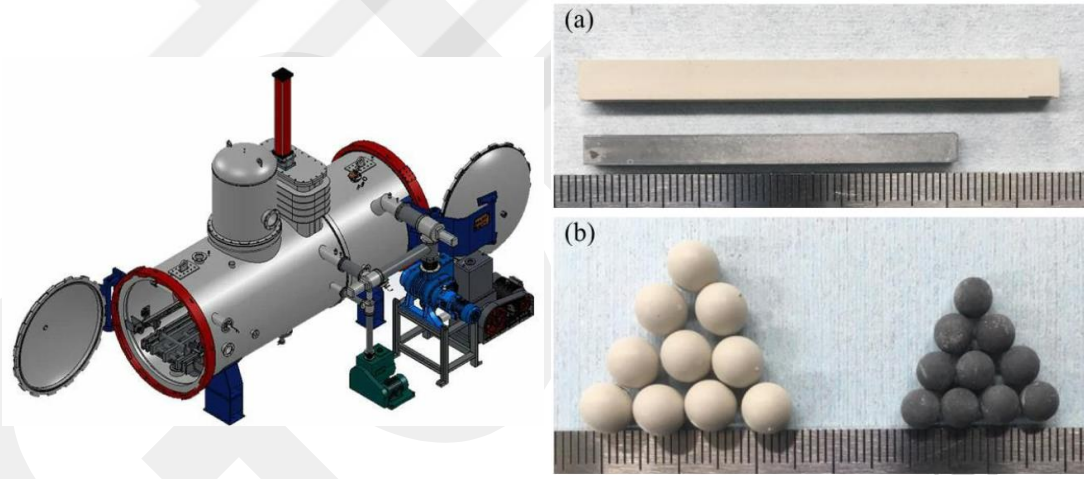

Figure 8: Plessureless Sintering Furnace and pressureless sintered Si_3N_4 ceramic balls by powder injection molding [20].

1.1.2.4 Gas Pressure Sintering (GPS)

The gas pressure sintering method, which is widely used in the production of Si_3N_4, allows the production suitable for the designed material by adding Ar or N_2 to the system at high temperatures and at different pressures.

This method is a method used for sintering materials containing additives that are unstable and volatile at high temperatures, or ceramics or metals that cannot be sintered at high density by other methods. With this method, it is possible to obtain the net-shape designed in the finished product.

It can be used for the production of Si_3N_4 in the temperature range of 1650-2100°C and 1-110 MPa. The sintering process, which consists of two stages, can be applied. In the first stage, no pressure is applied, until the closed pores becoming exist. Afterwards, high pressure is applied until the sintering is completed in order to contribute to the formation of condensation.

Si_3N_4 materials produced by GPS sintering method are superior to their competitors produced by traditional methods in terms of mechanical properties, either porous or non-porous [21].

Figure 9: Gas Pressure Sintering (GPS) [22].

1.1.2.5 Hot Isostatic Pressing (HIP)

Hot Isostatic pressing process has been developed for diffusion bonding and removal of porosity in the structure. It has long been used in powder metallurgy. It can be used to produce the material designed by powder metallurgy method or to improve the properties of the designed material.

In this manufacturing method, temperature and pressure are applied simultaneously on the powders. The pressure applied in the vacuum chamber can be an inert gas such as Ar or N_2. This pressure applied as isostatic can be determined in the range of 10-50 MPa. Therefore, deformation does not occur with the start of pressing.

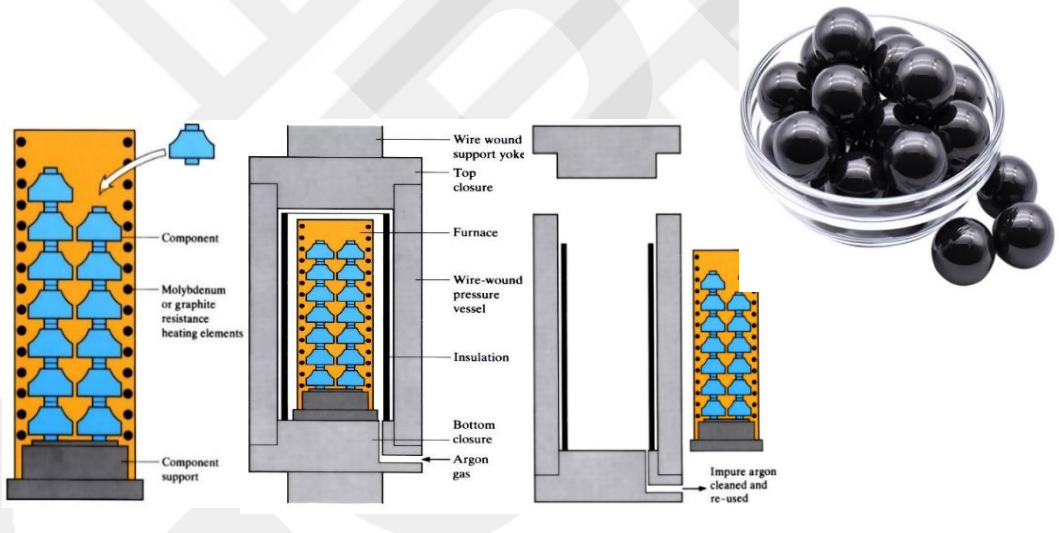

Figure 10: a.) Load components into the furnace. b.) Load furnace into pressure vessel. Raise pressure and temperature simultaneously, and hold.c.) Cool, release gas (clean and recycle) and remove furnace from pressure vessel. Remove components from furnace [24-25].

Graphite heaters in furnace can reach temperatures as high as 2000°C, so the powders are heated. It can be made for the production of materials with high density by the hip powder metallurgy production method. Internal pores without gas penetration or cavities in the solid with a rigid structure are sintered with high pressure and temperature [23].

1.1.2.6 Microwave Sintering

Microwave sintering method; it differs from the conduction or convection heat transport systems provided by traditional sintering methods because which is in an electromagnetic form that can penetrate the interior of the structure. The traditional methods heat the structure from the outside. The structure is heated from the inside with the microwave sintering method.

By definition, the microwave has a frequency in the range of 300 MHz (100 cm) to 300 GHz (0.1 cm). Microwaves cause movement at atomic scale within the structure they encounter. It results in the heating of the material. Microwaves are obtained from electrical energy.

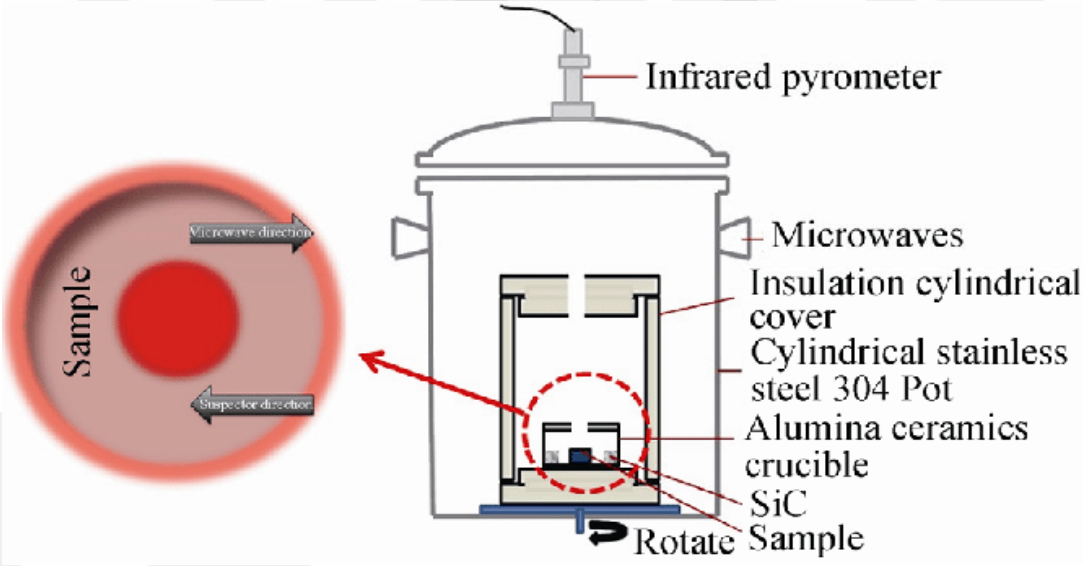

Figure 11: Shcematicaly drawing of Microwave Sintering Furnace [27].

The biggest advantage of this production method is that it is a fast sintering method due to the rapid access to high temperatures. The sintering processes are around 1-2 hours with traditional methods while the time can be reduced to 30 minutes with this method. On the other hand, products with high mechanical properties are obtained in near net shape by obtaining fine grains. This production technique is suitable for obtaining an FGM microstructure, but cannot be used for sintering Si_3N_4 powders [26].

1.1.2.7 Spark Plasma Sintering (SPS)/Field Assisted Sintering (FAST)

Spark plasma sintering method is obtained by applying pressure and current simultaneously on the material to be sintered. The powders are placed in a graphite container and intermittent direct current is applied and high pressure is applied to the powders at the same time. Therefore, heat is obtained and sintering occurs. In the case of pulsating current to the powders, the graphite container is also heated. For this reason, both the effective use of energy is ensured and the diffusion rate is increased thanks to the increase in mechanical tension and electric field. Result of that while there is a homogeneous heat distribution between the powders with the SPS method, homogeneous distributions are also observed in the microstructure.

The SPS method, fully dense structures can be sintered in a very short time without any growth in grain structures. In classical sintering methods such as HP, grain sizes tend to grow with the effect of temperature, time and are obtained in µm sizes. However, since grain growth is not allowed in the samples produced with SPS, nm sized structures can be observed. In this way, better mechanical properties can be obtained.

The working principle of the SPS system is as follows; instant high-temperature regions occur with sparks being sent to the contact points or particle spaces between the compressed particles. In the dusts around the temperature zones, melting occurs during SPS. The molten surfaces are pulled towards each other under vacuum and cause neck formation.

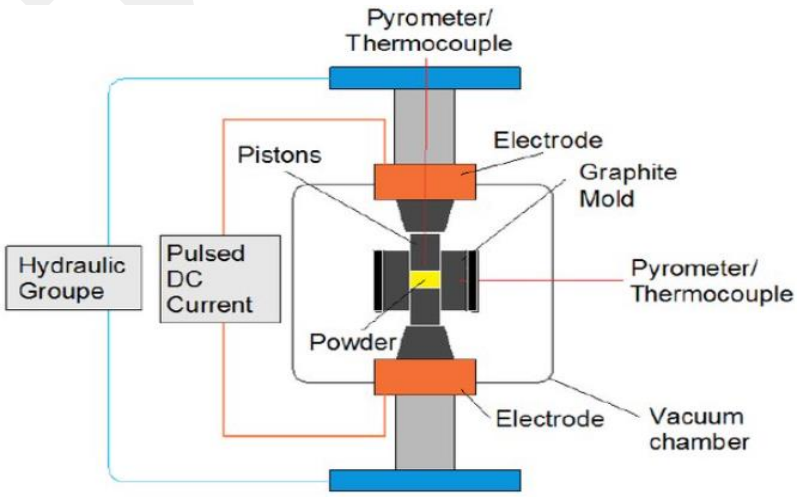

Figure 12: Schematicaly drawing of Spark Plasma Sintering (SPS) [28].

1.1.3 Porous Silicon Nitride (Si_3N_4)

Porosity is observed in the form of structural voids, channels or pores in the microstructure. Depending on the characteristics of the designed material, some gaps may be required or failure may occur due to the decrease in the mechanical properties of the material. The general condition of the porous materials, it contains 10-95 wt. % air and the remaining part contains dense bulk materials. These materials can have a metal, composite, ceramic or polymer bulk structures. Ceramic porous materials are used in molten metal filtration, catalysis, refractory insulation, hot gas filtration, etc. It can be used in the industrial field as well as for incubation centers with microroughness surfaces that it can form in the pores and it can also be used for bio integration processes due to increasing cell penetration. On the other hand, with the principle of less energy more work, it is aimed to reduce energy consumption by having low mass but high mechanical properties that can suitable for technological needs. Studies on the ratio, distribution and formation of pores in the microstructure are still continuing today. The properties exhibited when the characterization of porous materials is made; It is directly related to density, porosity, shape and structure. Coaxial pores while exhibit isotropic behaviour in terms of mechanical properties, long and rod-like pores exhibit anisotropic properties. Porous materials can also be examined in three classes according to their porous structures. The porous structure can be opened, closed and mixed. Open pores generate a structure that can form networks with each other in contact with the environment because they are on the surface or connected to the surface. The closed pores, on the other hand are pores structures that do not have a network structure in the bulk and are not related to the environment. The cell walls in the structures of materials with this pores structures causes an increase in mechanical properties. The mixed pores are formed by the presence of both opened and closed pores in the microstructure of the same material.

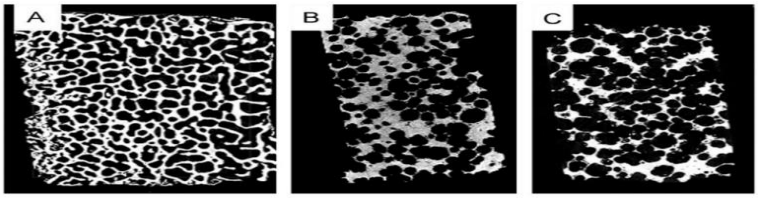

Figure 13: Sections from XRD microtomography of bone (64 vol% pores)—(A), air-sintered Si_3N_4 (65 vol% pores)—(B), SRBSN (73 vol% pores)—(C) [29].

1.1.4 Application areas of Silicon Nitride

Si_3N_4 has excellent physical and chemical properties thus has a wide range of application areas. It is used in applications requiring strength including high temperature as metal forming rolls, molds and cutting tools, as well as applications where abrasion resistance is important such as ball bearings, shafts, axles, turbine blades and wings. An engine parts waiting to stabilize at high temperature and cyclic load are also used in turbochargers [30].

Recently, there have been many studies in their use for biomedical purposes. These are used in many studies such as orthopaedic surgery, spinal fusion implants hip and knee joints dental implants and biocompatible features [31].

The figure 14, are products belongs of some silicon nitride applications [32]. In the first image, there is a Si_3N_4 bearing with a purity of 97-99 wt. %. Si_3N_4 bearing products can be used in many engineering applications with their high wear resistance, good corrosion resistance, low thermal conductivity and high working strength (800^oC). In the second image, there are thermocouples which has high thermal shock resistance due to Si_3N_4 structures. The good oxidation and wear resistance of S_3N_4, it is a suitable material for thermocouple production. It can be used in melting furnaces that require high temperature resistance. In the third image, there are nozzles which is used in many RF heating applications due to its low thermal conductivity and metallic chemical resistance. Si_3N_4 is used in many aerospace applications due to its high thermal shock resistance and high electrical insulation.

Figure 14: (Silicon carbide bearing ceramic products: Stanford Advanced Materials), (Silicon nitride bearing rollers: Stanford Advanced Materials) (Silicon nitride electrical insulator, Si_3N_4 2020) [33] [34].

The Si_3N_4 telemetries shown in Figure 15, can be used in oil fields and wells under corrosive chemicals and high pressure. It can record the data coming from the wells. It has high resistance to abrasion and corrosion. It also meets the high temperature requirements needed in deep water operations with its thermal shock resistance and thermal expansion coefficient. It is 60 wt. % lighter than steel. The plates in the image are used in mining and wear applications; It can be used as slabs and tiles with its corrosion resistance, electrical insulation, abrasion resistance, hardness, durability, thermal and impact resistance properties.

Figure 15: (3M™ Silicon Nitride Telemetry Tooling), (3M™ Silicon Nitride Wear Plate) [35] [36].

1.1.4.1 Biomedical Application of Silicon Nitride

Si_3N_4 is a very important biomaterial that is used in vivo in the structure of ceramic implant materials, especially in orthopaedic surgery and properties and stable structure that it protects in extreme body environments, its mimic mechanical properties make Si_3N_4 biomaterials attractive.

Figure 16: Si_3N_4 biomedical applications. [37].

Si_3N_4 is being developed for use in mobile body areas where bone wear is common in joint replacement. The images below are taken from the SINTX Technologies' (formerly Amedica) website [37]. There are cervical and lumbar produced with Si_3N_4, and Si_3N_4 based bio materials produced for fusion and fixation applications. Today, Si_3N_4-based ceramic biomaterials are produced with traditional production methods. In addition, Si_3N_4-based biomaterial studies are being developed with the additive manufacturing method. Application of additive manufacturing production method, that is possible to produce in bulk, FGM or coating form. This method supports, near net shapes, low tolerance dimensions and controllable microstructures can be obtained.

Figure 17: Prothesis applications of Si_3N_4 [37].

According to another study, it is mentioned that coatings and surfaces with roughness and porous structure are attached to the skeletons through implants. Two different Si_3N_4 biomaterials integrated into the body at different times are examined for 12 weeks and 9 months. Human bone grows at a rate of 1 μm per day, forming a porous structure. The pore sizes should be approximately 150-500 μm in order to promote bone growth. Otherwise, fibrosis affects tissue formation negatively and causes clinical failure [38].

Porous or rough surfaces and coatings have been developed and used successfully to provide skeletal attachment to orthopaedic implants through bone growth. Bone growth within porous coatings has been demonstrated to plateau in clinically successful post-mortem implants as soon as 12 weeks and at approximately

9 calendar months. It is also known that human bones transform into a porous structure at a rate of ~1 μm per day and the average pore size should be between 150 μm and 500 μm to promote bone growth. Poor implant placement resulting in a bone-implant cavity greater than 50 μm, small pores [39] and lack of interpore connectivity has been shown to promote the fibrous tissue encapsulation response. Formation of fibrous tissue layer on implant surfaces directly prevents bone apposition and skeletal adhesion and causes pseudarthrosis, joint instability and clinical failure [40].

1.2 FUNCTIONALLY GRADED MATERIALS (FGM)

Functionally graded materials (FGM' s) were developed in the 1980's by material science engineers due to the need for high thermal resistances. There are different specific properties of different layers in the micro and nano structures, porous structure network and chemical composition of these materials. This continuously variable structure, the mechanical, strength, thermal conductivity coefficient, chemical and electrical resistances of the designed material etc. features can be improved [41].

The desire to use different properties of metal materials with high toughness and refractory properties specific to ceramic materials simultaneously and the fact that this process can be achieved by reducing thermal stress, led to the creation of a project for the development of FGM architecture [42].

Materials produced by the FGM method in the 90's were chosen as one of the 10 developing technologies in Japan. Afterwards, the importance of FGM technology attracted the attention of many researchers and research on this subject gained momentum.

FGM materials produced today are examined under three main headings: chemical composition gradient FGM, pore difference gradient FGM, and micro/nano

structural gradient FGM. These heterogeneous materials replace homogeneous materials in some critical applications.

FGM materials are obtained by changing their chemical and mechanical properties in a controlled manner, in accordance with the target material, in a gradient manner for optimum performance in harsh working environments. These materials are defined as KMM. They are suitable materials for thermomechanical, high impact compressions, high voltages, high temperature and aggressive chemical environments.

Generally, application areas are turbo systems, aviation ground and air needs, automotive production sector, chemical production facilities, microsensors, electronic devices, biological implants and household appliances [43].

According to the chemical composition character of the material, FGM's contain different interactions of metal - ceramic, ceramic - ceramic, ceramic - plastic and many other materials with each other.

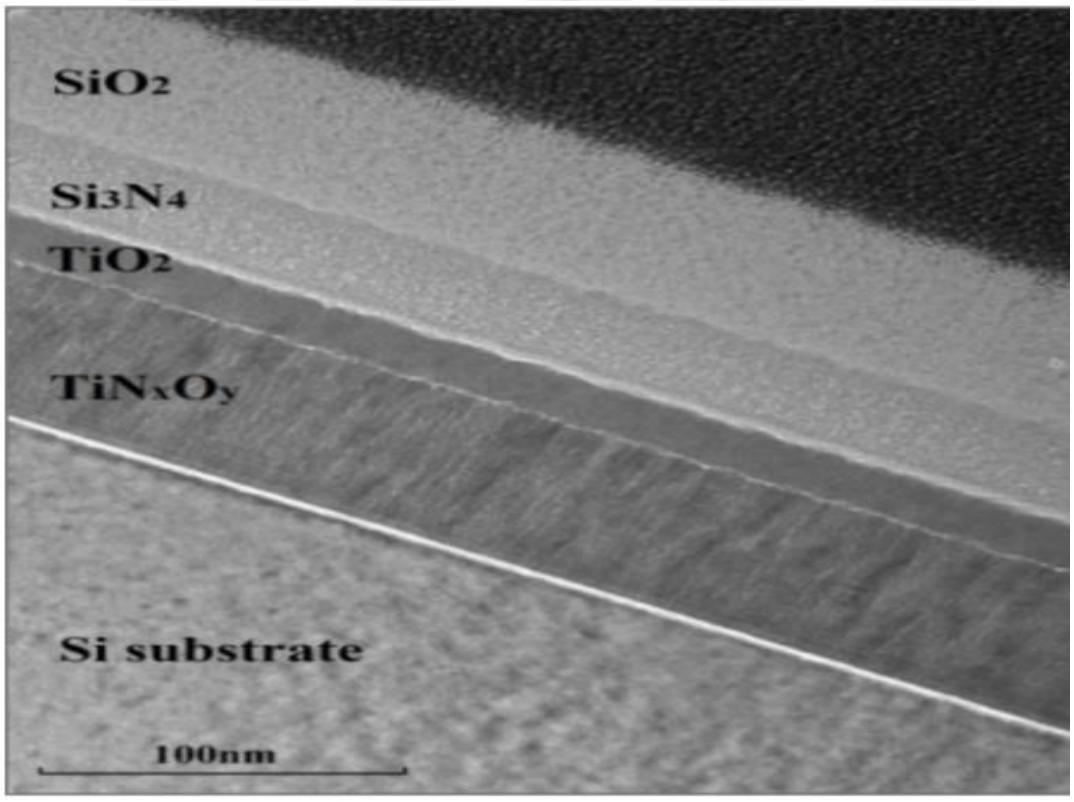

Figure 18: Transition areas of Si substrate, TinON, TiO_2, Si_3N_4 and SiO_2 The bright field cross-sectional transmission electron microscopy (TEM) micrograph of the multilayer absorber and the corresponding electron diffraction pattern [44].

In the figure 18, there is a sample that was produced in a monolithic form and the gradual transitions were observed. Here, there are TiN_xO_y, TiO_2, Si_3N_4 and SiO_2 layers on the Si substrate, respectively.

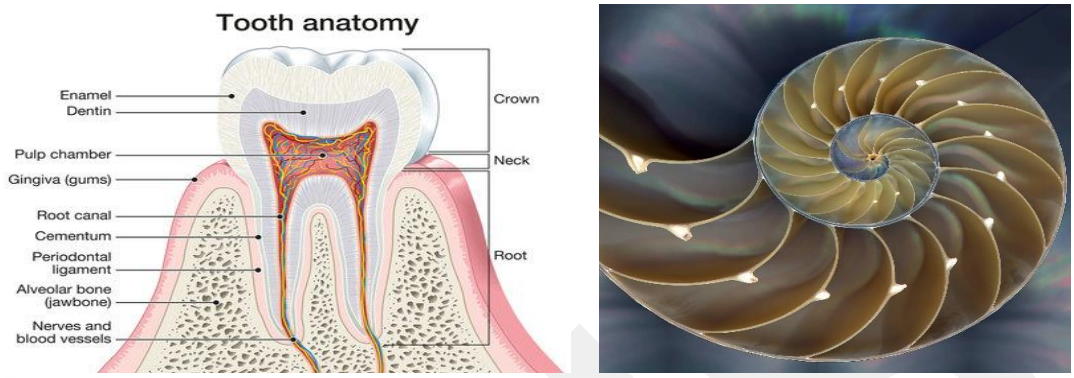

Figure 19: Schematical drawing of Tooth anatomy (Tooth Anatomy images) b.) Section view of seashell [45] [46].

There are functionally graded materials in many devices and machines we use today. On the other hand, unlike these artificially produced materials, there are many naturally developed natural FGM materials in order to adapt to environmental conditions in nature. Structures identified as FGM's are observed in plants, bamboo, shellfish, coconuts, and even in our bones and teeth.

The need for advanced materials with targeted properties became possible with the transition from bulk (monolithic) materials to composite (polylithic), FGM materials, they are second generation composite materials that cannot be achieved even with composite materials and were developed with the aim of achieving the targeted superior performance properties [39].

FGM materials can be in the form of a combination of many materials in layers, or in essence, the relationship of two different surface points with each other. Conventional composites while work homogeneously with each other, which is aimed that two different materials with the heterogeneous structures in FGM materials work in harmony in line with the targeted properties. Therefore, the selected features of both components coexist in a monolithic structure [47]. FGM materials can be found or produced as a thin coating on the surface or as a bulk material.

FGM production can be carried out in two ways. One of them is the bulk production method. This method covers functionally graded materials produced by powder metallurgy, infiltration, casting and additive manufacturing methods. If a secondary phase is desired to be formed on the material produced by the bulk production method, it can be done with one of the methods of PVD, CVD, thermal spray or other surface treatments.

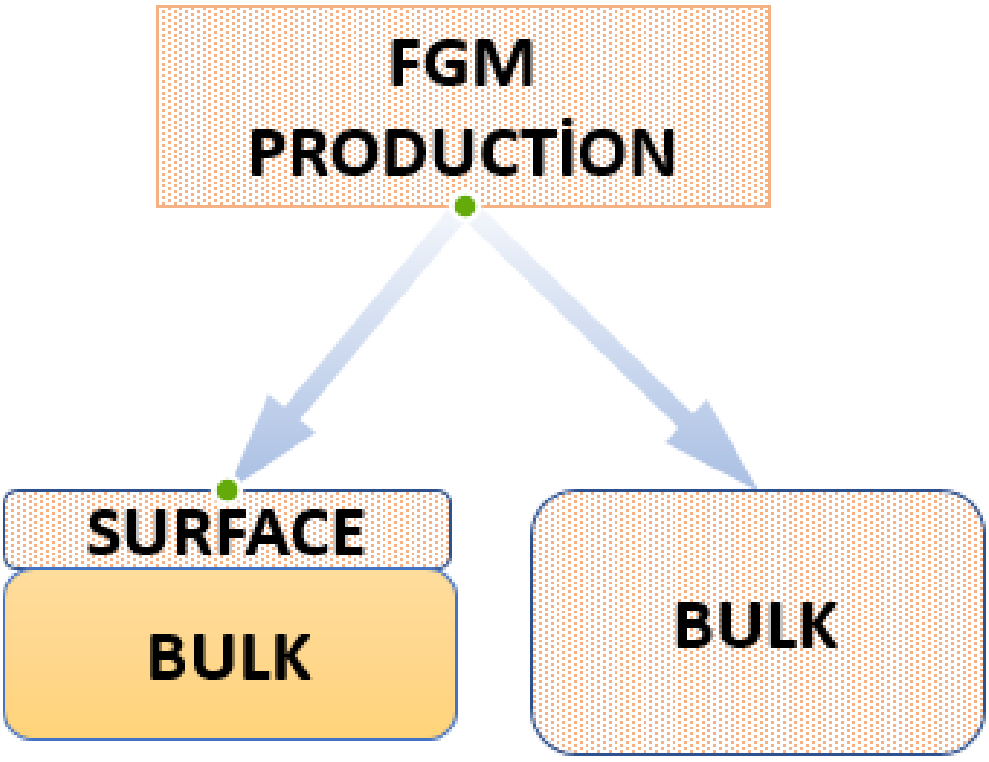

Figure 20: Difference of FGM Production

1.2.1 Bulk Production

Bulk FGM production methods differ from surface coatings both in terms of production methods and approach. The micro properties of the bulk material are determined by the pore size, pore density, chemical composition, as well as the shape, fraction, orientation and dimensions of the gradient.

Figure 21 shows examples of FGMs with different gradients that can be obtained. Figure 21.a, shows that the distribution of the secondary phase of the same shape and size is dispersed throughout the sample, forming a gradual gradient.

In Figure 21.b, it is seen that the gradient structure is arranged in equal layers throughout the entire microstructure. There is an equiaxed layer on one side of the sample, showing an elongated arrangement towards the other surface.

In Figure 21.c, it can be seen that the secondary particles are the same in shape and size. Here, the gradient structure is manifested by the difference in orientation, and in the bulk material it shows the varying properties of the material grains that differ along the x-y axis along the structure.

Lastly in Figure 21.d, the gradient formed is based on the different size of the secondary particles. There are denser and larger particles on one side of the structure and as it gets closer to the counter-face, shrinkage and a decrease in density are observed.

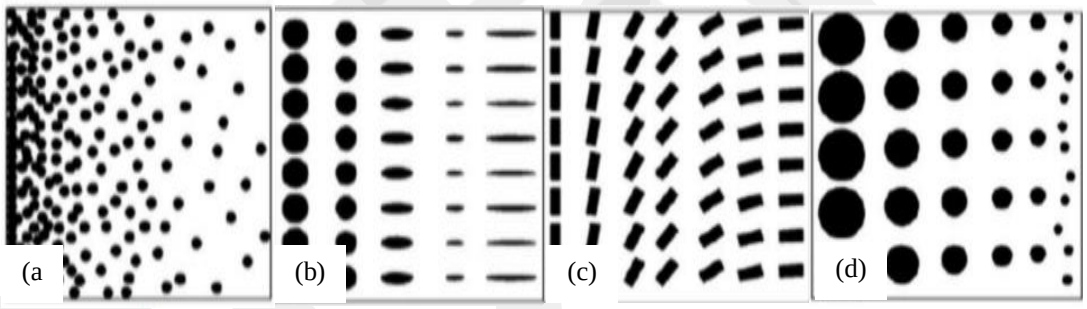

Figure 21: Scheamatic gradient drawings by density, shape, orientation and dimention [48].

1.2.1.1 Powder Metallurgy

The powder metallurgy method is the most commonly used method among the bulk production methods. It is preferred when it is difficult to control parameters such as microstructure, composition and obtaining a shape close to net shape with

other methods. Therefore, powder metallurgy is the most preferred production method in terms of requiring simpler tools for production and effective use of time.

Powder metallurgy consists of 6 steps as shown in table 2. The process starts with the production of powders. Alloys or pure materials to be used can be obtained using mechanical, electrolytic, chemical and atomization methods. In the second step, a homogeneous structure is obtained by mixing the powders. In the third step, the powders are pressed in a mold with different methods and shaped. In the fourth step, it is subjected to sintering process. Afterwards, if needed, heat treatment and/or post processes can be applied. FGM-Si_3N_4 samples, which are the subject of this thesis, were also produced using this method. The processes used are mentioned in more detail under the title of experimental procedure.

Table 2: Steps of Powder Metallurgy

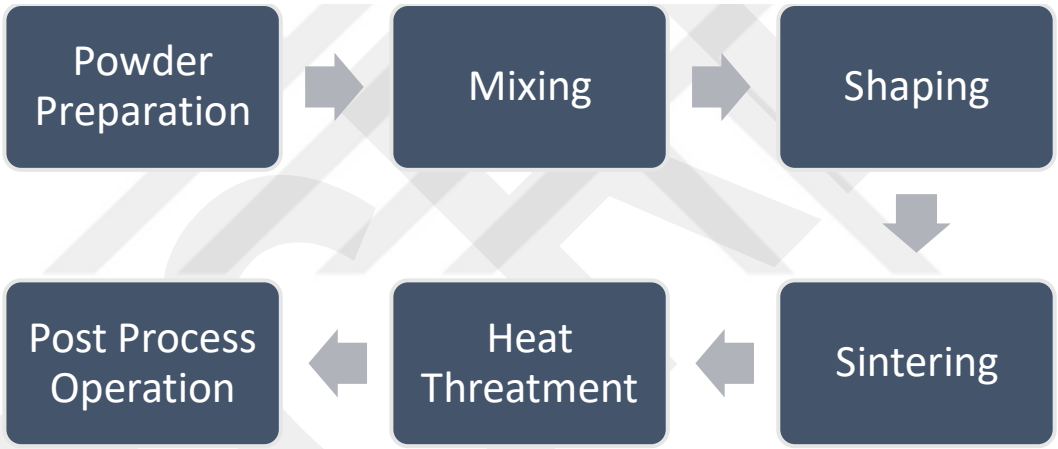

1.2.1.2 Infiltration Method

Infiltration method contains producing composite through leaking a molten metal and fill the forms through the channels of a porous ceramic preform. In the absence of wettability between the reinforcement and the matrix, it can be

accomplished by an external force; by vacuum, mechanical vibration, mechanically produced by an inert gas, by electromagnetic or centrifugal force or spontaneously. This method which can produce shapes with low residual porosity owing to infiltrating preforms and dimensions convenient to the required part is also relatively economic [49]. Definitions of infiltration methods that can be used in the production of FGM materials other than dispersion are explained in the relevant sections of the thesis.

Table 3: Liquic State Processes Table [50].

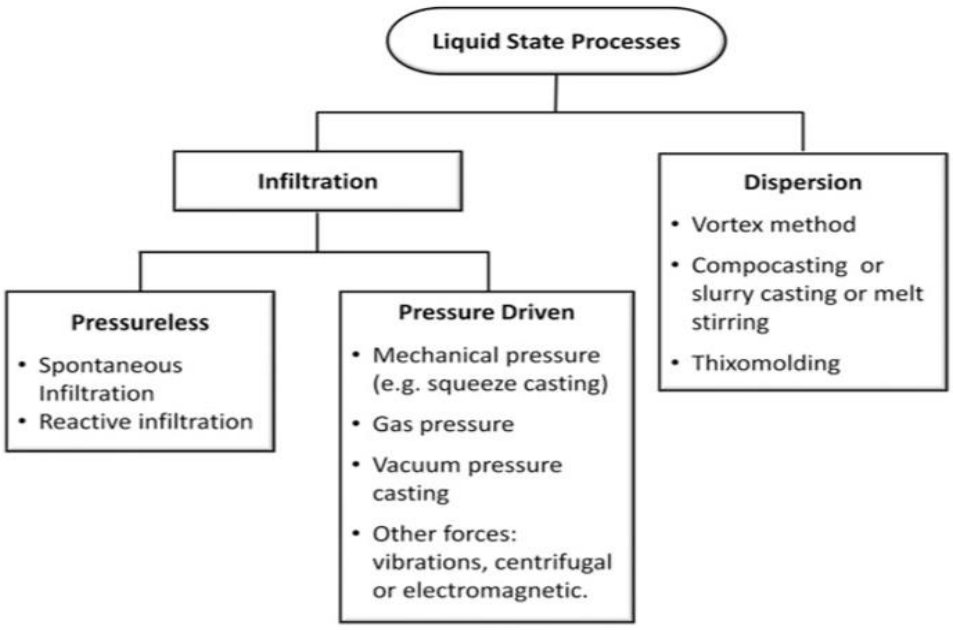

1.2.1.2.1 Gas pressure Infiltration Method

The mechanics of porosity causing infiltration penetration which is rare for RBSN, succeeded and open pores are filled with molten metals during process. The

samples are created by wetting RBSN by liquid metals some are having low specific gravity above 900^{o}C.

RBSN which has low density as 1800 kg.m^{-3} under “vacuum conditions” can be entirely infiltrated. Naturally, 200 Pa pressure is acceptable. RBSN which has medium density as 2000-2200 kg.m^{-3} during process needs greater temperatures or continued heating period for infiltration. Moreover, high density RBSN between the values (2400-2600 kg.m^{-3}) contains infallible pores which are submicrometric, the submicrometric pores of RBSN in this range can be adequately filled by minimizing internal oxidation in oxidizing environments. Liquid metals that are normally permeate-active can be energised by alloying with metals such as calcium, and new compounds formed by reactions including RBSN have been identified. Materials with cermet type character are created by this infiltration technique [51].

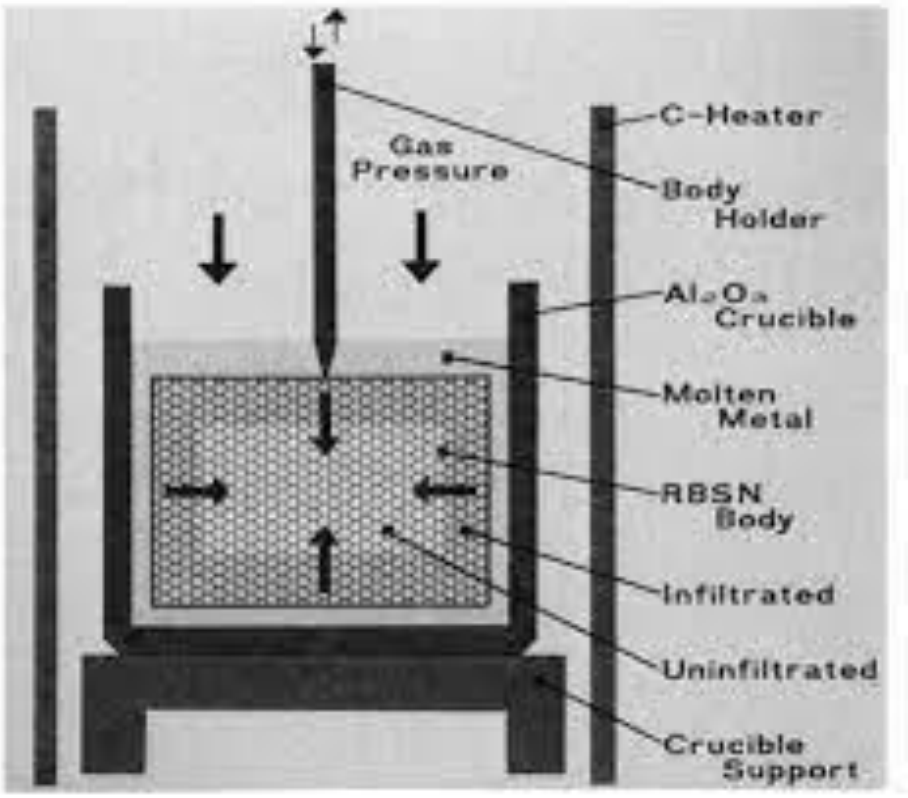

Figure 22: Gas Pressure Inflitration [52].

1.2.1.2.2 Pressure Die Infiltration

Si_3N_4 particles are poorly wetted by liquid aluminium, therefore; producing high performance Si_3N_4/Al composite is difficult. However, method of pressure

infiltration method (Fig. 23) is adequate to overcome poor wetting nature by forcing the molten metal alloy to infiltrate under high pressure. Moreover, this method has the advantages of simple production technology, high density and no restrictions on the alloy [53].

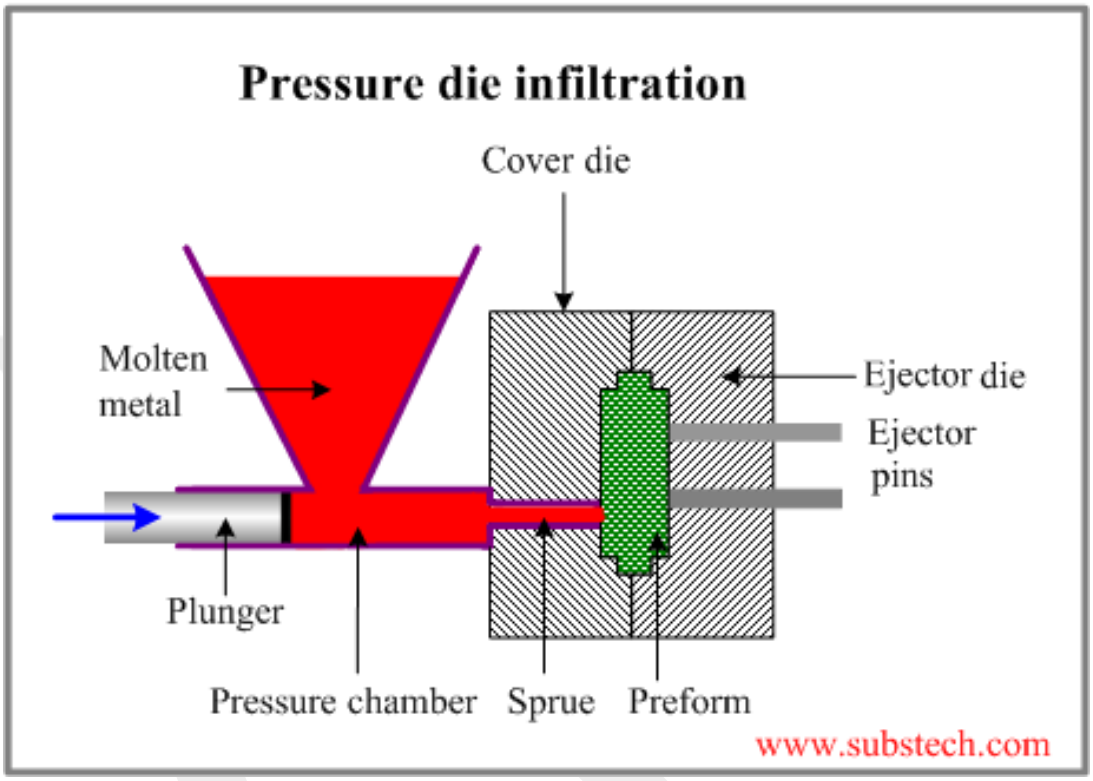

Figure 23: Pressure Die Infiltration [53].

1.2.1.3 Casting

1.2.1.3.1 Squeeze Casting (Liquid Metal Forging)

The fabrication method which solidification improved under high pressure and with a reusable mould as shown in Figure 24 is generically called squeeze casting (SC). Under high pressure within a reusable die. In squeeze casting, permanent die casting and die forging merges into a single process in which molten metal is solidified under implemented hydrostatic pressure. Phenomenal surface finish and approximately no porosity are achieved by SC-fabricated components. Furthermore, various sizes and shapes of products can be moulded which have improved mechanical properties in comparison to conventional casting, gravity die casting or more complex casting routes. Superior weldability and heat treatability are also asserted features of SC products.

Moreover, squeeze casting may continue in the absence of any feeding system, runner, gate; risers, shrinkage compensating units, etc. and is naturally a competent system which no scrap is created to recycle. In comparison with forging, lesser energy is required and single action is done during squeeze casting [54].

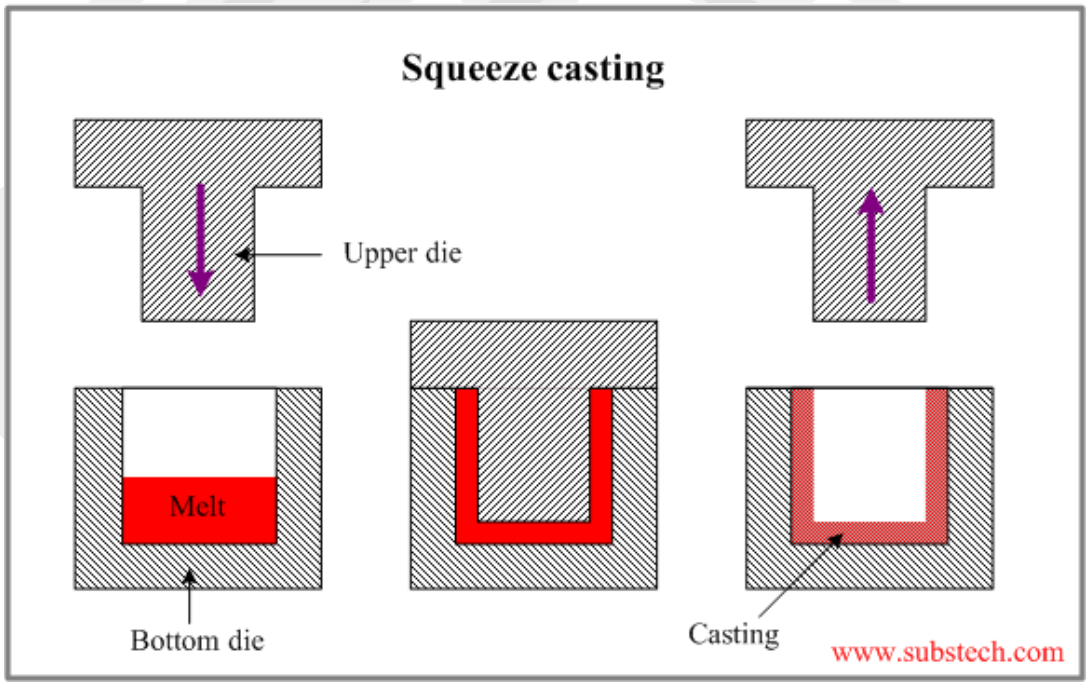

Figure 24: Squeeze Casting [53].

1.2.1.3.2 Stir Casting

Conventional stir casting is one of the commonly used processes due to its low cost, applicability to various materials and better bonding of the reinforcement particles with the metal matrix thanks to the mixing action of the composites with volumetric reinforcement ratio of up to 30%. In contrast to mass production of industrial fabrication stir casting cost is very low. Conventional stir casting is shown representatively in the Fig 25.

Moreover, stir casting method has capability of engineering very large size products with diverse shapes. Due to aforementioned properties, stir casting process can be employed in many applications [55].

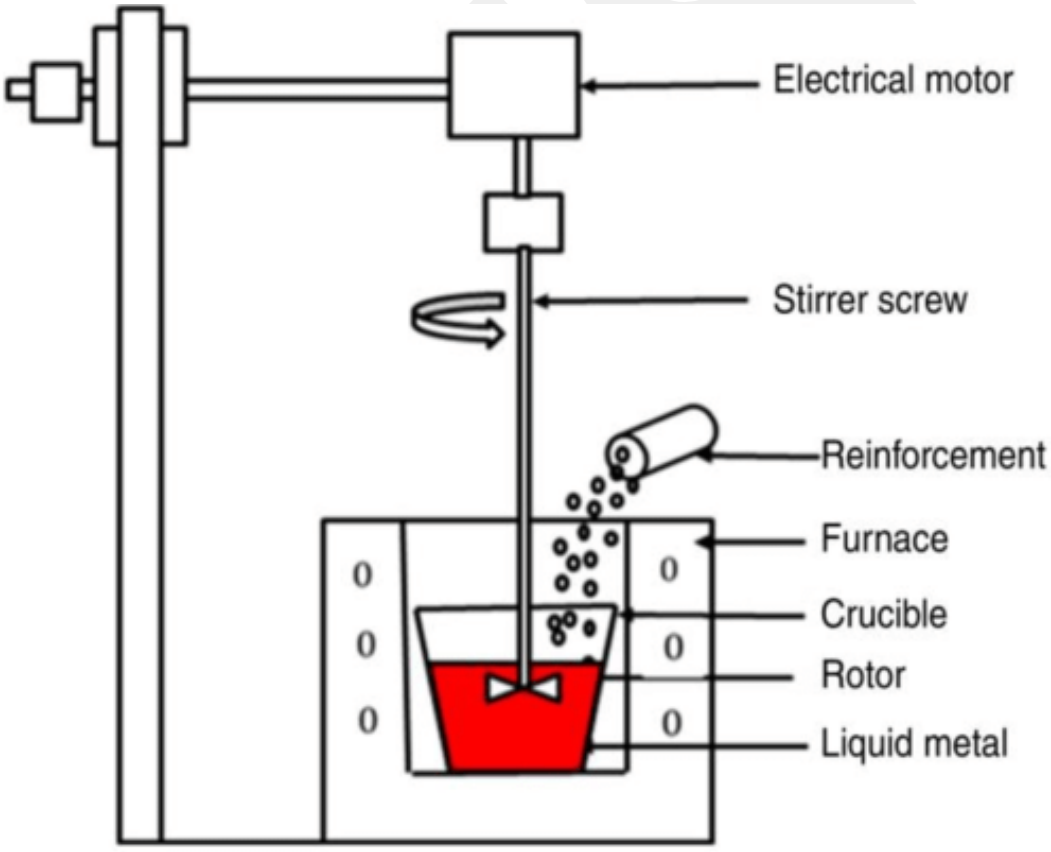

Figure 25: Stir Casting [56].

1.2.1.3.3 Compocasting

A semi-solid processing method in which ceramic reinforcement particles are supplemented to the semi-solid matrix alloy by mechanical mixing is defined as compocasting (Fig. 26). It has two types of combination, namely semisolid-liquid (SL) and semisolid-semisolid (SS). In both types, matrix alloy is in the semi-solid state while in the procedure of mixing and casting is fully or partially liquid, SL and SS types, respectively.

In comparison to conventional stir casting processes, combo casting is more favourable in many ways such as lower pouring temperature is needed, and it concludes to lesser interfacial reaction. In aforementioned low temperatures, a semisolid state can be formed and a defect- free final product can be engineered.

Apart from these advantages, compocasting method does not offer fully eliminated fibers and can cause residual pores. Moreover, main dramatic flaw of SS process are processing difficulties and unwanted porosity. Owe to high viscosity, the products can be defected and with heterogenous particle distribution [57].

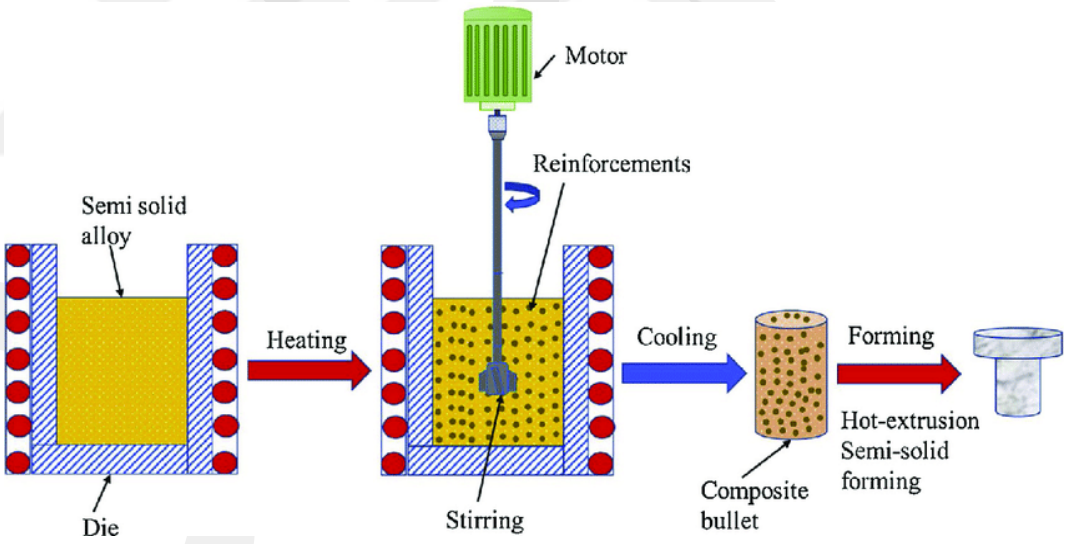

Figure 26: Compocasting [58].

1.2.1.3.4 Centrifugal Casting Method

The form of casting, which is made by entering the molten metal into a rotating mould while the casting solidifies, is called centrifugal casting. Centrifugal force while the process draws the molten liquid metal to penetrate the most detailed crevices of the mould [59].

Figure 27, demonstrates horizontal centrifugal casting method of functionally graded $Cu_{10}Sn_5Ni_{10}Si_3N_4$ composite and copper alloy [60].

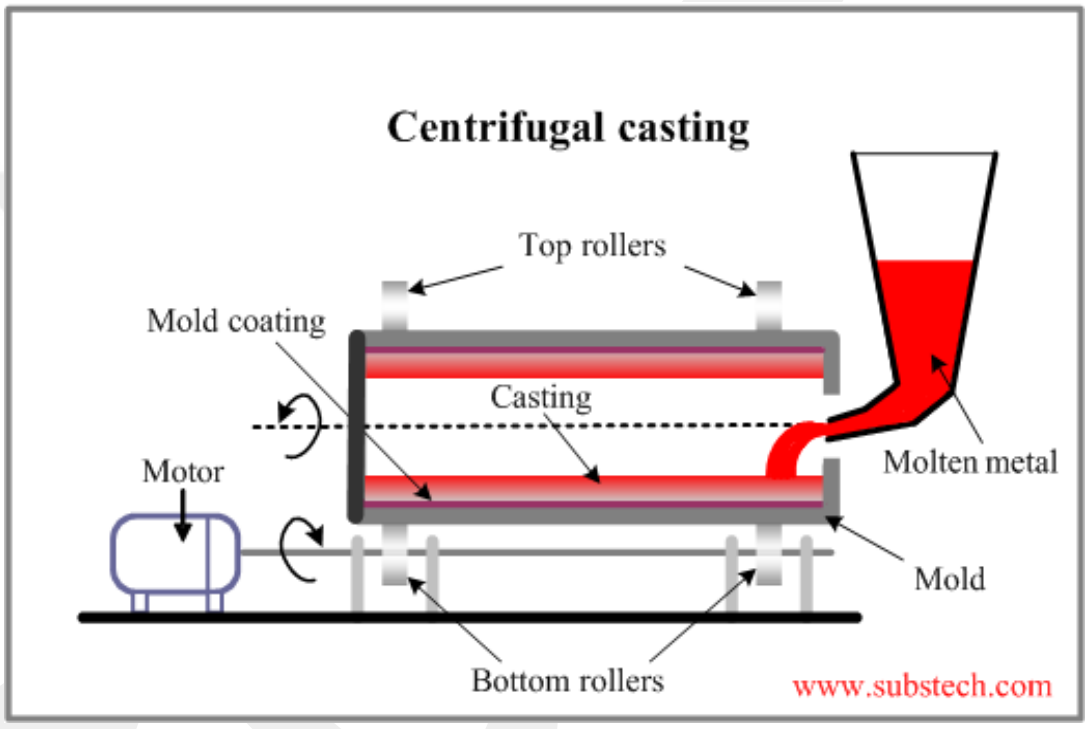

Figure 27: Centrifugal Casting [53].

1.2.1.3.5 Slip Casting

The slip method is formed by dispersing the fine ceramic powders and water with some chemicals that help to slip. This solid particle containing fluid is poured into a mould which eliminates the liquid from slip adjacent to mould walls. The reason of this attitude is capillary action between the porous mould and pore-wicking liquid [61].

It can be highlighted that manipulation ease of the colloidal suspension system leads to minimize interparticle reactions, as much as sample geometry and at least green density.

In the case of Si_3N_4, however, one of the biggest challenges is shear stabilization. It is complicated to prepare slurries with high solids loading that display the rheological behaviour required for this casting procedure. Moreover, if sintering additives are added, more stabilization problems are experienced in the suspension.

Sintering aids such as Al_2O_3, Y_2O_3, MgO or cordierite must be added when sintering at low temperature and without pressure with the addition of Al_2O_3 and Sialons are formed as a secondary phase due to the formation of a low melting point liquid phase between silica and oxide additives on the surface of Si_3N_4 particles [62].

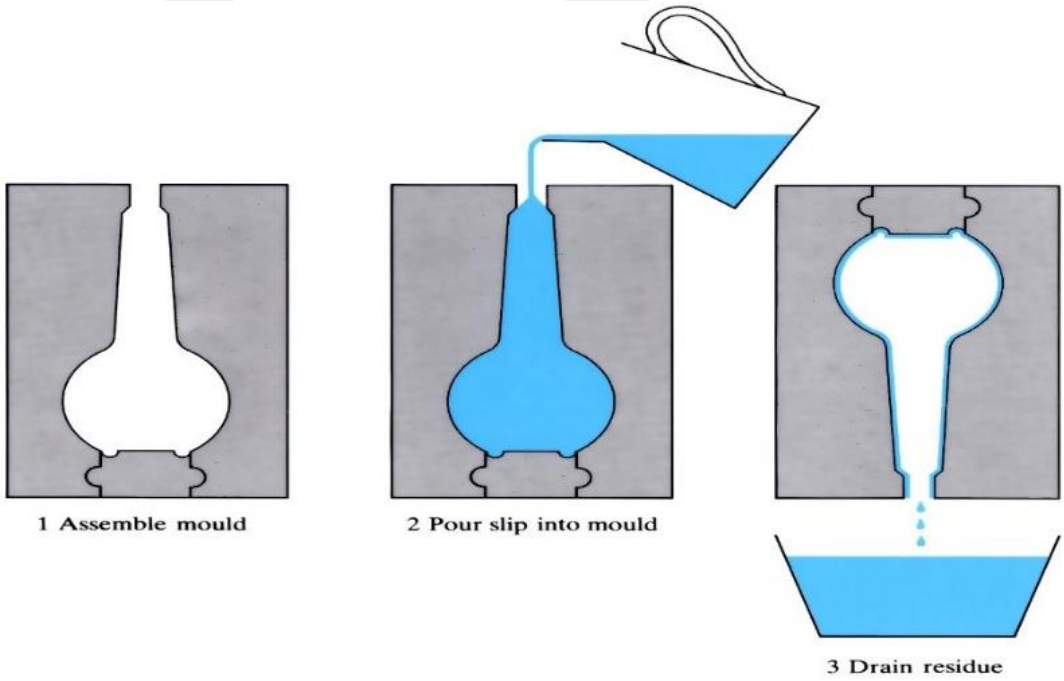

Figure 28: Slip Casting [63].

1.2.1.3.6 Tape Casting Method

Tape casting, also known as doctor blade casting or knife casting are the same processes. Thin two-dimensional structures are created with a thin scraping knife called “the doctor blade”. These structures are created in a large X and Y area with a cross-section. Tape casting has a very wide product range i.e. 1.2x2,4m squares which is used in fuel cells or small sheets used in thermistors, dimensions of 1.5mm x 1.5 mm.

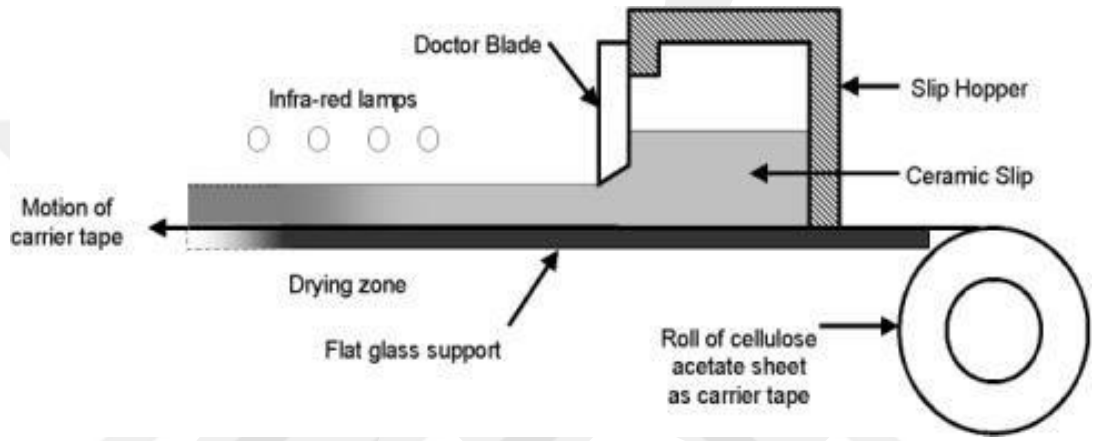

Figure 29: Tape Casting [64].

1.2.1.4 Additive Manufacturing (AM)

3D printing technology, which is one of the additive manufacturing methods such as the process of turning the first computers into a personal computer, has entered our homes today. In traditional production methods, there is a bottom up approach instead of the monopolized top bottom production methods. Materials atom by atom or molecules by molecules are produced according to the material designed. Combined with the competence of obtaining the desired composition at the desired point and the FGM understanding designed over CAD, which is possible to create high-tech innovative materials.

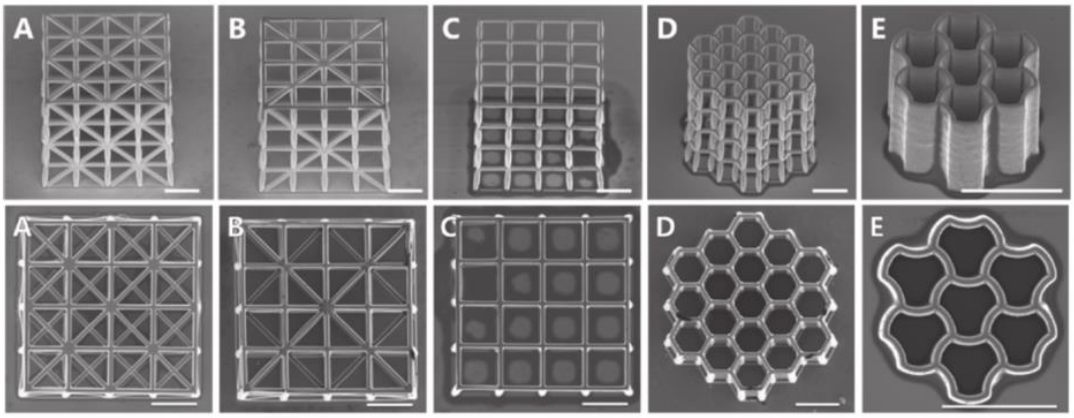

Figure 30: FGM samples produced with different support geometries produced by the Additive Manufacturing method [66].

AM is an effective method for fabricating FGM with excellent formability and optimized stress profiles. AM also provides the potential for spatial and temporal control of microstructure and complex geometry components in behalf of environmental benefits. Therefore efficiently produced using additive manufacturing, safely and greenly [65].

The most commonly used additive manufacturing methods for producing functionally graded materials are briefly summarized in the following subheadings.

1.2.1.4.1 Fused Deposition Modelling (FDM)

FDM technology is the cheapest 3D printing technology. Generally thermoplastic materials, which come in the form of filaments, they are heated in an extruder and the parts are built layer by layer, by selectively depositing molten material in a predetermined path. The most important parameters to be controlled here are the extruder temperature and the cooling rate of the created stages. Considering that the Si_3N_4 glass transition temperature is at high temperatures, this technology is not a suitable method for the production of Si_3N_4 samples. In addition, this technology is suitable for the production of metals, polymers and glass materials.

Figure 31: 3D printed products [67] [68] [69] [70].

1.2.1.4.2 Powder Bed

The Powder Bed Fusion process includes the following commonly used printing techniques; direct metal laser sintering (DMLS), electron beam melting (EBM), selective heat sintering (SHS), selective laser melting (SLM) and selective laser sintering (SLS).

Powder bed fusion (PBF) methods use either a laser or electron beam to melt and fuse material powder together. Electron beam melting (EBM), methods require a vacuum but can be used with metals and alloys in the creation of functional parts. All PBF processes involve the spreading of the powder material over previous layers.

There are different mechanisms to enable this, including a roller or a blade. A hopper or a reservoir below of aside the bed provides fresh material supply. Direct metal laser sintering (DMLS) is the same as SLS, but with the use of metals and not plastics. The process sinters the powders, layer by layer. Selective heat sintering differs from other processes by way of using a heated thermal print head to fuse powder material together. As before, layers are added with a roller in between fusion of layers. A platform lowers the model accordingly [71].

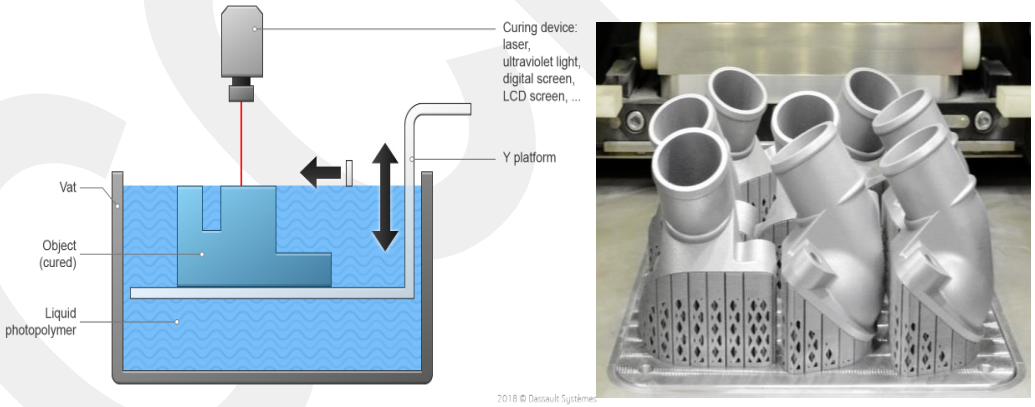

Figure 32: a.) Powder Bed Schematic drawing [72]. b.) 3D printed truck parts [73].

1.2.1.4.3 Directed Energy Deposition

Directed Energy Deposition (DED) covers a range of terminology: 'Laser engineered net shaping, directed light fabrication, direct metal deposition, 3D laser cladding', which is a more complex printing process commonly used to repair or add additional material to existing components [74].

A typical DED machine consists of a nozzle mounted on a multi axis arm, which deposits melted material onto the specified surface, where it solidifies. The process is similar in principle to material extrusion but the nozzle can move in multiple directions and is not fixed to a specific axis. The material, which can be deposited from any angle due to 4 and 5 axis machines, is melted upon deposition with a laser or electron beam. The process can be used with polymers, ceramics but is typically used with metals, in the form of either powder or wire [75].

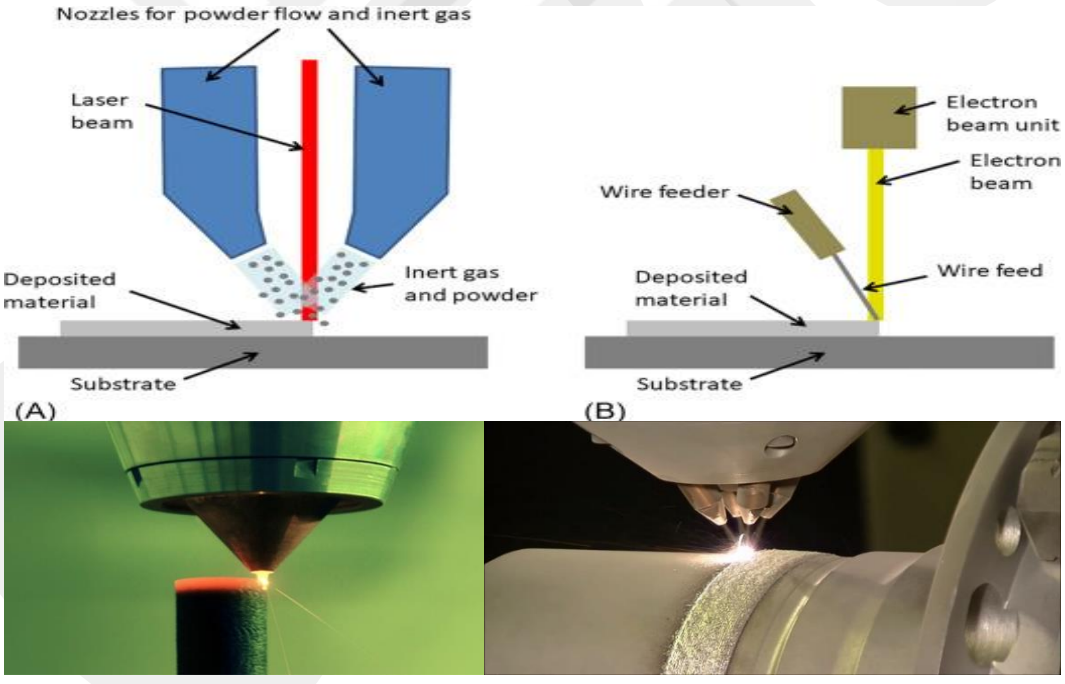

Figure 33: Directed Energy Deposition [76] [77].

1.2.1.4.4 Binder Jetting

Then, the selected CAD model is introduced to the system, the binder particles start to stick the powder particles to each other according to the designed model. The resulting product is near net shape. The densification is made in the sintering furnace. It can be made by PP (Plaster-based 3D printing) or PBIH (Powder bed and inkjet head 3D printing).

A layer of powder is formed, then the bottom piece is printed on the smooth surface of the powder by the printheads and the particles are adhered to each other. Followingly, when process is finished, the working platform is lowered by the piston and a new powder layer is applied. Printing continues gluing layers to previous layers and finishes until the sample is ended. All powders are reusable, as no solid or bonded supports used during the printing process are required [78].

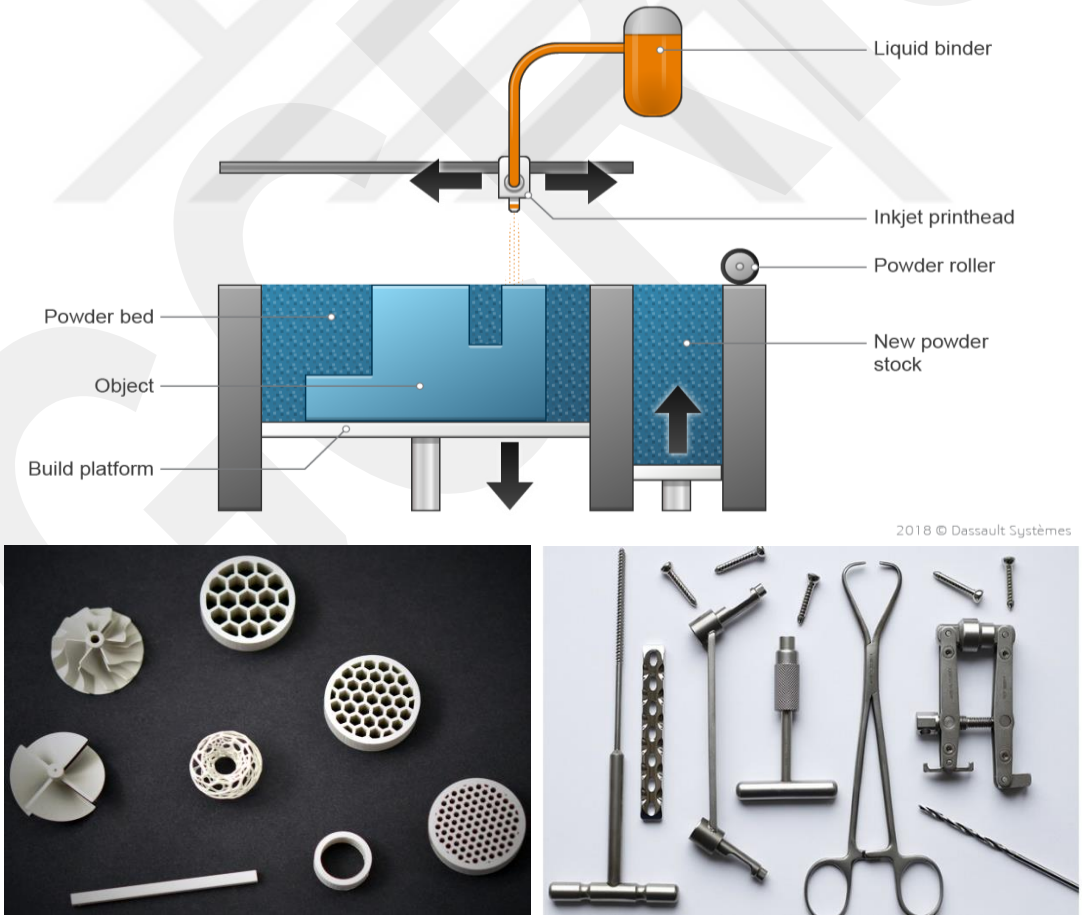

Figure 34: Binder Jetting device and applications [79] [80] [81].

1.2.1.4.5 Sheet Lamination

As a preliminary work of densification, laminating the structure improves the damage-critical material properties in ceramics. Building ceramics gain several features with this technique. First, the primary defect size can be reduced and even microstructural improvement can be achieved if attentively designed. Non-destructive failure modes and damage-tolerant interfaces can be exhibited by these ceramics even in bending cases. The lamination technique is considered as both a malleable and potent design method in a wide variety of material structures that are produced as prototypes and rapidly. Depending on the class of the material to be designed, vertical sheet pieces of reinforcement are brought together according to the direction of the reinforcements. They can be put together by adhesive bonding, clamping, ultrasonic welding or gluing. (Laminated object manufacturing of Si_3N_4 with enhanced properties.)

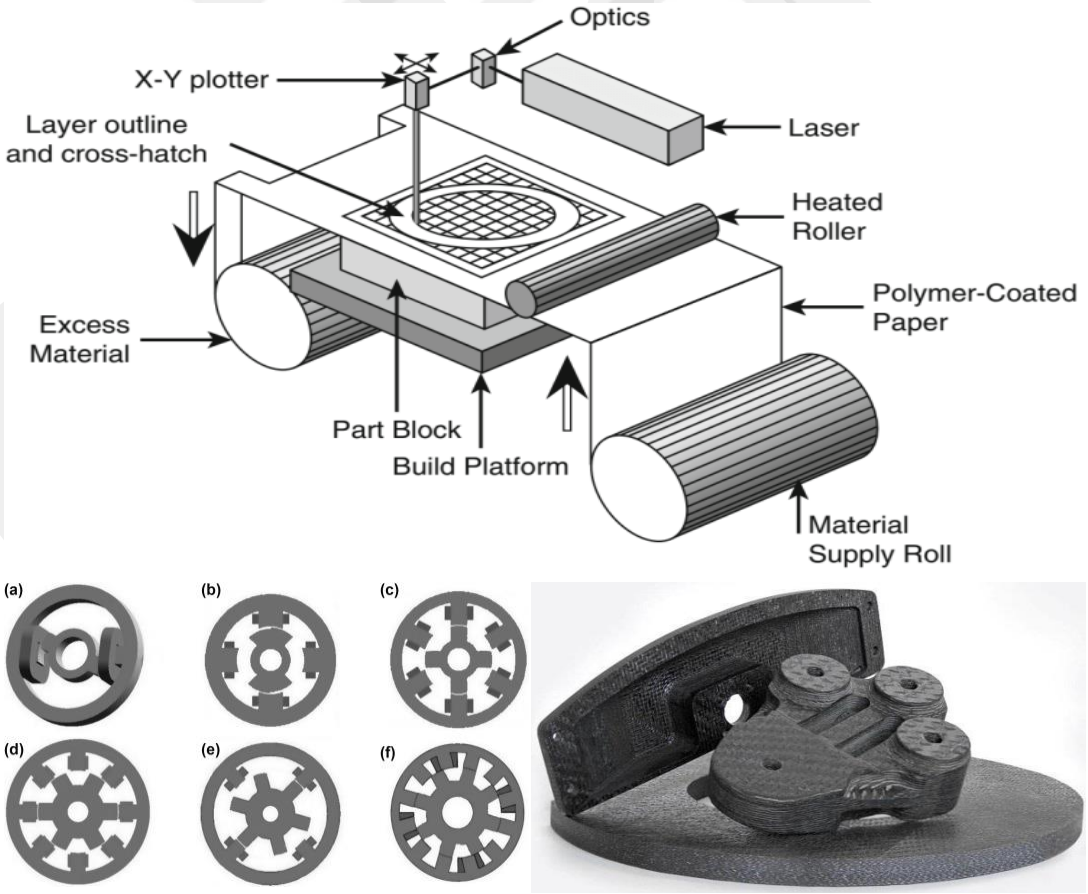

Figure 35: Sheet Lamination [82] [83] [84].

1.2.2 Surface Coating Production

Surface coatings are not made in the form of changes in the crystal structure or pore structure of the bulk materials by making a differentiation in the layers. Surface coatings represent customized exterior surfaces with the instructions given by the designed features. In this way, differentiation is observed on the surface without any change in the bulk part of the material. Conventionally used surface FGM methods are described below.

1.2.2.1 Physical Vapor Deposition PVD

Commonly known as thin film processes, physical vapor deposition processes aim to decompose evaporated material from a liquid or solid source. In this atomistic case, vacuum transported vapor which carry atoms or molecules condense into substrate when it is encountered low pressure gaseous plasma. PVD processed deposit films enable a wide range of thickness options of nanometres few to thousands, additionally, it is used to form free-standing structures, multilayer coatings, very thick deposits and graded composition deposits [85].

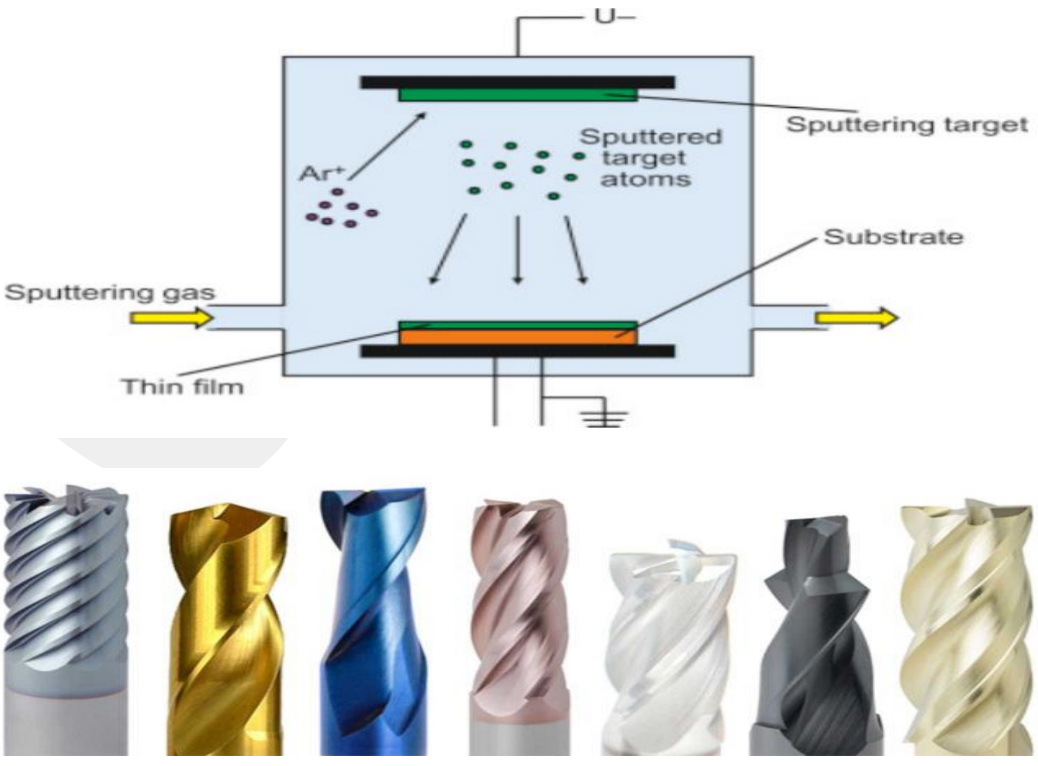

Figure 36: Physical Vapor Deposition PVD [86] [87].

1.2.2.1.1 Electron Beam-PVD

EB-PVD technology (Electron beam physical- vapor decomposition) overcomes complexity and defects compared to other methods of physical vapor decomposition processes, metal spray and chemical vapor decomposition; is more compatible, cost-efficient, and intense coating technology.

Through the agency of EB-PVD, comparatively high decomposition rates (up to 100-150 μm/minute with an evaporation rate approximately 10-15 kg/hour) can be obtained besides high thermal efficiency, low contamination, dense coatings, columnar and polycrystalline microstructures. At the relatively low temperatures, manifold metallic and ceramic coatings (carbides, oxides and nitrides) are deposited.

EB-PVD is a technique which has ability to achieve multicomponent and multi-layered metallic/creaming coatings on large components due to changes its variables such as ingot composition, part manipulation and electron beam energy. Dense coatings with improved adhesions are produced via ion beam source attachment to system of EB-PVD process [88].

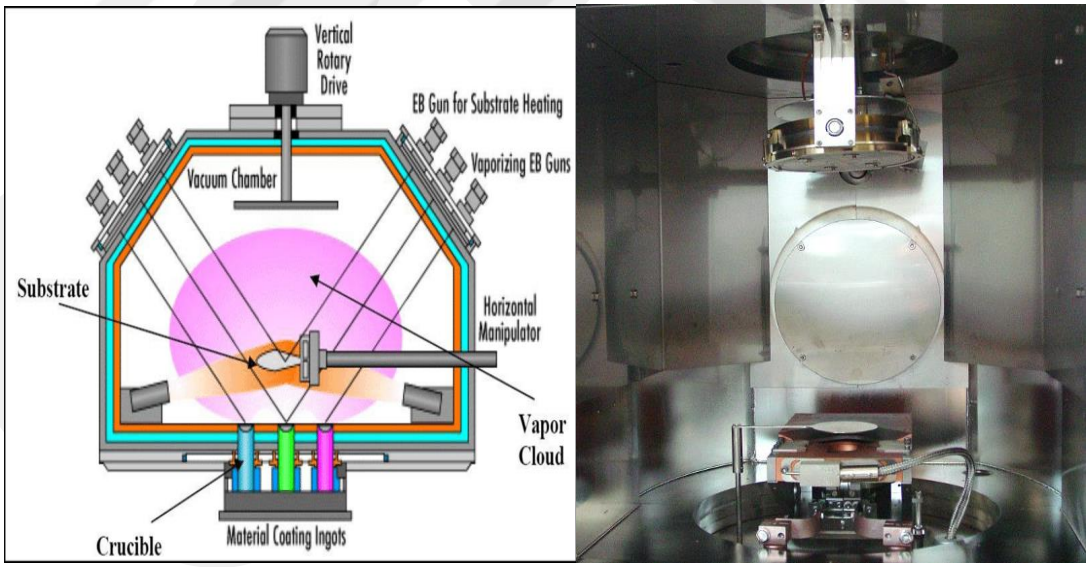

Figure 37: Electron Beam-PVD [89] [90].

1.2.2.1.2 Sputtering Based- PVD

Method of ion beam sputter deposition allows production of thin coatings with superior adhesion and high density exclusive of its many advantages. In this deposition process, the ionized argon gas is used to sputter atoms from a ceramic target. Sputtered atoms intensify on the metallic substrate that is settled in the path of the sputtered material [91].

It is a method used to combine the excellent bioactivity of ceramics with the mechanical properties of metals, using various techniques to coat metallic implants with calcium phosphate-based biomaterials. As a result of such a combination, it is aimed to improve the penetration between metal implants and newly formed bone. Clinical applications prefer adhesive, hard and dense calcium phosphate coatings as well as bioactivity.

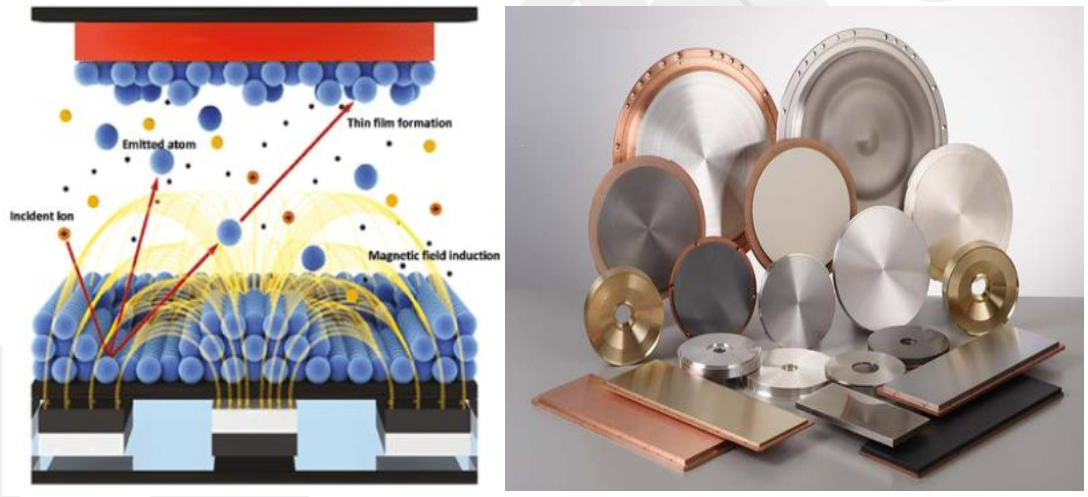

Figure 38: Sputtering Based- PVD [92] [93].

1.2.2.1.3 Plasma Spray Based –PVD (PS -PVD)

Plasma Spraying-PVD is a technique which powder particles are added into a growing plasma stream which heated and accelerated particles move towards the substrate. If the substrate and plasma streams move relatively to each other (nanoarray), particles solidify on substrate and constant thickness of layers are created [94].

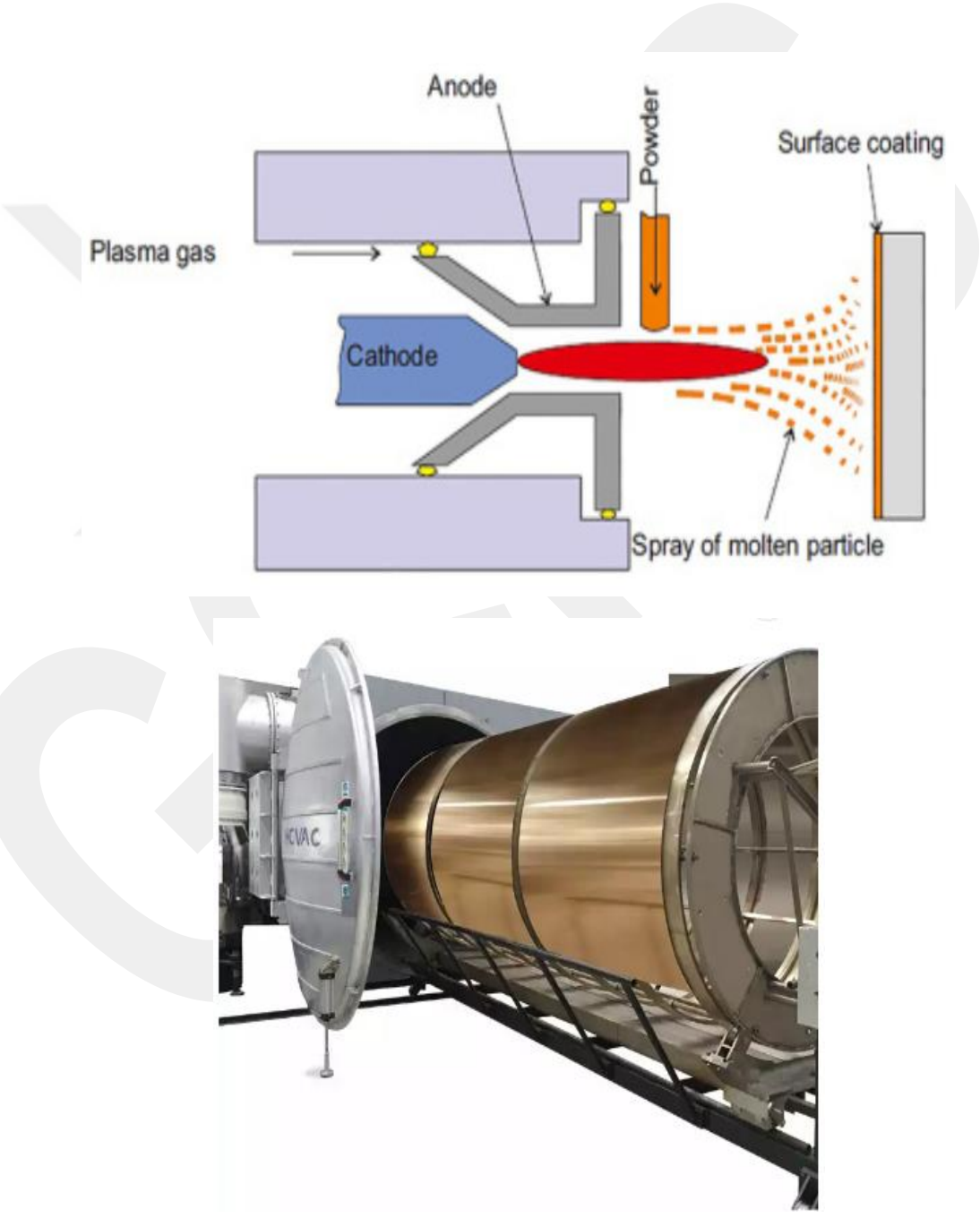

Figure 39: Plasma Spray Based – PVD (PS -PVD) [95] [96].

1.2.2.2 Chemical Vapor Deposition (CVD)

Chemical vapor deposition (CVD) is a deposition process in which endures decomposition and/or chemical reactions to mold stable solid products in which vapor forerunners must be activated (e.g., heat, plasma, light). Homogenous reaction which occurs in gas phase will cause formation of fine particles. On the contrary, on heated substrate or the reaction near to heated substrate would build a dense film. In substance, there are two methods; gas phase reaction and solid phase reaction. Succession of heterogenous and homogenous reactions would lead production of a porous film [97].

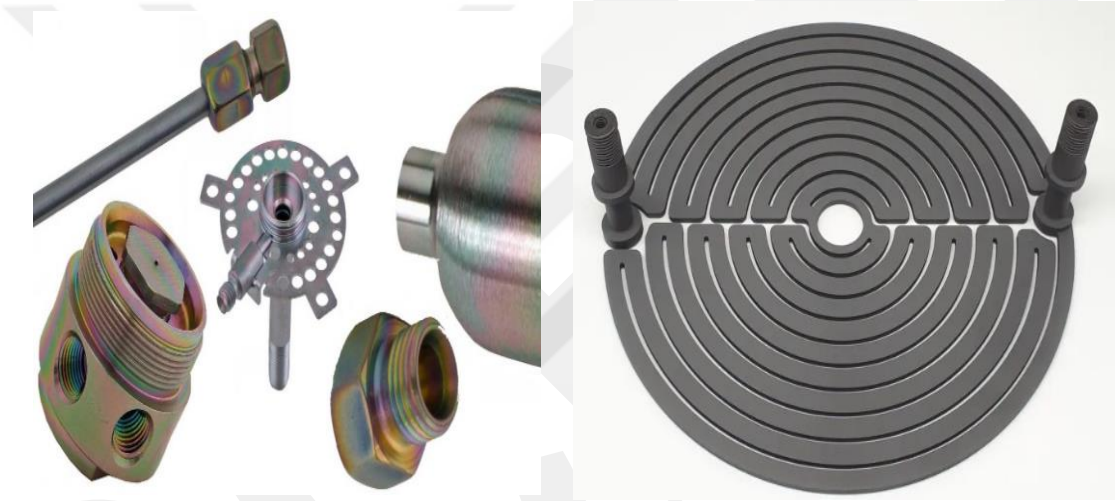

Figure 40: Chemical Vapour Deposition (CVD) [98] [99].

1.2.2.3 Thermal Spraying

Thermally spraying is one of the most commercial surface engineering application technologies which require resistance layer. Thermal spray coatings can be used to prevent corrosion, abrasion, erosion, scraping, prevent oxidation and hot corrosion, heat insulation, electrical conduction or insulation. It can also be used for renovation and repair, near-final production, renewable coating and decorative purposes.

Thermally sprayed coatings can be collected using several methods that provide various types of materials to be deposited. These materials are metals and their alloys and ceramics (mainly oxides and carbides). Other regularly sprayed products are composites of metal and ceramic alloys. It is also possible to spray polymers as another group of materials, and they are defined as polymethylmethacrylates (PMMA) and fluoropolymers residues of thermoplastic polymers, which are described in the literature.

Coatings can be practiced to protect underlying substrates of any material. Generally, alloys and metals are used as substrates. In addition, polymer or ceramic substrates can likewise be coated with this method [100].

In this technique, the coating material (powder/wire) is heated with the aid of an energy source and converted into a molten/semi-melt form and then the heated particles are accelerated by a gas or atomization jet. The heated and accelerated particles are impinged on the pre-prepared substrate and they are bonded to each other by taking the form of splat (flat particle).

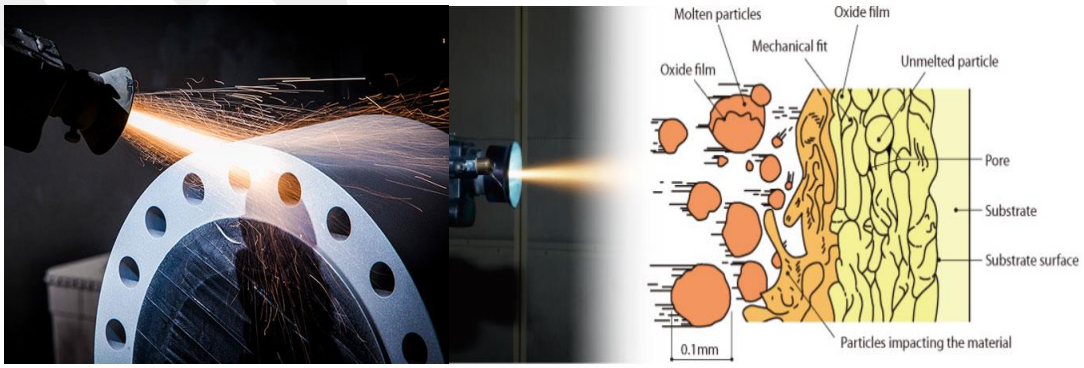

Figure 41: Thermal Spraying [101] [102].

1.2.2.4 Surface Treatments

Material surfaces can be improved with some processes and a different form can be achieved on the surface in terms of functionality. Examples of these improvements are nitriding and carburizing (cementation) processes.

Surface treatment processes are produced in accordance with the features of the designed material. These properties may be to improve the biocompatibility [103] or expand the lifetime of designed materials. The properties expected from the surface are generally high hardness and high corrosion resistance [104].

Figure 42: Surface Treatments, Gas nitriding, Carburizing [105] [106] [107].

1.3 STUDIES ABOUT THE SILICON NITRIDE FGM

The functionally grading of Si_3N_4 ceramics have been reported in a few research studies summarized and this topic creates a growing research area for multiple industries. These studies involve diverse probes, scanning and analysing techniques and explores manifold composite characteristics.

In the study reported by Ambigai et. al, reinforced aluminium alloy (ADC-14) was produced by spatial dispersion of Si_3N_4 particles by centrifugal casting, reinforced aluminium alloy (ADC-14) was produced by spatial dispersion of Si_3N_4 particles by centrifugal casting. While the rotation speed of the mould was optimized with the L4 orthogonal arrangement, two levels; 800 RPM and 1200 RPM were selected. L4 orthogonal array was also used to optimize mould speed i.e. volume fraction of Si_3N_4 and amount of reinforcement. The two levels were 12 wt. % and 8 wt. % and the reinforcement size was 100 μm and 50 μm, respectively. Fabricated FGMMC's (Functionally graded metal matrix composites) are characterized by use of optic microscopic images. The study concludes that improvement in hardness of 7 wt. % in comparison to material's core of casting to midpoint, 19 wt. % to core to shell. Climax hardness is reached by 50 μm of reinforcement by the ratio of 12 wt. %. The regression equation and 'ANOVA' analysis was performed to estimate the parameter most affecting stiffness. Si_3N_4 reinforced FGM is also examined via characterization apparatuses, SEM and EDS [108].

Moreover, in further research made to synthesize functionally graded $Cu_{10}Sn_5Ni/10Si_3N_4$ composite and copper alloy using horizontal centrifugal casting technique and to contrast its mechanical and adhesive wear properties. Engineered castings have dimensions of Ø out 100xØ inch 70×100 mm. The microstructural analysis revealed that the inner region of the composite had a denser concentration of reinforcement particles. In this region, it revealed that both the unreinforced alloy and the composite resulted in better hardness and tensile properties compared to the outer regions. Taguchi's method on pin-on-disc tribometer was used to calculate dry sliding wear performance under various conditions. Analysis of variance signal to noise ratio showed that applied load had the most influence on wear rate and coefficient of friction followed by sliding velocity and sliding distance. Worn surface

morphologies of composite specimens revealed a transition from mild to severe wear at high loads. The composites are applicable for tribological sliding [109].

In the study reported by Radhika, that is worth to note focuses on wear resistance issues of functionally graded composite and homogeneous LM25 aluminium (Al) composites were produced by liquid metallurgy and centrifugal casting respectively by incorporating Si_3N_4 (10% wt. 40 μm) particles. The performance of unreinforced alloy product composites was compared. Microstructural behaviours of homogeneous composite, unreinforced alloy and functionally graded composite (outer, middle, and inner) surfaces were investigated by means of an optical microscope. Mechanical properties of these surfaces were also considered. Wear rate was also measured by an abrasive wear test to determine its affects. As a result of studies microstructural investigations which was observed that the reinforcement particles were uniformly distributed in the homogeneous composite while a particle-rich region was discovered on the outer surface of the functionally graded composite material. Whereas homogeneous composite displayed higher tensile strength, the exterior region of the functionally graded material showed greater hardness. The abrasive wear rate escalated with the increase in load while which declined inversely with the increase in speed and decreased with the increase in speed and the particle-rich outer surface exhibited a lesser wear rate. Moreover, fewer scratches were discovered by scan of electron microscopy. Owing to these characteristics, study suggests that functionally graded composites can be evaluated for use in parts such as cylinder liners in automotive tribo-components, as they exhibit high wear resistance [110].

Si_3N_4 ceramic radomes, which include material preparation and optimal design of the radome wall structure are the subject of another study. A low dielectric constant core layer is covered by a multilayer radome wall structure with high dielectric constant skins and is used for broadband application. As a competitor material for both the exterior and core layer, controlled dielectric constant in the range 3.0~7.5 Si_3N_4 ceramics were prepared by adding different content of sintering aids such as zirconium phosphate binder, alumina, silica, magnesia and deciding appropriate sintering methods. According to design requirements for the wall structure of Si_3N_4 multilayer ceramic radome based on microwave equivalent network method is carried out CAD (A computer aided design) was done. Power transmission efficiency

of multilayer ceramic radome is adjusted by enhancing thickness of core and skins layer. The study contains results such as while the dielectric constant of core layer in the range 3.5~4.0, and skins is in between the range 6.0~7.5 the power transmission efficiency is above 85 wt. % with frequency of 2~18 GHz. The thickness of skins is less than 0.03 λ and the thickness ratio of skins to core layer is less than 1:15 [111].

In the study reported by Lian-meng et. al, pore gradient structured Si_3N_4 ceramics were prepared using spark plasma sintering (SPS) technique. The process has been carried out an unpressurized nitrogen atmosphere and operation temperature is applied at 1100°C. Green body had prepared by ceramic with different controlled porosities with ZrP_2O_7 as a binder material. The obtained porosity of Si_3N_4 ceramics were 34-47 wt. %, moreover, porous structure was homogenously distributed. At 1400~1600°C with sintering aids MgO and Al_2O_3 fully dense Si_3N_4 ceramics sintering could be accomplished. The pore gradient structure was formed by laminating Si_3N_4 porous ceramics and using a powder mixture to obtain fully dense ceramics and then sintered at 1400-1600°C. The microstructure of the sintered samples was observed the change of phase compositions with a scanning electronic microscope (SEM) and X-ray diffraction were analysed by (XRD) respectively. This research results demonstrate that samples exhibited dense surface layer with well porous graded structure. Moreover, α phase is the major phase of Si_3N_4 ceramics [112].

In the study reported by Belmonte et. al, examined whether FGM's could enhance the performance of components under harsh operating conditions. The reduction of residual stresses across the gradient and adapting this to the manufacturing process of mass production contains of some limitations. As a solution to these study presents a one-step approach for processing continuous FGM-Si_3N_4 materials from a pure homogeneous powder composition, using spark plasma sintering as a density improvement method. α and β phase samples as well as samples with a continuous variation in grain size were achieved by controlling the temperature profile inside the compact. In these samples, hardness, toughness and continuity in gradation of mechanical properties were measured. This approach offers unprecedented opportunities to design custom-made Si_3N_4 components because it relies on exploiting the capabilities of field-assisted sintering methods [113].

1.4 AIM OF THIS STUDY

Pore ratio and pore size are critical for a biomaterial in terms of effect on mechanical properties, effect on cell proliferation, antibacterial effect. Porous network (interconnection) is necessary to distribute oxygen as well as nutrients and to eliminate waste material. Therefore, over 50 wt. % of porosity is ideally preferred for bone replacement cases. However, load bearing is important for applications such as spinal spacer, which is the only Si_3N_4 application on the biomedical market, and better osteointegration and antibacterial resistance are still needed. Therefore, size and quantity controlled porosity is believed to increase the success of such biomaterials.

Hulbert et al. reported the minimum pore size required to generate mineralized bone as 100 μm [124]. It was also demonstrated in another study that only pores sizes above 300 μm result in vascularized tissue formation [125]. In contrast, if the pores are too large, the decrease in surface area limits cell adhesion and increasing porosity affects the load-bearing capacity [125].

Therefore, porosity and pore size have to be within a specific range to maintain the balance between the optimal pore size biological and mechanical stability. Based on this idea The ultimate aim of the thesis is to develop a new, reliable, cost-effective and reproducible technique for the preparation of novel Si_3N_4-based functionally graded biomaterials with a unique structure with graded porosity, appropriate mechanical properties and improved bioactivity sufficient for bone tissue ingrowth.

The functionally graded Si_3N_4 bio ceramics by means of different porosity levels is produced using powder metallurgy, followed up by the sintering. The final materials consist of three distinct layers; a more bioactive part with high amount of porosity, a transition zone (interlayer) between highly porous and dense parts, and a highly dense part. The bioactive porous part is designed to ensure good integration with human body fluid, while the dense bulk part ensures appropriate mechanical properties. The role of the interlayer-decreases the potential residual stresses in the

material due to a “sharp” change in chemical composition between the porous and dense parts.

The reason of the production of FGMs is the elimination of the macroscopic boundary in materials in which the material’s mechanical, physical and chemical properties change continuously and have no discontinuities within the material. Thus, these materials exhibit superior mechanical properties when compared to basic (monolithic) and composite materials. This technique provide biomaterials with a unique structure, appropriate mechanical properties and improved bioactivity sufficient for bone tissue ingrowth. Dense inner side will improve mechanical and structural properties.

Y_2O_3 was selected as the sintering additive in this thesis, as it is one of the commonly used oxides to obtain superior mechanical properties and is also the additive currently used in the commercial Si_3N_4 bioceramic material that has taken its place in the market.

CHAPTER II
EXPERIMENTAL PROCEDURE

2.1 POWDER PREPARATION

A ceramic product with the desired microstructure and properties can be obtained by proper shaping and sintering the high purity powders having optimum particle size and particle size distribution. For this reason, high purity (>95 wt. %) Si_3N_4 powders UBE E10 which available from Industries of Tokyo, Japan is selected as the Si_3N_4 starting material. The particle sizes are cumulatively distributed in the 0.2-10 μm range.

Y_2O_3 (99 wt. % purity) powders used as sintering additives were obtained from Sigma-Aldrich. The reason for using Y_2O_3 powder as a sintering additive is that it provides high bulk density, has a high α to β-Si_3N_4 transition percentage and is known as an advantageous sintering additive against both gram positive and gram negative bacteria.[16].

The purpose of using sintering addition is to form eutectic liquid phase at low temperature with SiO_2 layer around Si_3N_4 grains and to reduce sintering time and temperature. Liquid phase sintering is discussed in more detail under the heading of sintering.

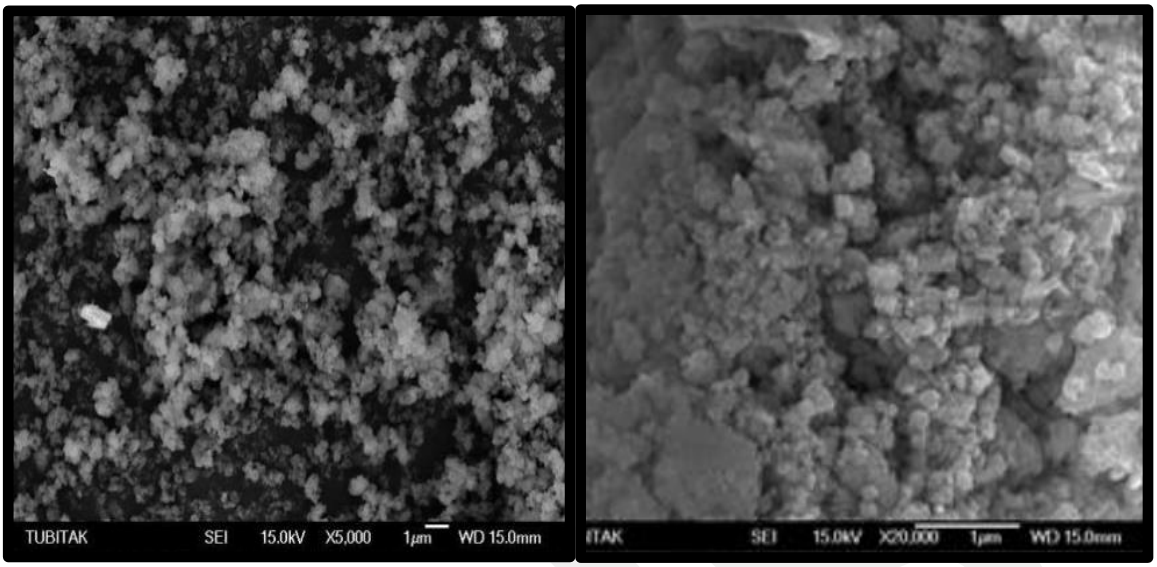

Figure 43: SEM images of Si_3N_4 powders.

- 1st powder group was prepared by mixing 5 gr (10 wt.%) Y_2O_3 and 45 gr (90 wt.%) Si_3N_4 to obtain a total of 50 gr powder mixture.

- 2nd powder group was prepared by mixing 10 gr (20 wt.%) Y_2O_3 and 40 gr (80 wt.%) Si_3N_4 to obtain a total of 50 gr powder mixture.

2.1.1 Raw Materials

The Table 4 shows the purity of the raw materials, their grain size and origin. Carbamide and semolina are used as pore forming agent materials, in order to form large sized porous structure. For that purpose, agent capsules with grain sizes between 0.125 mm and 0.355 mm were selected by screening method.

Table 4: Properties of Raw Materials

Name	Chemical Formula	Brand	Purity	Contents - impurities	Size	Origin
Silicon Nitride	Si_3N_4	Ube E10	High purity	α- phase >95 wt.%	0.25-5 µm	Japan
Itriyum (III) Oxide	Y_2O_3	Sigma Aldrich	High purity	>99.99 wt. % trace metals basis	<100 nm	Germany
Semolina	73 wt. % Carbohydrate	Market Product	High purity	>99 wt. %	125-140 µm	Turkey
Carbamide (Urea)	NH_2CONH_2	Sigma Aldrich	High purity	>0.99 wt. %	325-127 µm	Switzerland

2.1.2 Ball Mill

Powder mixtures were milled in a planetary ball mill (Fritsch GMBH) featuring a Si_3N_4 jar and milling ball.

Si_3N_4 balls (1:1.5 ratio with Si_3N_4 powders) was placed in a jar which inner side is Si_3N_4 because of the reduction of the contamination.

Propanol (1:2 ratio with Si_3N_4 powders) was added to the jar to increase the homogeneity of the both powder mixtures cause of which can be easily removed from the mixture during the evaporation step.

The spinning operation was performed at 300 RPM for a total of 90 minutes. Rotation was stopped every 30 minutes and then reverse rotation was performed.

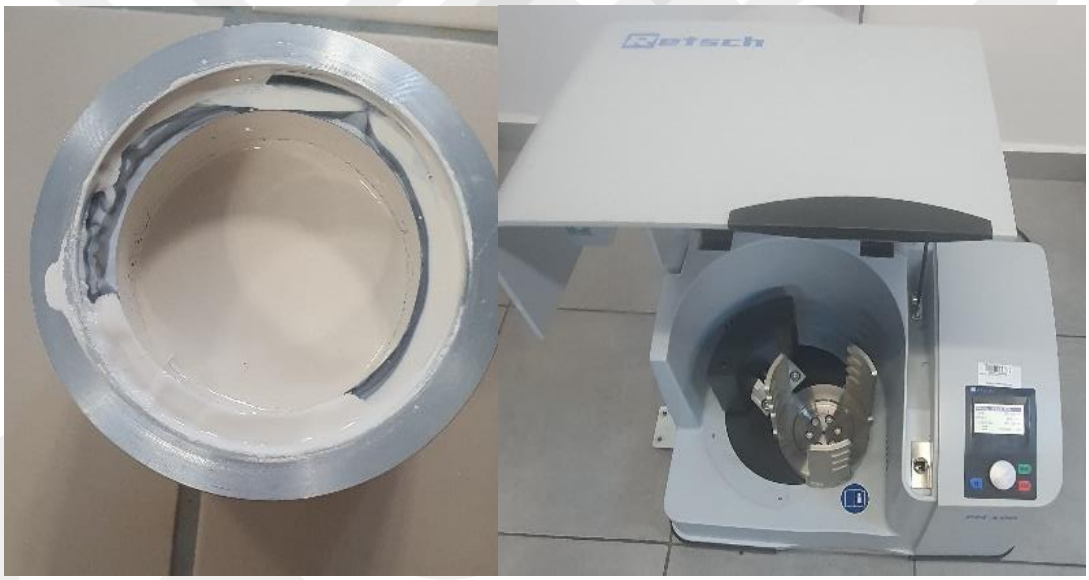

Figure 44: Planetary ball milling device and the Si_3N_4 jar with slurry inside.

2.1.3 Evaparator

Slurry was dried using a rotary evaporator to obtain homogeneity during drying process. The slurry in the jar was taken into the glass evaporating flask to be dried via rotary evaporator equipment. Slurry was rotated at 30 RPM and 55°C for 45 minutes. Total drying process took 45 minutes under these conditions. The resulting powders was stored in desiccator prior to screening for homogeneity.

Figure 45: Rotary evaporator equipment.

2.1.4 Screening

The dried powders with grain size below 355 µm were screened separately in both powder groups and barcoded in plastic containers to be used in subsequent operations and stored in a desiccator.

Figure 46: Screening.

2.1.5 Turbula Mixing

Pore forming agents with different ratios (10 wt. % and 20 wt. %) were added to the screened Si_3N_4 powder mixtures at this stage. In order to improve homogeneity, each mixture is mixed separately for 30 minutes in turbula mixer (Figure 48). The mixtures are stored in plastic containers (Figure 49). One of the main reason for adding carbamide to the mixture at this stage is that the urea (carbamide, CH_4N_2O) dissolves in alcohol, as explained by Lee et al. [113]. Another reason why pore-forming additives are not added during ball milling is to prevent the agents from breaking during the process.

Figure 47: Turbula Mixer.

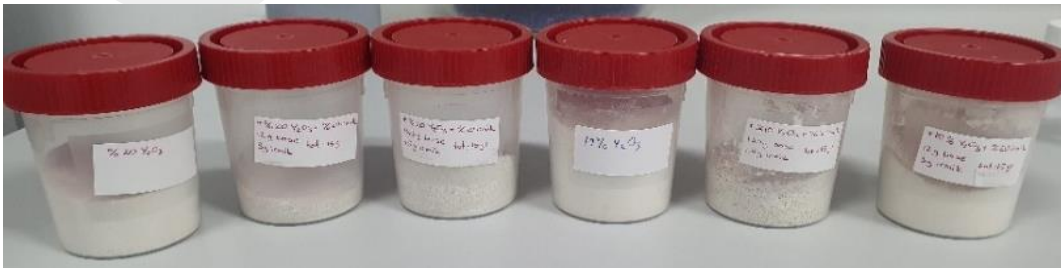

Figure 48: Si_3N_4 samples mixed with pore-forming materials and placed in plastic containers, prior to turbula mixing.

2.1.6 Green Body Preparation

Carbamide and semolina, the pore forming agents, were added as 10 wt. % and 20 wt. % ratio to two different Si_3N_4 mixtures containing 10 wt.% and 20 wt.% Y_2O_3 as sintering additives. The codes and details of the relevant powder mixtures are given in Table 5.

Table 5: Green body composition table

Sample Code	Si_3N_4 Ratio (wt. %)	Y_2O_3 Ratio (wt. %)	Pore Forming Agent Type	Pore Forming Agent Ratio (wt. %)
1Y	90	10	none	none
2Y	80	20	none	none
1Y1C	90	10	Carbamide	10
1Y2C	90	10	Carbamide	20
1YCF	90	10	Carbamide FGM	0 & 10 & 20
2YFCF	80	20	Carbamide FGM	0 & 10 & 20
1YSF	90	10	Semolina FGM	0 & 10 & 20
2YSF	80	20	Semolina FGM	0 & 10 & 20

2.2 FGM GREEN BODY PREPARATION

FGM structures were formed by stacking 3 different powders with a uniaxial press and then burning the pore-forming agents. The schematic representation of this layered structure is given in Figure 49 and the content of the powders is given in Table 6.

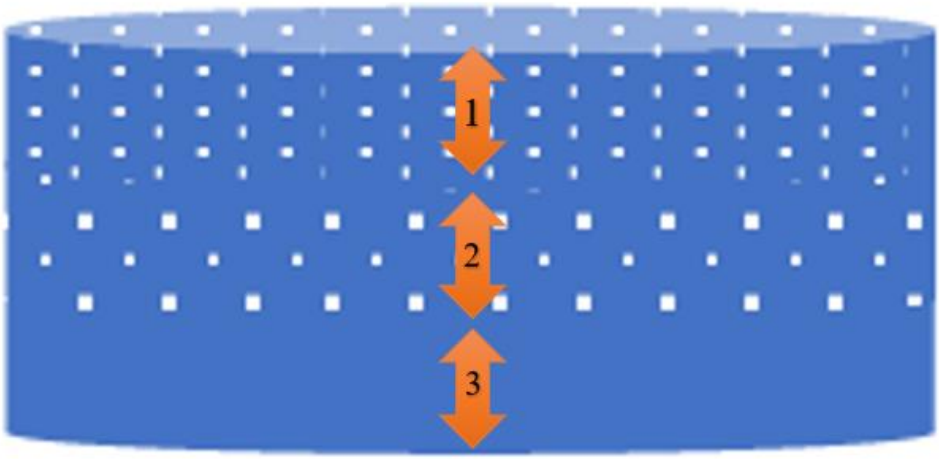

Figure 49: Schematic drawing of FGM - Si_3N_4

Table 6: Table of FGM content

Composition	Base material	Additive	Pore forming agent ratio
1	Si_3N_4	Y_2O_3	20 wt.%
2	Si_3N_4	Y_2O_3	10 wt.%
3	Si_3N_4	Y_2O_3	none

The thickness of the individual layers is typically between 0.2 mm and 1mm.

In the first layer of the designed material, pore formations larger than 100 µm were targeted in order to increase osseointegration. Moreover, the formation of nano roughness surfaces on the walls of these pores is believed to support antibacterial resistance.

The amount of pores in the second layer of the designed structure was determined as 10 wt. % with the aim of ensuring integrity between the first and third layers and creating an intermediate layer with a smooth transition.

In the third layer of the designed structure, it was aimed to improve the mechanical properties. Therefore, for this reason, a denser structure was obtained by not using a pore forming agent in that part.

Powder mixtures used in FGM production were also prepared separately in order to facilitate characterization studies, and they were sintered together with FGM samples.

2.2.1 Pressing

Powder mixtures were compacted into pellets by uniaxial pressing. Mixtures were filled into a steel die and uniaxially pressed at 40 MPa at RT to form cylindrical pellets. While pressing the FGM samples, after each powder mix addition, powder was fixed with the punch, and then the other powder mixture was added.

Figure 50: a.) Uniaxial Press [114] b.) Si_3N_4 pressed samples

2.2.2 Cold Isostatic Pressing

Some samples were subjected to cold isostatic pressing to investigate the effect of increased green density on the final structure and the properties.

The samples were packed in a vacuumed protective latex to prevent the contact with the working fluid.

The fluid used in isostatic pressing was a liquid containing boron oil and water. Samples are compacted at 300 MPa approximately 5 minutes in this liquid and after this process, samples were carefully removed from the protective latex.

Figure 51: Cold Isostatic Press (CIP).

2.2.3 Pore Forming Agent Burn Out

The samples were burned in the muffle furnace for 12 hours at 650^{o}C to remove the pore-forming agent material from the pellets.

Figure 52: Muffle Furnace [116].

2.3 SINTERING

2.3.1 Gas Pressure Sintering (GPS)

The sintering operation is carried out in two separate procedures:

1. 5 bar pressure was applied at 1750^{o}C for 1 hour. Then the temperature was increased to 1830^{o}C and kept at 95 bar pressure for 1.5 hours. Finer grain size was expected in the resulting material. Contents of GPSed-Si_3N_4 samples are showed in Table 7 in order to understand coding later in the thesis.

2. The temperature was kept constant at 1920^{o}C and the pressure was increased from 5 bar to 20 bar by increasing for 30 minutes. Coarser grain size was expected to be observed as the temperature increases in the resulting material (Samples; 1Y, 2Y, 1Y1C, 1Y2C, 1YCF, 2YFCF, 1YSF and 2YSF).

Table 7: Si_3N_4 samples and their codes sintered via GPS.

Sample Code	**Si_3N_4 Ratio (wt. %)**	**Y_2O_3 Ratio (wt. %)**	**Pore Forming Agent Type**	**Pore Forming Agent Ratio (wt. %)**
1Y1C /83	90	10	Carbamide	10
1Y2C /83	90	10	Carbamide	20
1YCF /83	90	10	Carbamide FGM	0 & 10 & 20

Figure 53: Gas Pressure Sintering (GPS) Furnace [117].

2.3.2 Spark Plasma Sintering (SPS)

The condensation profile of the samples was examined using a SPS furnace. This furnace was used as a dilatometer in this operation. It was observed in which regions the liquid phase started to form first. As the liquid phase is formed, the grains begin to slide over each other and approach together. Therefore, the appropriate temperature for GPS is determined depending on the data achieved by this furnace.

Figure 54: Spark Plasma Sintering (SPS) Furnace [117].

2.3.3 Density and open porosity measurements

The open porosity, is the volume of the open pores into which a liquid can penetrate as a percentage of the total volume.

Density determinations are carried out by means of Archimedes Principle (The Buoyancy Method), which states that an object immersed in a liquid loses an amount equal to the weight of the liquid it apparently replaces.

During the measurements, the samples are immersed in the liquid with a metal hanger and the measurement is made with a balance with an accuracy of ±0.01 gr. Distilled water (density 1 g/cm^3) was used for the measurements.

During this operation, the suspended, wet and dry weights of the samples were measured.

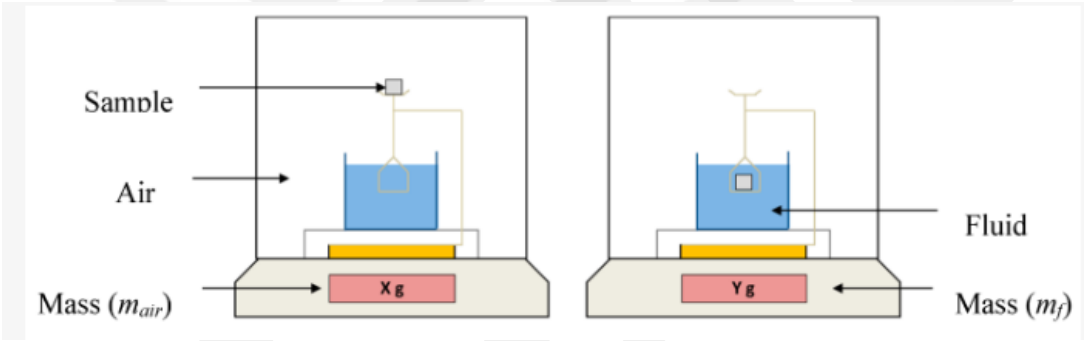

Figure 55: Archimedes principle [118].

2.4 PHASE CHARACTERİSATION BY X-RAY DIFFRACTION (XRD)

The X-Ray Diffraction method (XRD) is based on the principle that each crystal phase refracts X-rays in a characteristic pattern depending on their unique atomic arrangement.

The samples were analysed at Yıldırım Beyazıd University which using the Rigaku Miniflex XRD system shown in figure 56, 3.5. XRD scans were taken over 2θ in a range of 10 to 70° with a 2°/minute scan speed using Cu-Kα radiations (λ=1.54 Å).

Figure 56: XRD device [119].

2.5 SCANNING ELECTRON MICROSCOPY (SEM)

Scanning electron microscope (SEM) was used to obtain three-dimensional images as a result of focusing electrons accelerated by high voltage on the sample placed on the aluminium stab and scanning the sample surface.

The microscopic features of the samples were observed with SEM, HITACHI SU5000 FE-SEM device in the Central Laboratory of Middle East Technical University (METU). Images were obtained by detecting the surface with the secondary electrons. In addition, energy dispersive X-ray spectrometer (EDX) is used to detect the characteristic X-rays of some of the samples in order to make elemental anlysis. For instance, after the bioactivity test, the formation of Hydroxyapatite (HAp) was evaluated by the Ca/P atomic ratio in the structures formed on the surface.

Figure 57: Scanning Electron Microscopy (SEM) [120].

During the SEM analysis, fracture surfaces of the samples were examined.

2.6 BIOACTIVITY TEST - SIMULATED BODY FLUID (SPS) PREPARATİON

A body fluid-like structure was artificially prepared to observe the biocompatibility of the samples in vitro. In this context, a total of 1000 ml mixture was prepared by adapting the recipe given in Table 9, specified by Kokubo et al. In order to mimic the body fluid, the pH of the liquid obtained as a result of the mixture should be less than or equal to 7.45.

Likewise, the mixture should be in the range of 36.5-37^{o}C in order to mimic the body environment .

Table 8: The mixture of Simulated Body Fluid (SBF)

Compounds in the mixture	**Quantities of the compounds in the mixture**
NaCl	8.035 gr.
$NaHCO_3$	0.355 gr.
KCl	0.225 gr.
K_2HPO_4. $3H_2O$	0.231 gr.
$MgCl_2.6H_2O$	0.312 gr.
1.0 M= HCl	39 ml.
$CaCl_2$	0.292 gr
Na_2SO_4	0.072 gr.
Tris	6.118 gr.

Figure 58: pH meter

Samples from each group were placed in appropriate plastic containers together with the prepared SBF. Lids are paraffinized to ensure impermeability.

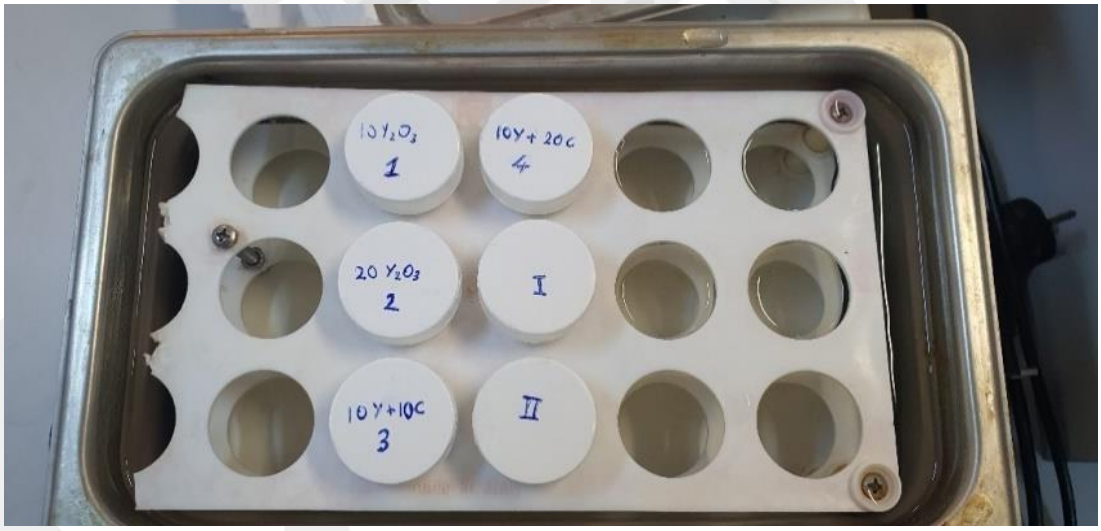

Figure 59 : Samples waiting in water at 37 ^{o}C.

Samples were cleaned individually (15 minutes each) with acetone, ethanol and deionized water before being tested for bioactivity in simulated body fluid (SBF) and soaked in SBF for 28 days at a constant temperature of 36.5 ±0.5°C. The SBF solution was refreshed every other day to stabilize the ion concentration. The samples were washed in distilled water to remove any residual salts on the surface and dried at room temperature at the end of 28 days. The bioactivities of the surfaces

were evaluated via Scanning Electron Microscope (SEM) by examining the HAp (hydroxyapatite) formation as described in the previous section.

Figure 60: Ultrasonic cleaner, used for keeping the water hence the samples, at a constant temperature

2.7 ANTIBACTERIAL TEST

Sintered samples were cleaned of dust and dirt with methyl alcohol and deionized water before being tested for bacteria. In order to avoid any wetness in the pores, it was exposed to evaporation in a vacuum oven for 30 minutes.

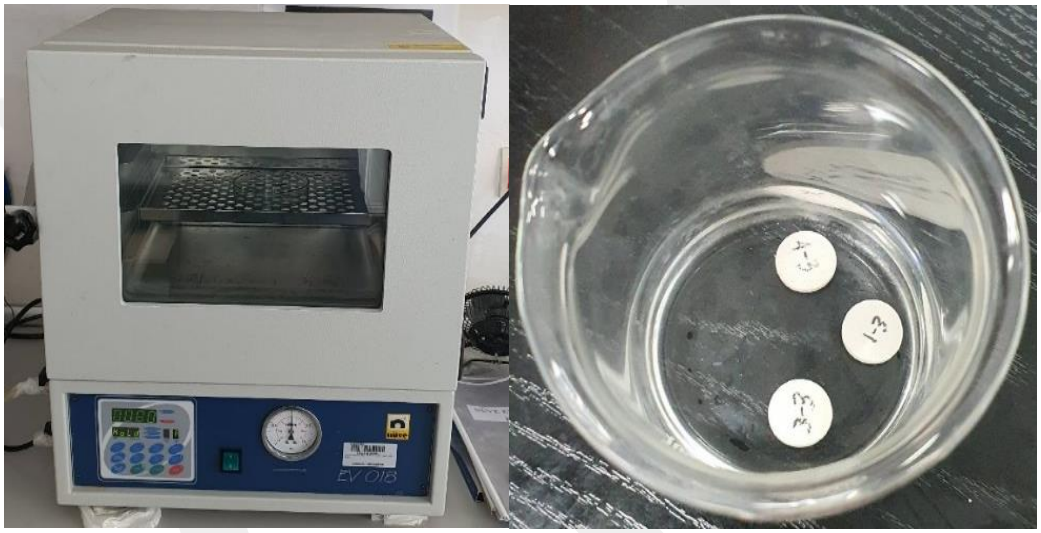

Figure 61: a.) Vacuum Etuv b.) Samples 1Y/92, 1Y1C/92 and 1Y2C/92

Samples 1Y/92, 1Y1C/92 and 1Y2C/92 were subjected to bacteria tests. Agar well diffusion method is used to evaluate and compare the antibacterial resistance of the samples. The complications caused by bacteria were examined in studies on patients who were subject to bioactive implant applications, *Staphylococcus aureus* (*S. aureus*) gram-positive bacteria is preferentially used in this test [121].

S. Aureus bacteria samples were obtained from Ankara University to be used in bacterial tests. These bacteria were spread into petri dishes impregnated with food for a week in METU microbiology laboratories. The samples were marked and taken into petri dishes and kept at 37°C for a week.

In another petri dish, antibiotic-dropped pellets were placed for the control study. These pellets, the results of which are discussed in the experimental section, have developed resistance against different types of bacteria.

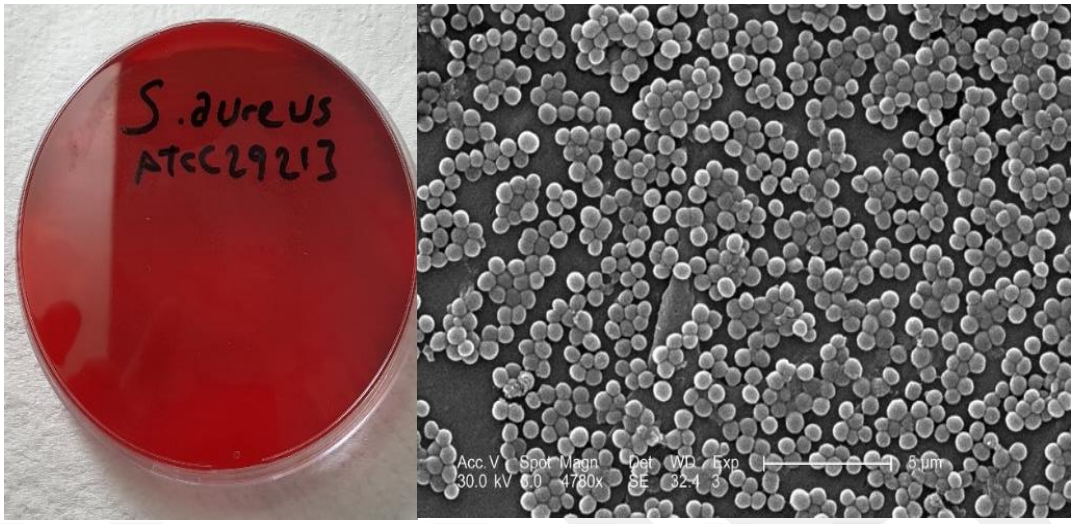

Figure 62: Staphylococcus aureus bacteria [122].

CHAPTER III
RESULTS AND DISCUSSIONS

Si_3N_4 samples, 1Y /92, 1Y1C /92, 1Y2C /92 and 1YCF /92 were sintered under nitrogen gas atmosphere via gas pressure sintering furnace in two steps. In the first step; samples were sintered at 1750^oC, 5 bar pressure for 1 hour and in the second condition; further densification was achieved at 1830^oC, under 95 bar for 90 minutes sintering conditions. There were observed that sufficient post-sintering density could not be achieved in the samples. (Even in the carbamide-free sample).

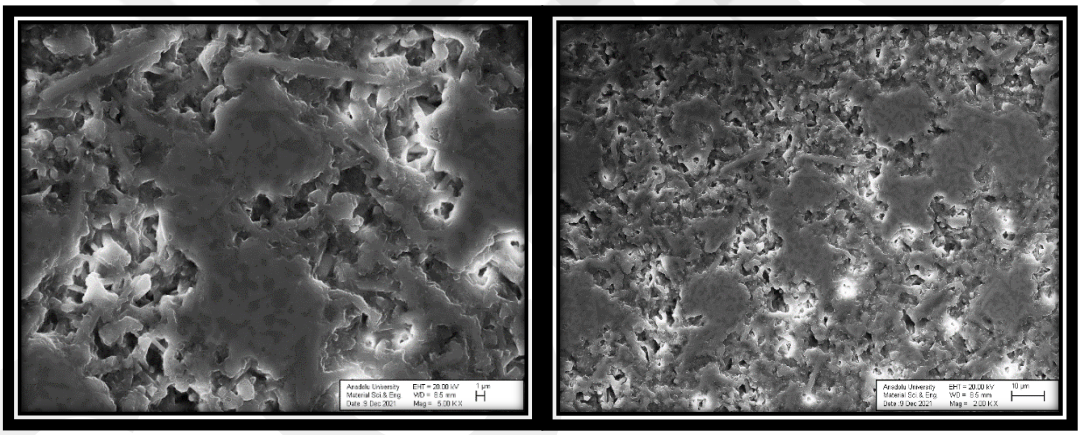

Figure 63: SEM images of Sintered Si_3N_4 sample - 1Y /92.

According to the density results of samples 1Y1C /92, 1Y2C /92 and 1YCF /92, given in Table 10, it is obvious that sufficient sintering could not be achieved under these sintering conditions. Figure 63, corresponds to back scattered electron images (BEI) of sample 1Y /92 after polishing the fractured surface. Although there is no pore forming agent in the structure which is observed that, there are still pores in the material which is in good correlation with the density results.

It is a known fact that the biggest disadvantage of Si_3N_4 compared to SiAlON ceramics is the difficulty in full densification. The reason of poor densification and some alternative methods applied in the thesis study to overcome this problem are given below:

1. **Possible reason:** Insufficient amount of sintering additive. **Alternative solution:** 10 wt.% Y_2O_3 increased to 20 wt.%. Even though minimum grain boundary phase amount is desired by means of mechanical properties, this change in composition was applied in order to observe its effect on densification.
2. **Possible reason:** Insufficient green density value by uniaxial pressing. **Alternative solution:** Cold isostatic pressing (CIP) carried out after shaping by uniaxial press.
3. **Possible reason:** The effect of carbamide pore-forming agent. **Alternative solution:** Instead of carbamide, semolina was also used as a pore-forming agent.
4. **Possible reason:** Failure to provide a suitable sintering regime. **Alternative solution:** A new sintering regime was applied and this is SPS method was applied.

Considering these possible reasons, new compositions were prepared. (1Y /92, 2Y /92, 1Y1C /92, 1Y2C /92, 1YCF /92, 2YFCF /92, 1YSF /92, 2YSF /92).

Since the pore size to be obtained in the study is desired to be over 100 micrometers and to reach 300 microns if possible, the alternatives given in Table 9 were evaluated and considering this size requirement, it was seen that poppy seed and semolina could be used instead of carbamide.

Table 9: Diameter of some pore forming agents [123].

Sample	Density (g/cm^3)	Characteristic diameter (µm)	Type of characteristic diameter
Rice semolina	1.5	4.8 MIA 4.4 LD	Median
Corn starch	1.5	12.9 MIA 14.2 LD	Median
Potato semolina	1.5	46.3 MIA 49 LD	Median
Lycopadium	1.2	33.1 MIA 30.6 LD	Median
Poppy seed	1.1	265 MIA (max Feret) 1038 MIA (min Feret)	Arithmetic mean
Coffee	1.3	405 LD	Modus
Fine flour	1.5	32.7 LD	Modus
Semolina	1.5	25.5 LD 561 LD	Modus

However, due to the difficulty of obtaining a compact structure in the case of poppy seed use, semolina was preferred as a pore forming agent simultaneously with carbamide in the remainder of the study.

In order to evaluate the possibility that the densification problem observed in the samples after sintering was due to the insufficient green density being achieved by uniaxial pressing, the samples were subjected to CIP after pressing.

As another solution to the densification problem, the amount of sintering was increased and the Y_2O_3 addition was prepared as 20 wt.% apart from 10 wt.%.

Figure 64: Samples containing semolina dispersed after the burn out process.

It was evaluated that while there was no dispersion in the samples containing carbamide due to the expansion that occurred during burn out process, it was found in the samples containing semolina. Therefore, it was understood that these samples could not be continued (Due to the fact that compact samples could not be obtained.) and it was found appropriate to continue with the carbamide system.

In order to apply the appropriate new sintering regime, the sample with sample Y/92, free of pore forming agents and with the addition of 10 wt. % Y_2O_3, was sintered using the SPS furnace in dilatometer mode. Thus, the first liquid phase formation temperature and the temperatures at which densification is achieved were determined and the optimum sintering regime was determined. The relevant SPS graph is given in Figure 65.

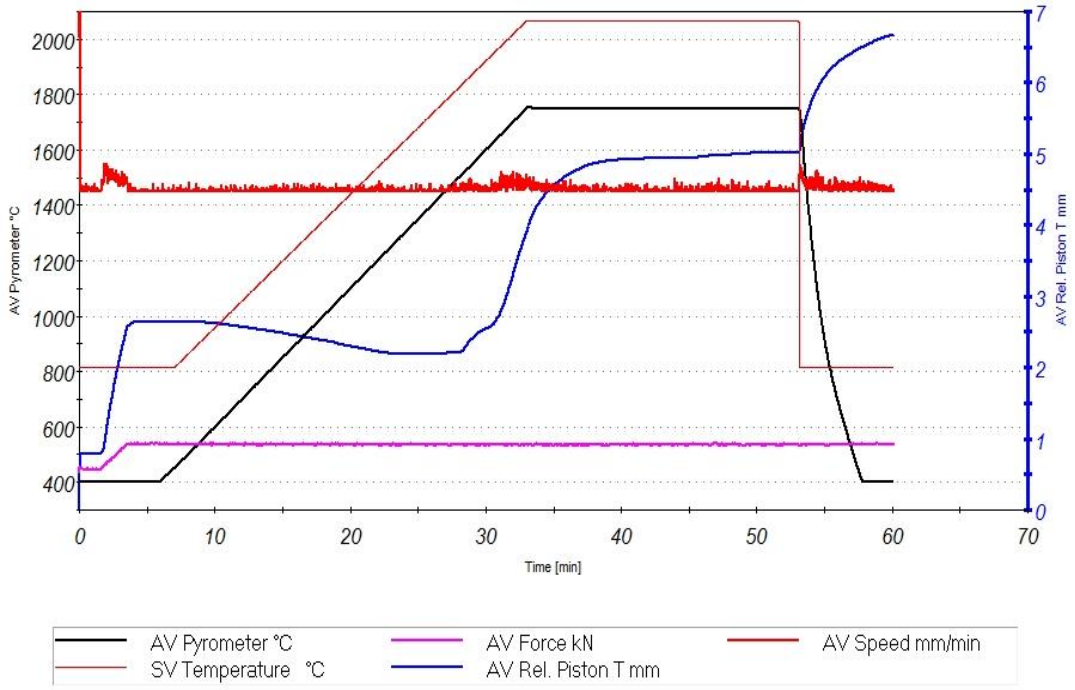

Figure 65: Temperatur vs Time graph taken from SPS during sintering of 1Y sample

According to this graph, the temperature at which the liquid Y_2O_3-SiO_2 phase is formed is approximately 900°C. The sintering regime was arranged under these conditions. Accordingly, the results of the samples obtained under these conditions are shared under the following sub-headings.

3.1 DENSITY AND OPEN POROSITY

Density and open porosity results of the samples 1Y, 1Y1C, 1Y2C and 1YCF, having 10 wt. % Y_2O_3 additive and pore formers, sintered at 1830°C and 1920°C (after CIP) were measured by Archimedes method and the results are given in Table 10.

According to these bulk density results, it was observed that full densification could not be obtained even in the samples without pore forming agents. Also, increasing the sintering temperature from 1830ºC to 1920ºC and applying additional CIP treatment provided only a minor improvement in densification behaviour. In the samples sintered at 1920ºC, increasing sintering additive (Y_2O_3) from 10 to 20 wt. %, increased bulk density from 2.34 to 2.77 g/cm^3.

On the other hand, when the amount of Y_2O_3 was kept constant at 10 wt. % and the amount of carbamide was increased to 10 and 20 wt. %, a decrease in bulk density and an increase in the percentage of open pores were observed, as expected.

Table 10: Bulk density and open porosity of the samples

Sample	**Suspended Weight (g) (W_3)**	**Wet Weight (g) (W_2)**	**Dry Weight (g) (W_1)**	**Bulk Density (g/cm^3) D=W1/W2-W3**	**Open Porosity wt% i: (w2-w1)/(w2-w3)**
1Y /92	0.31	0.52	0.49	2.34 +/- 0.02	14.26 +/- 0.59
2Y /92	0.34	0.52	0.50	2.77 +/- 0.01	8.55 +/- 1.61
1Y1C /92	0.26	0.48	0.43	1.97 +/- 0.15	22.64 +/- 4.61
1Y2C /92	0.25	0.47	0.40	1.80 +/- 0.02	29.98 +/- 2.16
1YCF /92	0.35	0.61	0.55	2.07 +/- 0	26.35 +/- 1.15
1Y /83	0.24	0.47	0.41	1.84 +/- 0.31	24.06 +/- 4.48
2Y /83	0.19	0.42	0.35	1.48 +/- 0.01	31.82 +/- 0.41
1YCF /83	0.22	0.46	0.40	1.68 +/- 0.10	26.82 +/- 7.62

3.2 XRD ANALYSIS

The samples for which XRD analysis was performed and their characteristics are given in Table 11. For ease of measurement and explanation of the results, characterization studies were applied to monolithic samples instead of FGM samples. These results are significant for understanding FGM systems. The phase analysis results of these samples, given in Figures 66 and 67, revealed similar patterns in different systems. These XRD patterns showed that the main crystalline phase was β-Si_3N_4 with traces of either $YSiO_2N$ or $Y_4Si_2O_7N_2$ depending on the sintering temperature. According to these results, the grain boundary phase formed is not amorphous but crystalline form. The patterns given in Figure 67, show that $YSiO_2N$ is the grain boundary phase in the system observed at both sintering temperatures, and the $Y_4Si_2O_7N_2$ phase is also formed when the sintering temperature is increased to 1920ºC. These patterns also reveal that peak intensities decrease when the amount of sintering additive is kept constant and the amount of carbamide is increased from 10% to 20%. Similar trend was observed at both temperatures.

Table 11: XRD samples

Sample	Additive	Pore forming Agent
1Y1C /83	10 wt.%	Carbamide 10 wt.%
1Y2C /83	20 wt.%	Carbamide 20 wt.%
1Y1C /92	10 wt.%	Carbamide 10 wt.%
1Y2C /92	20 wt.%	Carbamide 20 wt.%

.

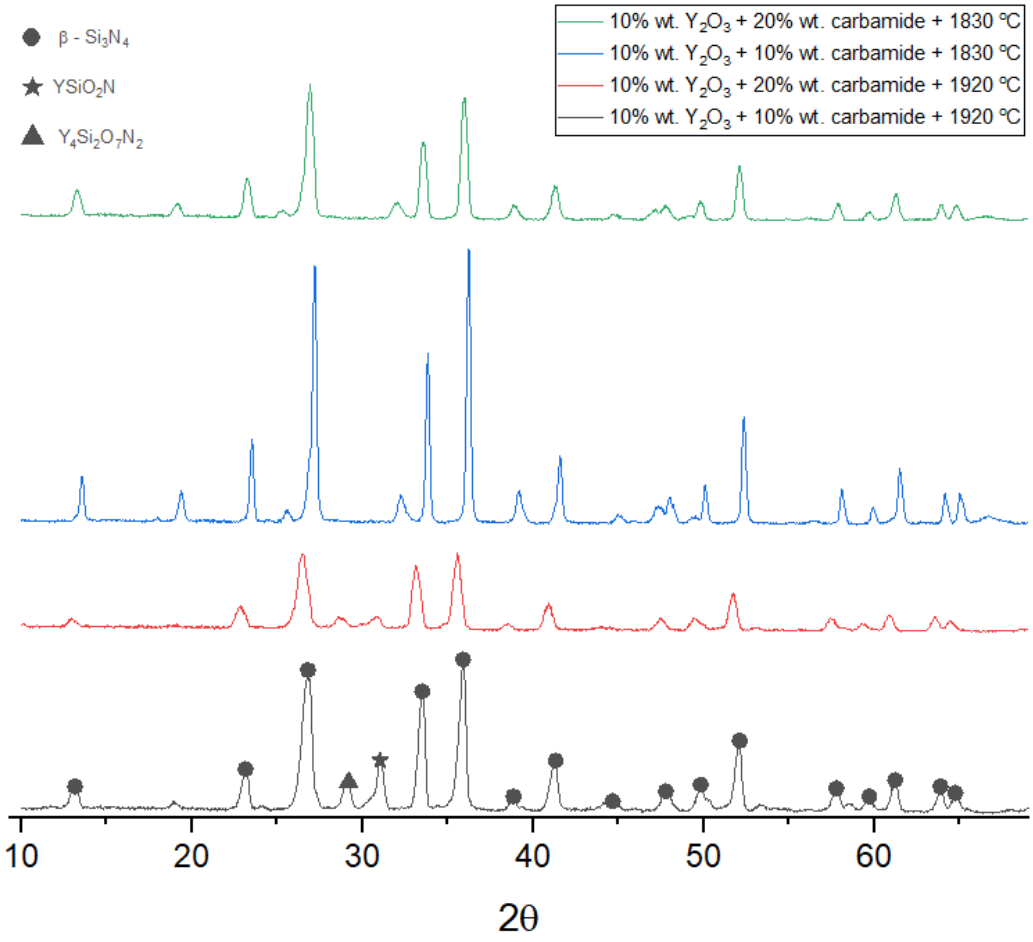

Figure 66: a.) 1Y1C/92 b.) 1Y2C/92 c.) 1Y1C/83 d.) 1Y2C/83

Effect of sintering additive amount on the phase characterization results was investigated by comparing 1Y and 2Y samples (without any pore forming agents) by keeping the sintering temperature constant at 1920ºC). Results of these two samples showed that 1Y sample having 10 wt. % Y_2O_3 and 2Y sample with 20 wt. % Y_2O_3 have similar patterns, only with a difference in grain boundary phase/Si_3N_4 phase ratio, according to the most severe peak intensities. This indicates an increase in the amount of grain boundary phase, as expected. This is also the result that supports the increase in the density value.

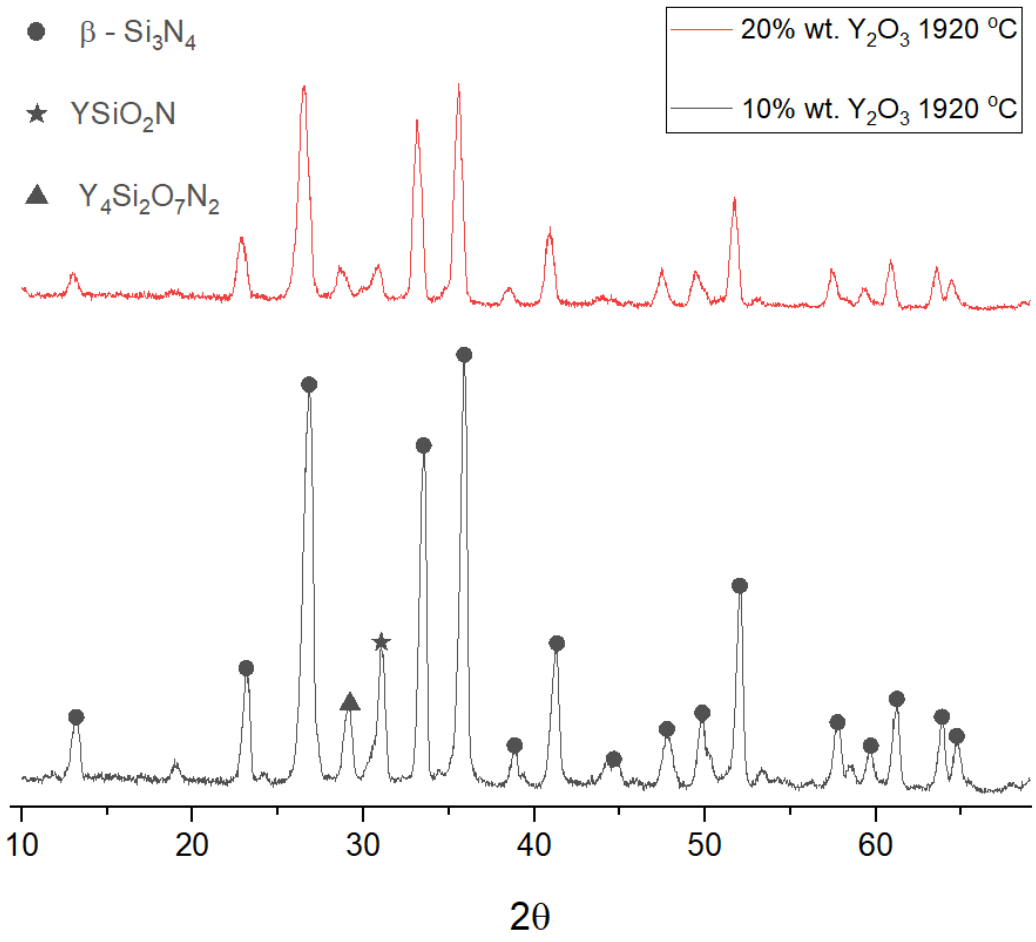

Figure 67: a.) 1Y /92 b.) 2Y /92

3.3 SEM ANALYSIS

In Figure 68, are the low magnification secondary electron images of Si_3N_4 FGM samples with 10 wt. % Y_2O_3 sintering additive. These samples having 1YCF/83 and 1YCF/92 codes corresponds to the FGMs sintered at 1830 and 1920°C, respectively. Images were taken from the fracture surfaces of the samples. The smooth transition between the layers is clearly visible in the images. These layers consist of structures containing 0%, 10% and 20% pore-forming substances (carbamide) from bottom to top.

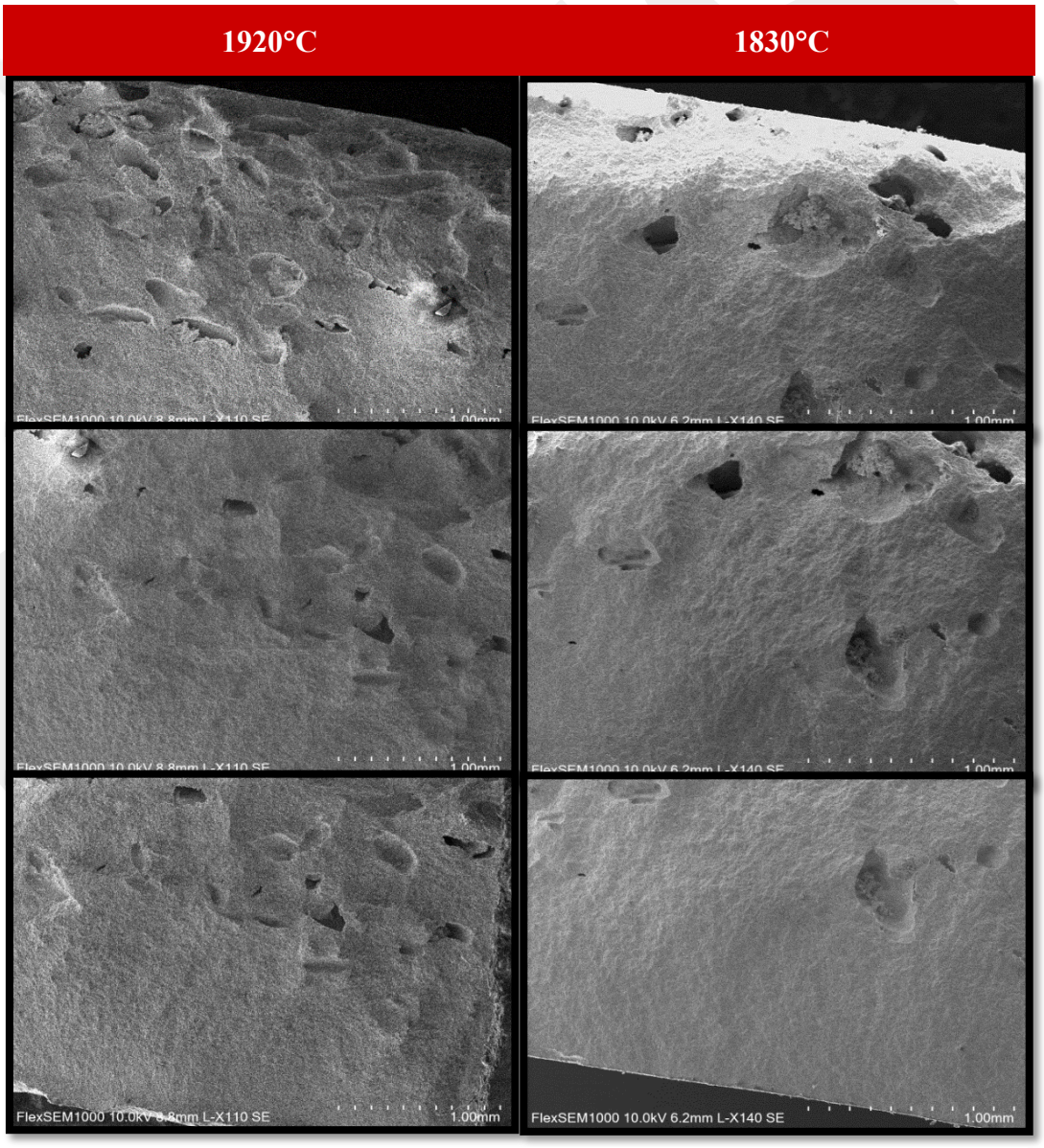

Figure 68: SEM images of FGM samples

Thus, when these images in Figure 68, are examined, it is clear that FGM samples with no pores on one side and 20% pores on the other, with a smooth transition in terms of pore ratio between these two surfaces, were produced. To conclude, it was observed that samples with an FGM structure in terms of pore ratio were successfully produced at both temperatures.

Backscattered SEM images of the same 1YCF /83 and 1YCF /92 samples at different magnifications are given in Figure 69. A representative pore image with a diameter of approximately 300 μm is seen at 500 x magnification. Since this pore size is compatible with the initial dimensions, it was evaluated that the expansion we observed in the semolina application was very limited in the carbamide containing samples.

In addition, these pores will be important as incubation centers for cell penetration in Si_3N_4 implant applications. The interior surfaces of the pores were also examined at higher magnifications. The presence of open and closed pore shapes in the network structure shows that it has a mixed pore structure. Microroughness is observed at the interior side of the pores because of the formation of rod-like Si_3N_4 grain formation. At 10kx magnification, it is observed that these rod-like grains are coarser in the samples sintered at 1920°C compared to the ones sintered at 1830°C as a result of grain coarsening at higher temperature. Since it is known that nanorough surfaces especially show antibacterial resistance [124], antibacterial test was carried out within the scope of the study.

1920°C	1830°C
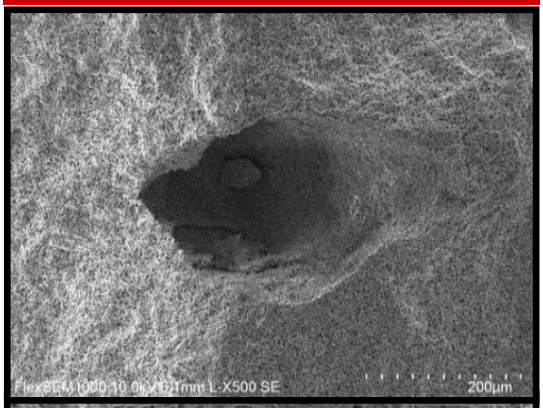	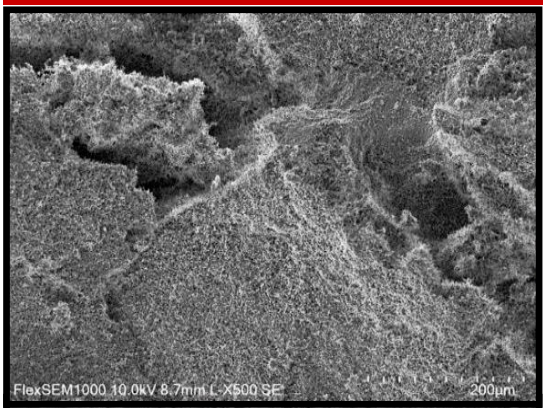
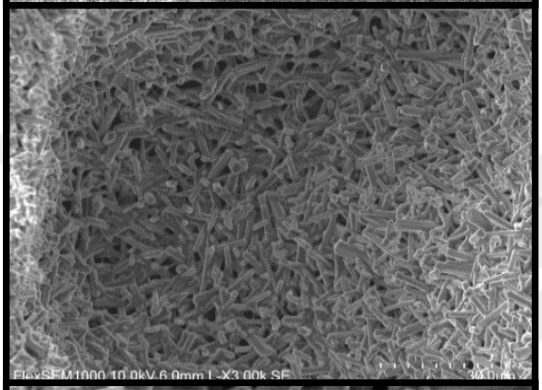	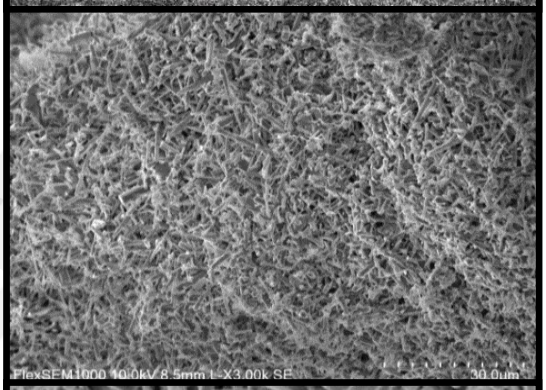
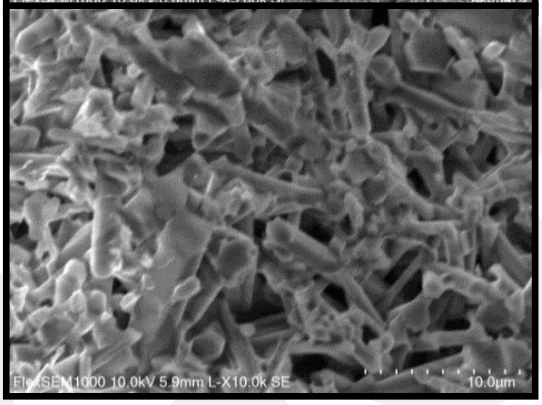	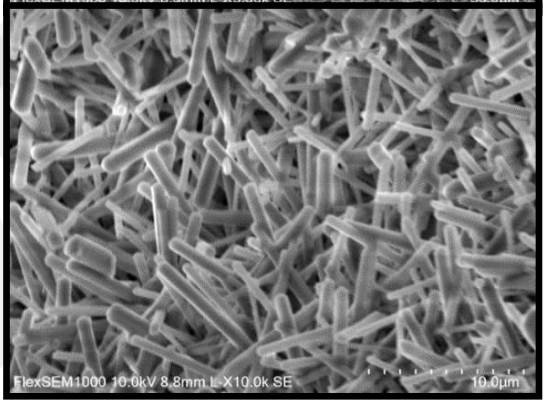

Since this current thesis was a part of a bilateral project, is it possible to compare the results with the other FGM production techniques carried out in this project. The unsuccessful transitions in the FGM samples obtained by stacking the tape casted layers, which are similar to the composition used in this thesis, are given in Figure 70.

While a smooth transition cannot be achieved with the gradual stacking of cast strips, it has been observed that this transition is achieved with gradual powder pressing within the scope of this thesis.

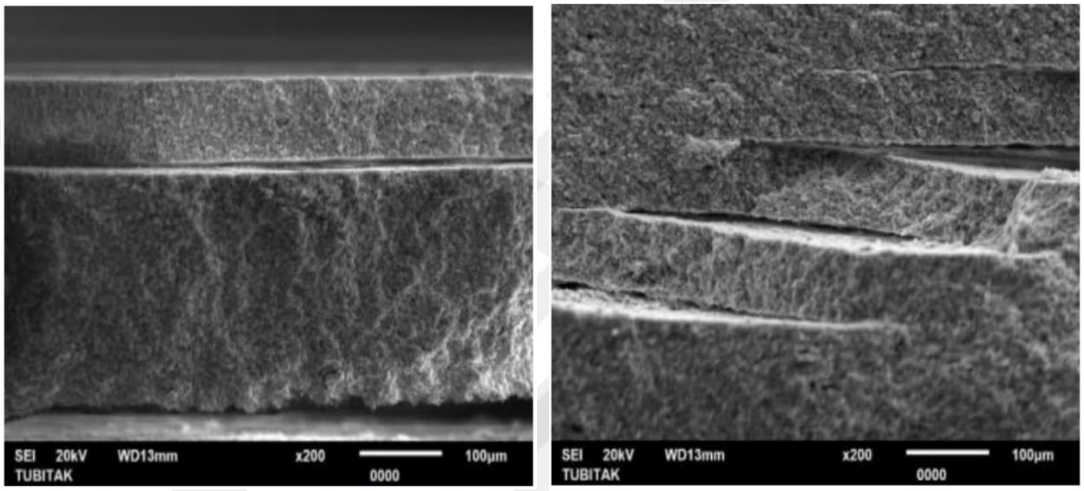

Figure 70: SEM Images of FGM samples produced by stacking the tape casted layers [126]

3.4 ANTIBACTERIAL TEST RESULTS

According to the results of the bacteria tests performed in the METU microbiology laboratory; In the control plate, an antibacterial effect was observed to prevent the bacteria from reaching the discs on which antibiotics were dripped. In addition, no antibacterial effect was found in Si_3N4 samples 1Y /92, 1Y1C /92 and 1Y2C /92 [120].

According to this agar well diffusion test, it was observed with the naked eye that although the samples did not repel bacteria (diffusion zone did not form), they did not allow bacterial growth on their surfaces and the bacteria did not cover the surface.

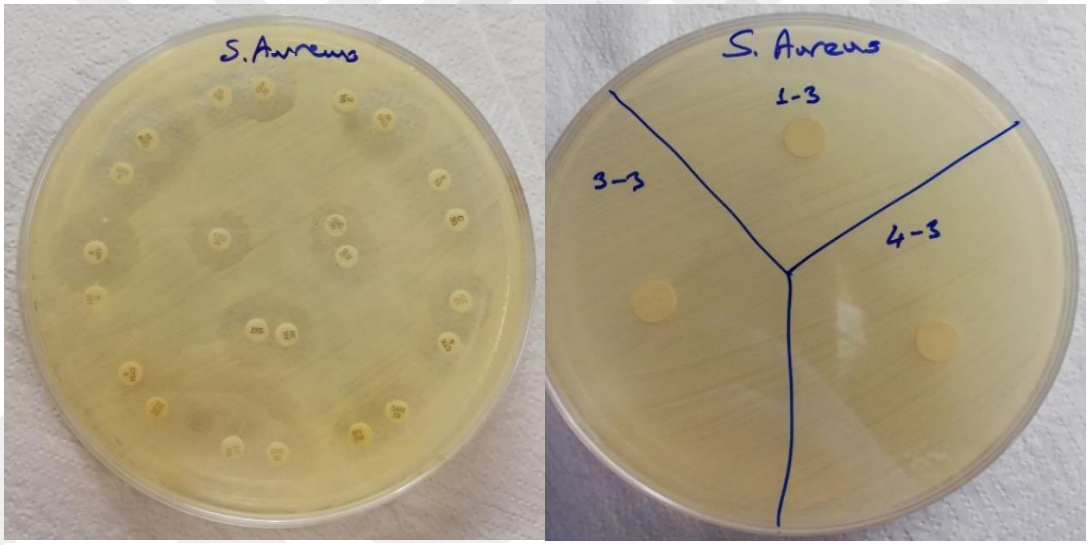

Figure 71: Control and 1Y /92, 1Y1C /92 and 1Y2C /92 samples S.Aureus bacterias.

In addition, no significant effect of the change in the amount of pores on antibacterial behaviour was observed in samples 1Y /92, 1Y1C/92 and 1Y2C /92, where the porosity amount was prepared as 0 wt. %, 10 wt. % and 20 wt. % respectively.

3.5 SBF ANALYSIS

Si_3N_4 ceramics with different grain boundary phase amounts and porosity levels were soaked in SBF for 28 days to investigate and compare their bioactive potential by evaluating the HAp formation with SEM and EDX.

Figure 72.a, shows the secondary electron image and EDX results of Sample 1Y with 10 wt.% Y_2O_3 without and pore forming agent. Needle like Si_3N_4 grains are clearly observed in this image with some typical "cauliflower-like" grains, which is a typical appearance of HAp, and also some more angular grains which probably corresponds to precipitated salt. EDX survey from one of these cauliflower-like globules is given in Figure 72.b, to examine the Ca/P atomic ratio. According to these results, it is clear that salts were not totally removed from the system, even after the washing proses after removing the samples from SBF test, since we still observed the peaks like Cl and Na. When the Ca/P ratio was examined according to these EDX peaks, it was also evaluated that the Ca/P atom ratio was 1.24 which is not very close to the stoichiometric atomic ratio of HAp (1.667).

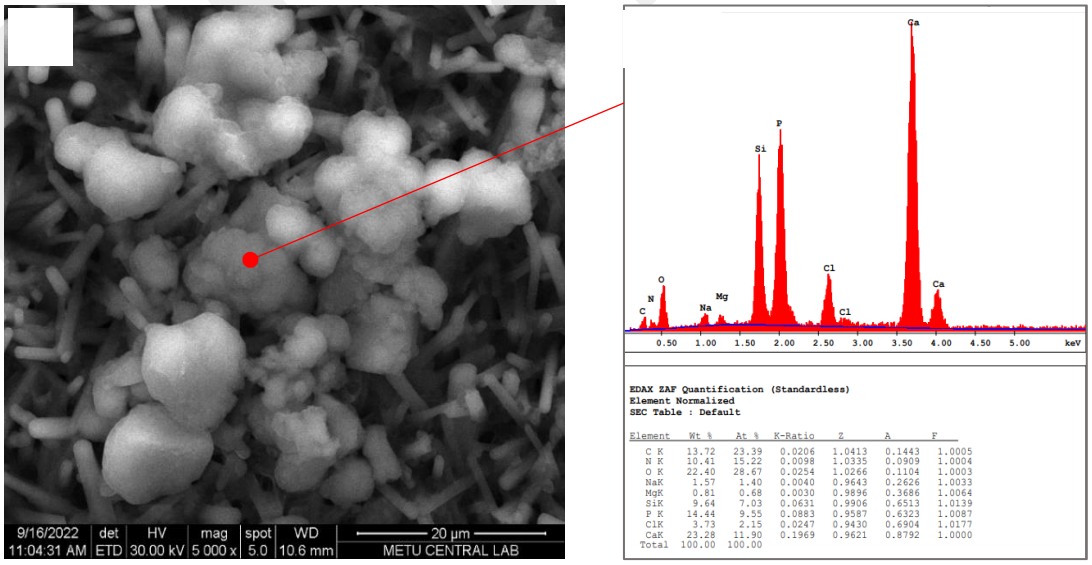

Figure 72: a.) Secondary electron image of sample 1Y after immersion in SBF for 28 days and (b) EDX spectum of a point analysis. b.), SEI (with different magnifications) and EDX results of sample 2Y.

In Figure 73, SEI (with different magnifications) and EDX results of sample 2Y with 20 wt. % Y_2O_3 without and pore forming agent is given.

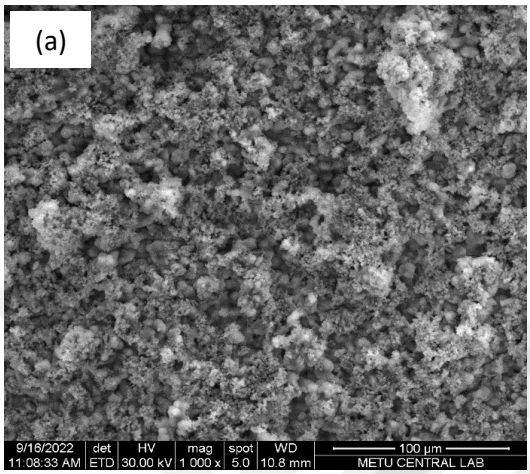

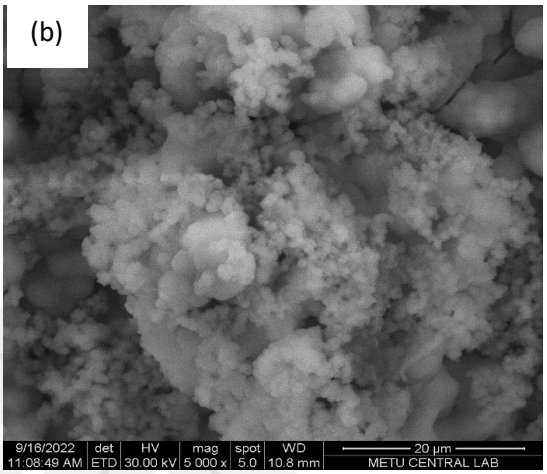

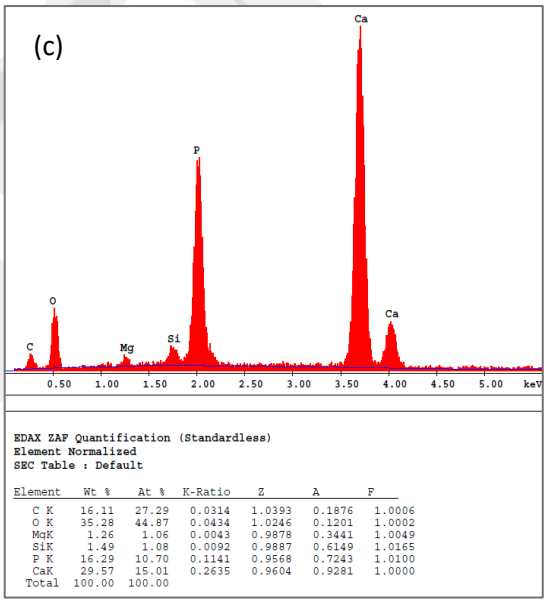

Effect of grain boundary phase amount on the bioactivity of Si_3N_4 samples is obvious when the SEI of Figure 74.a and Figure 74.b are compared. In Figure 74.b, all the surface is totally covered by calcium phosphate layer and therefore Si_3N_4 grains cannot be observed on the surface. Increasing the grain boundary phase amount and hence increasing the O/N content on the surface resulted in an increase of surface bioactivity. The Ca/P atomic ratio in Figure 74. c was calculated as 1.4, which is closer to the stoichiometric atomic ratio of HAp compared to that obtained in sample 1Y.

The effect of its porosity on bioactivity was evaluated with samples 1Y /92, 1Y1C /92 and 1Y2C /92 on the composition containing 10wt % Y_2O_3, in systems with 0 wt. %, 10 wt. % and 20 wt. % carbamide addition, respectively.

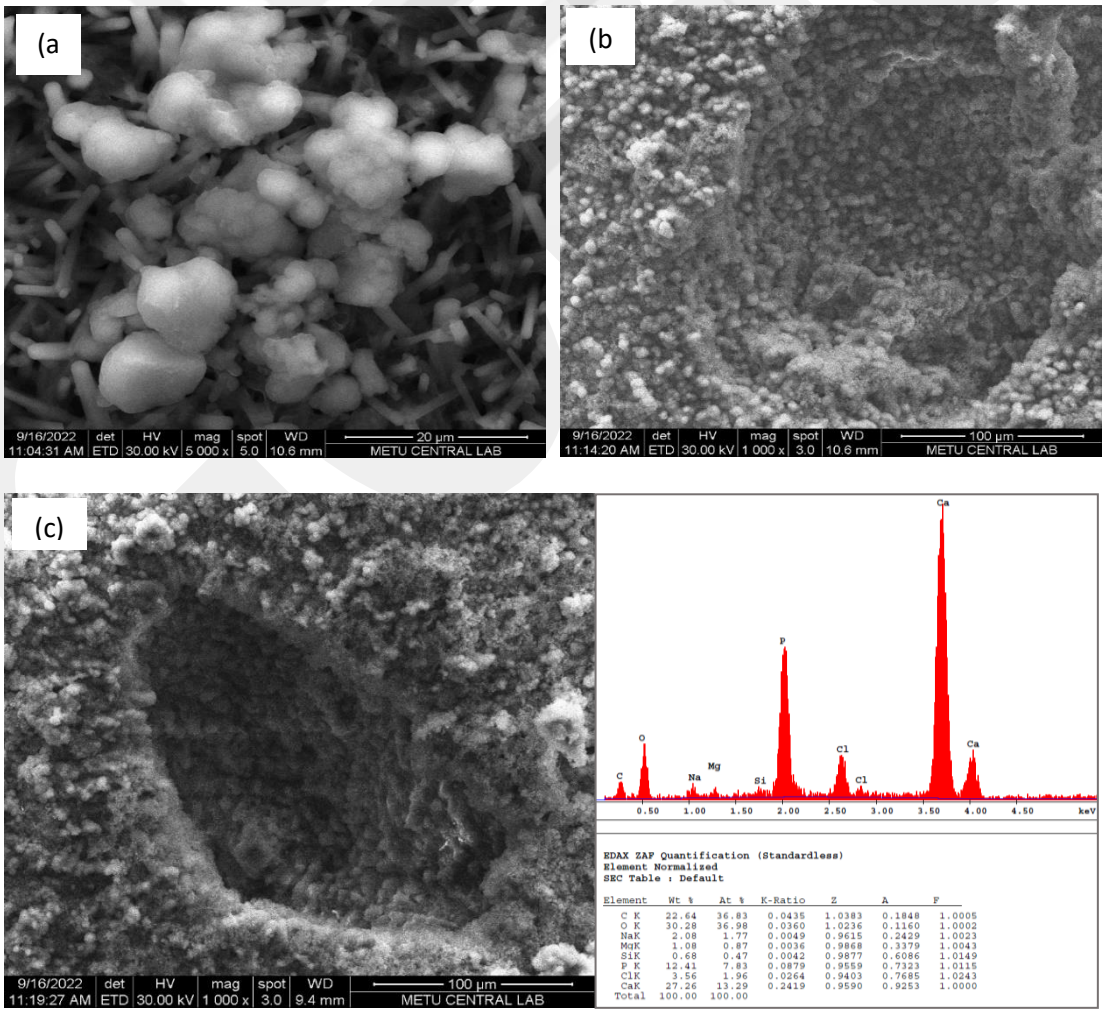

Figure 74: SEI of samples after immersion in SBF for 28 days (a) Sample 1Y /92 (b) Sample 1Y1C /92 and (c) Sample 1Y2C /92. (d) is the EDX inspection field of the area given in (c)

In figure 75.a and figure 75.b, it is observed that in the porous samples, the surfaces are completely covered with a calcium phosphate layer, although the grain boundary phase is still the same as in sample 1Y /92. The pores are also perfectly covered with this coating phase. It is believed that, these voids formed by pore forming agents, served as nucleation sites for the precipitation of calcium phosphate grains. When the Ca/P atomic ratio of sample 1Y2C /92 was calculated from the EDX spectra, a value of 1.69 was obtained, which is very close to the ratio of HAp (1.667).

Similarly, the bioactivity results of the samples containing 10 wt. % and 20 wt. % carbamide but sintered at lower temperature were similar to those sintered at high temperature and the relevant SEI images are given in Figure 77.

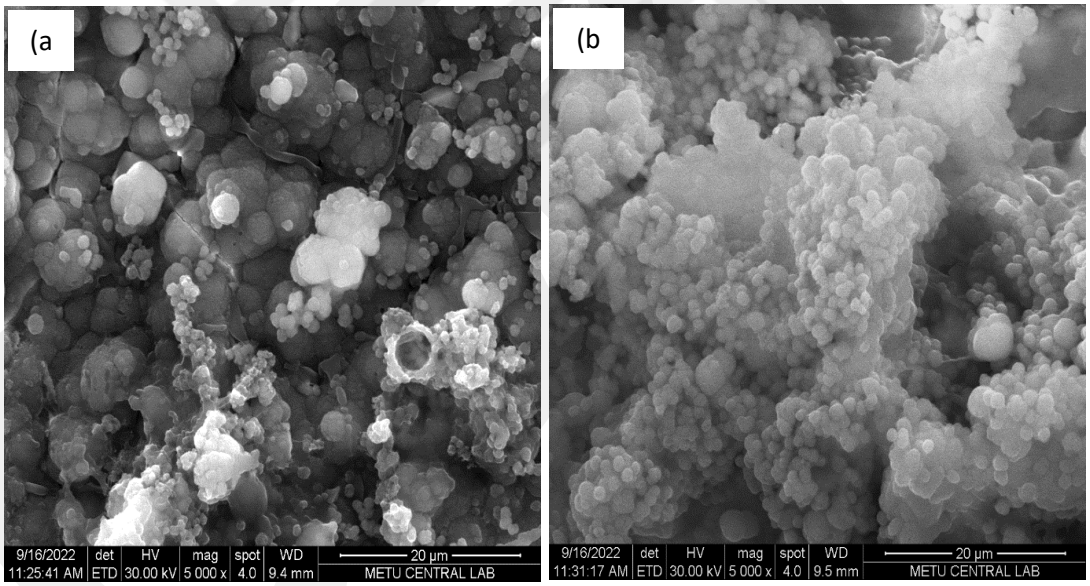

Figure 75: SEI of samples after immersion in SBF for 28 days (a) Sample 1Y /92 (b) Sample 2Y /92.

CHAPTER IV
CONCLUSION

- Sintering at 1830°C for 1.5h under 95 bar sintering conditions was not sufficient for densification of Si_3N_4 ceramics with 10 wt. % Y_2O_3 addition, with a density of 2.22 g/cm^3 and open porosity of ~21%
- For the same composition, changing the sintering procedure as 1920°C for 1.5h under 20 bar (according to the SPS results) and CIP application prior to sintering resulted in a better densification. Density was increased to 2.34 g/cm3 and open porosity was decreased to 14%. However, it is clear that the full densification could not be achieved according to these results even at 1920°C.
- Using semolina instead of carbamide as a pore forming agent caused disintegration of the pellets after the burn-out process.
- Increasing sintering additive amount from 10 wt. % to 20 wt. % caused an increase in density, as expected, from 2.34 to 2.77.
- 0 wt. %, 10 wt. % and 20 wt. % carbamide addition resulted in 15%, 29% and 23% open porosity, respectively.
- Even though phase analysis results revealed similar patterns for each different system. At higher temperatures, $Y_4Si_2O_7N_2$ (JCPDS card no. 01-086-1106) was formed as a grain boundary phase in addition to $YSiO_2N$ (JCPDS card no. 01-083-1204), which was also observed even at lower sintering temperature.
- SEM images revealed a smooth gradual transition by powder metallurgy, in terms of porosity content between the layers.
- Needle-like Si_3N_4 grains were observed in the pore regions, giving the interior of the pores a micro-rough structure.

- According to the results of the bacteria tests performed by the agar well diffusion method, it was observed with the naked eye that although the samples did not repel bacteria (diffusion zone did not form), they did not allow bacterial growth on their surfaces and the bacteria did not cover the surface.
- "Cauliflower-like" grains, which is a typical appearance of HAp is observed in all systems. In the samples with 10 wt. % of sintering additive, without pore forming agent, needle like Si_3N_4 grains were also clearly observed and the surface is not fully covered. However, with the increase of the sintering additive and thus the amount of grain boundary phase, it was observed that the surface is fully covered.
- In the samples produced with pore forming agents, it was examined that the pores are also perfectly covered with this coating phase. It is believed that, these voids acted as nucleation sites for the precipitation of calcium phosphate grains. When the Ca/P atomic ratio of sample was calculated from the EDX spectra, a value of 1.69 was obtained, which is very close to the ratio of HAp (1.667).

REFERENCES

[1] Deville H. C. and Wöhler (1857), "Ueber das stickstoffsilicium", *Annalen Der Chemie Und Pharmacie,* Vol. 104, No 2, pp. 256-256, DOI:10.1002/jlac.18571040224.

[2] Collins J. F. and Gerby R. W. (1955), "New refractory uses for silicon nitride reported", *JOM,* Vol. 7, No 5, pp. 612-615, DOI:10.1007/bf03377548.

[3] Lee M. R., Russell S. S., Arden J. W. and Pillinger C. T. (1995), "Nierite (Si_3N_4), a new mineral from ordinary and enstatite chondrites", *Meteoritics,* Vol. 30, No 4, pp. 387-398, DOI:10.1111/j.1945-5100.1995.tb01142.

[4] Riley F. L. (2004), "Silicon nitride and related materials", *Journal of the American Ceramic Society,* Vol. 83, No 2, pp. 245-265, DOI:10.1111/j.1151-2916.2000.tb01182.

[5] Klemm H. (2010), "Silicon nitride for high-temperature applications", *Journal of the American Ceramic Society,* Vol. 93, No 6, pp. 1501-1522, DOI:10.1111/j.1551-2916.2010.03839.

[6] Boberski C., Hamminger R., Peuckert P., Aldinger F., Dillinger R., Heinrich J. and Huber J. (1989), "High-performance silicon nitride materials", *Advanced Materials,* Vol. 1, No 11, pp. 378-387, DOI:10.1002/adma.19890011104.

[7] Substech (2012), *Nitride Ceramics* http://www.substech.com/dokuwiki/doku.php?id=nitride_ceramics. DoA.11.09.2022.

[8] Wei C., Zhenglin L., Dongqiang G. and Xu A. (2015), ''Study on Preparation and Physical Mechanical Properties of Si_3N_4 Composite Ceramics'', *MATEC Web of Conferences*, Vol. 22, No 05019, pp.1-6, Shaanxi, China, DOI: 10.1051/matecconf/20152205019.

[9] Kyocera (2022), *Silicon nitride: Fine ceramics (advanced ceramics),* https://global.kyocera.com/prdct/fc/list/material/silicon_nitride/silicon_nitride.html., DoA. 11.09.2022.

[10] Singhal S. (1976), "Thermodynamic analysis of the high-temperature stability of silicon nitride and silicon carbide", *Science Direct*, Vol. 2, No 3, pp. 123-130, DOI: 10.1016/0390-5519(76)90022-3.

[11] Krstic Z. and Krstic V. D. ''Silicon nitride: the engineering material of the future'', *Journal of Materials Science,* Vol. 47, pp. 535–552, DOI: 10.1007/s10853-011-5942-5, DoA. 11.09.2022.

[12] Touchdown (2022), *Silicon Nitride (Si_3N_4) applied to ceramic product: Ceramic Parts Supply for over 30 years*, https://www.touchdown.com.tw/en/material-property/Silicon-Nitride-SiN-applied-to-ceramic-product/material-property_silicon-nitride.html, DoA.11.09.2022.

[13] Singh P., Harbola M. K. and Johnson D. D. (2017), "Better band gaps for wide-gap semiconductors from a locally corrected exchange-correlation potential that nearly eliminates self-interaction errors", *Journal of Physics: Condensed Matter*, Vol. 29, No 42, pp. 2-3, DOI:10.1088/1361-648x/aa837b.

[14] Uchino K. (2017), "Manufacturing methods for piezoelectric ceramic materials", *Advanced Piezoelectric Materials*, Vol. 2, pp. 385-421, DOI:10.1016/b978-0-08-102135-4.00010-2.

[15] Gawronski A., Patzig C., Höche T. and Rüssel C. (2014), "Effect of Y_2O_3 and CeO_2 on the crystallisation behaviour and mechanical properties of glass–ceramics in the system $MgO/Al_2O_3/SiO_2/ZRO_2$", *Journal of Materials Science*, Vol. 50, No 4, pp. 1986-1995, DOI:10.1007/s10853-014-8765-3.

[16] Kuşhan Akın Ş. R. (2021), "Reaksiyon Bağlı Silisyum Nitrür Seramiklerinde Sinterleme İlavesinin Mikroyapı ve Antibakteriyel Davranışa Etkisinin İncelenmesi" , *International Journal of Engineering Research and Development* , Vol. 13, No 2 , pp. 375-381, DOI: 10.29137/umagd.793123.

[17] Falco S., Dancer C. E. J., Todd R. I. and Petrinic N. (2013), "A new anisotropic constitutive model for ceramic materials failure'', *Ceramic Engineering and Science Proceedings,* Vol. 33, No 10, pp. 93-103, DOI:10.1002/9781118217542.ch9.

[18] Moustafa S., Daoush W., Ibrahim A. and Neubaur E. (2011), "Hot forging and hot pressing of alsi powder compared to conventional powder metallurgy route",

Materials Sciences and Applications, Vol. 2, No 8, pp. 1127-1133, DOI:10.4236/msa.2011.28152.

[19] Meng Q., Zhao Z., Sun Y., Li X. and Ji H. (2017), "Low temperature pressureless sintering of dense silicon nitride using BaO-Al2O3-SiO_2 glass as sintering aid", *Ceramics International*, Vol. 43, No 13, pp. 10123–10129, DOI: 10.1016/j.ceramint.2017.05.033.

[20] Vacfurnace (2022), *Vacuum heat treatment furnace*, https://www.vacfurnace.com/vacuum-furnace-product/vacuum-heat-treatment-furnace/, DoA.11.09.2022.

[21] Biswas S. K. and Riley F. L. (2001), "Gas pressure sintering of silicon nitride — current status", *Materials Chemistry and Physics,* Vol. 67 No 1-3, pp. 175–179, DOI: 10.1016/s0254-0584(00)00436-3.

[22] FCT Anlagenbau (2022), *Laboratory Furnace*, https://www.fct-anlagenbau.de/en/sintering-machinery-and-plants/vacuum-sintering-systems/laboratory-furnace, DoA.11.09.2022.

[23] Bhandhubanyong P. and Akhadejdamrong T. (1997), "Forming of silicon nitride by the hip process", *Journal of Materials Processing Technology*, Vol. 63 No 1-3, pp. 277–280, DOI: 10.1016/s0924-0136(96)02635-0.

[24] Open.edu (2022), *Hot isostatic pressing (HIP)*, https://www.open.edu/openlearn/science-maths-technology/engineering-technology/manupedia/hot-isostatic-pressing-hip, DoA. 11.09.2022.

[25] Sinoma (2022), *Silicon Nitride (Si_3N_4) Balls*, http://www.sinomanitride.com/Product/Ceramic-Balls/Silicon-Nitride-Balls/90/HIP-Silicon-Nitride-_Si_3N_4_-Ball/, DoA. 11.09.2022.

[26] Azom (2018), *Microwave sintering of metals*, https://www.azom.com/article.aspx?ArticleID=937, DoA.11.09.2022.

[27] Ibrahim M., K., Hamzah E., Saud S. N., Abu Bakar E. N. and Bahador A. (2017), "Microwave sintering effects on the microstructure and mechanical properties of Ti−51%Ni Shape memory alloys", *International Journal of Minerals, Metallurgy, and Materials,* Vol. 24, No 3, pp. 280-288, DOI:10.1007/s12613-017-1406-5.

[28] Guillon O., Gonzalez-Julian J., Dargatz B., Kessel T., Schierning G., Räthel J. and Herrmann M. (2014), "Field-assisted Sintering Technology/Spark Plasma

Sintering: Mechanisms, Material's and technology developments", *Advanced Engineering Materials*, Vol. 16, No 7, pp. 830–849, DOI:10.1002/adem.201300409.

[29] Bodišová K., Kašiarová M., Domanická M., Hnatko M., Lenčéš Z., Nováková Z. V. and Šajgalík P. (2013), "Porous silicon nitride ceramics designed for bone substitute applications", *Ceramics International*, Vol. 39, No 7, pp. 8355-8362, DOI:10.1016/j.ceramint.2013.04.015.

[30] Azom (2020), *Silicon Nitride (Si_3N_4) properties and applications*, https://www.azom.com/article.aspx?ArticleID=53#:~:text=The%20material%20is%20used%20currently.tools%20and%20hot%20metal%20handling, DoA.11.09.2022.

[31] Bal B. and Rahaman M. (2012), "Orthopedic applications of silicon nitride ceramics", *Acta Biomaterialia*, Vol. 8, No 8, pp. 2889-2898, DOI:10.1016/j.actbio.2012.04.031.

[32] Stanford Advanced Materials (2022), *Global Supplier of Fabricated Products & Machining Parts*, https://www.samaterials.com/, DoA. 11.09.2022.

[33] Stanford Advanced Materials (2022), *Silicon carbide bearing ceramic products: Stanford Advanced Materials*, https://www.samaterials,com/silicon-nitride/909-silicon-nitride-bearings.html, DoA. 11.09.2022

[34] Stanford Advanced Materials (2022), *Silicon nitride bearing rollers*, https://www.samaterials.com/silicon-nitride/1935-silicon-nitride-bearing-rollers.html., DoA.11.09.2022

[35] 3M (2022), *Silicon Nitride Telemetry Tooling* https://www.3m.com/3M/en_US/p/d/b40070804/, DoA.11.09.2022.

[36] 3M (2022), *Silicon Nitride Wear Plate*, https://www.3m.com/3M/en_US/p/d/b5005303016/, DoA. 11.09.2022.

[37] Amedica Website, *CTL Amedica*, https://www.ctlamedica.com/portfolio, DoA.11.09.2022.

[38] Rahaman M. and Xiao W. (2017), "Silicon nitride bioceramics in healthcare", *International Journal of Applied Ceramic Technology*, Vol. 15, No 4, pp. 861-872, DOI:10.1111/ijac.12836.

[39] Besisa D. H. and Ewais E. M. (2016), "Advances in functionally graded ceramics – processing, sintering properties and applications", *Advances in*

Functionally Graded Materials and Structures, Vol.1, pp.1-3, DOI:10.5772/62612.

[40] Anderson M. C. and Olsen R, (2009), "Bone ingrowth into porous silicon nitride", *Journal of Biomedical Materials Research Part A*, Vol 92, No 4, pp. 605-1598, DOI:10.1002/jbm.a.32498.

[41] Koizumi M. (1997), "FGM activities in Japan", *Composites Part B: Engineering*, Vol. 28, No 2, pp. 1-4, DOI:10.1016/s1359-8368(96)00016-9.

[42] Miyamoto Y. (1996), "The applications of functionally graded materials in Japan", *Materials Technology*, Vol. 11, No 6, pp. 230-236, DOI:10.1080/10667857.1996.11752708.

[43] Ebhota W. S. and Jen T. (2018), "Casting and applications of functionally graded Metal Matrix Composites", *Advanced Casting Technologies*, Vol.1, pp. 59, DOI:10.5772/intechopen.71225.

[44] Chen F., Wang S. W., Yu L., Chen X. and Lu W. (2014), "Control of optical properties of TiN_xO_y films and application for high performance solar selective absorbing coatings", *Optical Materials Express*, Vol. 4, No. 9, pp. 11-13, DOI:10.1364/ome.4.001833.

[45] StockAdobe (2022), *Tooth Anatomy*, https://stock.adobe.com/tr/search?k=tooth%2Banatomy&asset_id=335829657, DoA.11.09.2022.

[46] Pinterest (2012), *Nautilus shell cross section*, https://www.pinterest.com/pin/nautilus-shell-cross-section--504544582958089 12/, DoA.11.09.2022.

[47] Azom (2020), *Functionally graded materials (FGM) and their production methods*, https://www.azom.com/article.aspx?ArticleID=53#:~:text=The%20material%20is%20used%20currently,tools%20and%20hot%20metal%20handling, DoA.11.09.2022.

[48] El-wazery M. S. and El-Desouky A. R. (2015). "A review on Functionally Graded Ceramic-Metal Materials''. *Journal of Materials and Environmental Science*, Vol. 6, No 5, pp. 1369-1376, https://www.researchgate.net/publication/334108229_A_review_on_Functionally_Graded_Ceramic-Metal_Materials. DOI :10.1.1.719.2979.

[49] Contreras C. A., Bedolla B. E., Martínez M. S. and Lemus R. J. (2018), "Joining of composites", *Metal Matrix Composites,* Vol. 1, pp. 187-226, DOI:10.1007/978-3-319-91854-9_5.

[50] Khanna V., Kumar V. and Bansal S. A. (2021), "Mechanical properties of aluminium-graphene/carbon nanotubes (CNTS) metal matrix composites: Advancement, opportunities and perspective", *Materials Research Bulletin,* Vol. 138, pp. 1-3, DOI:10.1016/j.materresbull.2021.111224.

[51] Bradt R. C. (1985), "Progress in Nitrogen Ceramics", *Materials Science and Engineering,* Vol. 68, No 2, pp. 268-269, DOI:10.1016/0025-5416(85)90417-3.

[52] Travitzky N. A. and Claussen N. (1992), "Microstructure and properties of metal infiltrated RBSN Composites", *Journal of the European Ceramic Society,* Vol. 9, No 1, pp. 61–65, DOI:10.1016/0955-2219(92)90078-r.

[53] Subtech (2012), *Liquid state fabrication of Metal Matrix Composites,* https://www.substech.com/dokuwiki/doku,php?id=liquid_state_fabrication_of_metal_matrix_composites, DoA. 11.09.2022.

[54] Ghomashchi M. and Vikhrov A. (2000), "Squeeze casting: An overview", *Journal of Materials Processing Technology,* Vol 101, No 1-3, pp. 1-9, DOI:10.1016/s0924-0136(99)00291-5.

[55] Ervina Efzan M. N., Siti Syazwani N. and Al Bakri Abdullah M. M. (2016), "Fabrication method of Aluminum Matrix Composite (AMCS): A Review", *Key Engineering Materials,* Vol. 700, pp. 102-110, DOI:10.4028/www.scientific.net/kem.700.102.

[56] Thandalam S. K., Ramanathan S. and Sundarrajan S (2015), "Synthesis, microstructural and mechanical properties of ex situ zircon particles ($ZrSiO_4$) reinforced metal matrix composites (mmcs): A Review", *Journal of Materials Research and Technology,* Vol. 4, No 3, pp. 333–347, DOI: 10.1016/j.jmrt.2015.03.003.

[57] Ervina E. M. N., Siti S. N. and Al-Bakri A. M. M. (2016), "Fabrication method of Aluminum Matrix Composite (AMCS): A Review", *Key Engineering Materials,* Vol. 700, pp. 102-110, DOI:10.4028/www.scientific.net/kem.700.102.

[58] Ramanathan A., Krishnan P. K. and Muraliraja R. (2019), "A review on the production of metal matrix composites through stir casting – furnace design, properties, challenges, and research opportunities", *Journal of Manufacturing Processes,* Vol.42, pp. 213-245, DOI:10.1016/j.jmapro.2019.04.017.

[59] Altan Türkeli (2022), *Centrifugal Casting,* https://mimoza.marmara.edu.tr/~altan.turkeli/files/cpt-9-centrifugal_casting.pdf, DoA.11.09.2022.

[60] Radhika N., Thirumalini S. and Jojith R. (2019), "Development and properties of centrifugally cast silicon nitride reinforced functionally graded copper matrix composite", *Silicon,* Vol. 11, No 4, pp. 2103-2116, DOI:10.1007/s12633-018-0030-y.

[61] Ceramics (2014), ''Teacher instructions ceramic processing'', *Ceramic Processing: Slip Casting*, https://ceramics.org/wpcontent/uploads/2014/04/Slip-Casting-Lesson,pdf, DoA.11.09.2022.

[62] Hostaša J., Silvestroni L., Piancastelli A., Sciti D., Martino D. D. and Esposito L. (2012), "Slip casting of a Si_3N_4-based system", *International Journal of Applied Ceramic Technology,* Vol. 9, No 2, pp. 246-258, DOI:10.1111/j.1744-7402.2011.02718.x.

[63] OpenEdu (2022), *Slip Casting*, https://www.open.edu/openlearn/science-maths-technology/engineering-technology/manupedia/slip-casting, DoA.11.09.2022

[64] Jabbari M. and Hattel J. (2012), ''Numerical Modeling of the Flow of a Power Law Ceramic Slurry in the Tape Casting Process. AES-ATEMA International Conference Series'', *Advances and Trends in Engineering Materials and their Applications*, Vol. 1389, pp. 151-157.

[65] Zhang C., Chen F., Huang Z., Jia M., Chen G., Ye Y. and Lavernia E. J. (2019), "Additive Manufacturing of functionally graded materials: A Review", *Materials Science and Engineering: A,* Vol. 764, pp-1-5, DOI:10.1016/j.msea.2019.138209.

[66] Alemnis (2022), *Additive Manufacturing*, https://alemnis.com/additive-manufacturing/, DoA.11.09.2022

[67] Tritech3D (2022), *Vero Clear: Rigid Transparent*, https://www.tritech3d.co.uk/materials/transparent/, DoA.11.09.2022.

[68] Sourced (2022), *How 3D Printed Shoes Quietly Took Over The World*, https://www.3dsourced.com/feature-stories/3d-printed-shoes/, DoA.11.09.2022.

[69] 3DPBlock (2022), *Metal Filament for 3D Printer – Metallic Filament 30% Metal Content Filaments – Copper Brass Bronze Aluminum 1.75mm*, https://3dpblock.com/product/metal-filament/, DoA.11.09.2022.

[70] Villainouspropshop (2022), *High Quality Design and 3D Printing Services*, https://villainouspropshop.com/, DoA.11.09.2022.

[71] Loughborough University (2022), *About Additive Manufacturing: Powder Bed Fusion*, https://www.lboro.ac.uk/research/amrg/about/the7categoriesofadditivemanufacturing/powderbedfusion/, DoA.11.09.2022.

[72] Make3Dexperience (2022), *Photopolymerization – VAT, SLA, DLP, CDLP*, https://make.3dexperience.3ds.com/processes/powder-bed-fusion, DoA.11.09.2022.

[73] 3D Natives (2017), *Mercedes-Benz 3D prints their first metal part for trucks*, https://www.3dnatives.com/en/mercedes-benz-3d-printed-part070820174/#, DoA.11.09.2022.

[74] Gibson I., Rosen D. and Stucker B. (2015), ‘‘Additive Manufacturing Technologies 3D printing”, *Rapid Prototyping, and direct digital manufacturing*.

[75] Loughborough University (2022), *About Additive Manufacturing: Powder Bed Fusion*, https://www.lboro.ac.uk/research/amrg/about/the7categoriesofadditivemanufacturing/directedenergydeposition/, DoA.11.09.2022.

[76] Sing S., Tey C., Tan J., Huang S. and Yeong W. Y. (2020), “3D printing of metals in rapid prototyping of biomaterials: Techniques in additive manufacturing”, *Rapid Prototyping of Biomaterials*, Vol. 2, pp. 17-40, DOI:10.1016/b978-0-08-102663-2.00002-2.

[77] 3D Natives (2022), *The Complete Guide to Directed Energy Deposition (DED) in 3D printing, 3DNatives*, https://www.3dnatives.com/en/directed-energy-deposition-ded-3d-printing-guide-100920194/, DoA. 11.09.2022

[78] Rabinskiy L., Ripetsky A., Sitnikov S., Solyaev Y. and Kahramanov R. (2016), "Fabrication of porous silicon nitride ceramics using binder jetting technology", *IOP Conference Series: Materials Science and Engineering*, Vol. 140, pp.1-7, DOI:10.1088/1757-899x/140/1/012023.

[79] Nancy Crotti (2019), ''Binder jetting and debinding'', *Medical Design and Outsourcing*, https://www.medicaldesignandoutsourcing.com/what-are-binder-jetting-and-debinding/, DoA.11.09.2022.

[80] Céline Montanari, (2017), *Additive Manufacturing of Silicon Nitride*, http://www.diva-portal.org/smash/get/diva2:1107442/FULLTEXT01.pdf, DoA. 11.09.2022.

[81] 3D Experience Marketplace (2018), *3D Printing – Additive*, https://make.3dexperience.3ds.com/processes/binder-jetting, DoA. 11.09.2022

[82] Stefanos N. Manias (2017), ''Introduction to Motor Drive Systems'', *Introduction to Motor Drive Systems*, Vol. 1, pp. 843-967, DOI: 10.1016/B978-0-12-811798-9.00012-3.

[83] Engineering Product Design (2019), *Sheet Lamination*, https://engineeringproductdesign.com/knowledge-base/sheet-lamination/, DoA. 11.09.2022.

[84] Matthew J. P., Patterson M.C.L., Zimbeck W. and Fehrenbacher M. (1997), ''1997 International Solid Freeform Fabrication Symposium'', *Laminated Object Manufacturing of Si_3N_4 with Enhanced Properties*, Vol.1 pp. 529-536, DOI:10.15781/T2XP6VP98

[85] William Andrew and Donald M. Mattox (2010), ''Handbook of Physical Vapor Deposition (PVD) Processing'', *Atomistic Film Growth and Some Growth-Related Film Properties*, Vol.2. pp.333-438, DOI: 10.1016/C2009-0-18800-1.

[86] Ghader Faraji, H.S. Kim and Hessam Kashi (2018), ''Severe Plastic Deformation'', *Methods, Processing and Properties*, Vol.1, pp.1-17, DOI: 10.1016/B978-0-12-813518-1.00020-5.

[87] Eifeler (2022), *High – Tech Coationgs*, https://www.eifeler-austria.com/en/. DoA. 11.09.2022.

[88] Wolfe D. Movchan M. and Singh J. (1997), "Architecture of functionally graded ceramic/metallic coatings by electron beam-physical vapor deposition", *Applied Research Laboratory (ARL), Materials Research Institute (MRI),* Vol.118, No 4, pp. 93-110, https://pennstate.pure.elsevier.com/en/publications/architecture-of-functionally-graded-ceramicmetallic-coatings-by-e., DoA.12.09.2022.

[89] OpenPR (2020), *Global Electron Beam Physical Vapor Deposition Coating Market Analysis (2020-2025),* https://www.openpr.com/news/2210596/global-electron-beam-physical-vapor-deposition-coating-market, DoA. 11.09.2022.

[90] Nano-Master Inc. (2022), *E-Beam Systems,* http://www.nanomaster.com/e-beam.html, DoA. 11.09.2022.

[91] Wang C., Chen Z., Guan L., Wang M., Liu Z. and Wang P. (2001), "Fabrication and characterization of graded calcium phosphate coatings produced by Ion Beam Sputtering/mixing deposition", *Nuclear Instruments and Methods in Physics Research Section B: Beam Interactions with Materials and Atoms,* Vol. 179, No 3, pp. 364-372, DOI:10.1016/s0168-583x(01)00585-7.

[92] Qadir M. Li. Y. and Wen C. (2019), "Ion-substituted calcium phosphate coatings by physical vapor deposition magnetron sputtering for biomedical applications: A Review", *Acta Biomaterialia,* vol. 89, pp. 14-32, DOI:10.1016/j.actbio.2019.03.006.

[93] Teknotip (2022), *Sputtering Target,* https://www.teknotip.com.tr/urun/sputtering-target/, DoA. 11.09.2022.

[94] Heuer S., Matějíček J., Vilémová M., Koller M., Illkova K., Veverka J., Weber T., Pintsuk G., Coenen J.W. and Linsmeier C. (2019), ''Atmospheric plasma spraying of functionally graded steel/tungsten layers for the first wall of future fusion reactors'', *Surface and Coatings Technology,* Vol. 366, pp. 170-178, DOI:10.1016/j.surfcoat.2019.03.017.

[95] Renjith Devasia, Anil Painuly, Deepa Devapal and K.J. Sreejith (2021), ''Continuous fiber reinforced ceramic matrix composites'', *Composites Science and Engineering, Fiber Reinforced Composites,* Vol.1, pp. 669-751, DOI: 10.1016/B978-0-12-821090-1.00022-3.

[96] Alibaba (2022), *PVD plasma spray gold plating machine for stainless steel sheet furniture*, https://www.alibaba.com/product-detail/PVD-plasma-spray-gold-plating-machine_50041906045.html, DoA.12.09.2022.

[97] Coltelli M. B. and Lazzeri A. (2019), *Chemical vapour infiltration of composites and their applications*, DOI: 10.1201/9781315117904-8.

[98] Silcotek (2022), *What is a CVD coating?*, https://www.silcotek.com/blog/what-is-a-cvd-coating, DoA.11.09.2022.

[99] CGT Carbon GmbH (2022), *Silicon Carbide Coating (CVD)*, https://cgt-carbon.com/coating/silicon-carbide-coating-cvd, DoA.11.09.2022.

[100] Łatka L., Pawłowski L., Winnicki M., Sokołowski P., Małachowska A. and Kozerski S. (2020), Review of functionally graded thermal sprayed coatings, *Applied Sciences*, Vol. 10, No 15, pp. 5153, DOI:10.3390/app10155153.

[101] Austin Hayes Group (2022), *Thermal Metal Spray*, http://www.austinhayes.com/what-we-do/thermal-metal-spray/, DoA. 11.09.2022.

[102] Osaka Fuji Corporation (2022), *Thermal Spraying*, https://www.ofic.co.jp/en/r_and_d/thermalspraying/, DoA. 11.09.2022.

[103] Laurent W., Yaël N., Marc N., Pascal L. and Thierry G. (2019), ‘‘On the use of Functionally Graded Materials to differentiate the effects of surface severe plastic deformation, roughness and chemical Composition on cell proliferation’’, *Metals*, Vol. 9, No 12, pp. 1344. DOI:10.3390/met9121344.

[104] Ocylok S., Weisheit A. and Kelbassa I., (2010), “Functionally graded multi-layers by laser cladding for increased wear and corrosion protection”, *Physics Procedia*, Vol. 5, pp. 359-367, DOI: 10,1016/j,phpro,2010,08,157.

[105] Enercon (2022), *Flame Plasma Treaters and Flame Treatment*, https://www.enerconind.com/plasma-treating/technologies/flame.aspx, DoA. 11.09.2022.

[106] NITREX (2022), *Gas Nitriding*, https://www.nitrex.com/en/solutions/furnaces-technologies/nitriding-nitrocarburizing/nitreg-technologies/gas-nitriding-nitreg/, DoA.11.09.2022.

[107] Teknovak (2022), *Carburizing Applications*, https://www.teknovak.com/en/carburizing-applications/, DoA.11.09.2022.

[108] NITREX, *Gas nitriding*, https://www.nitrex.com/en/solutions/furnaces-technologies/nitriding-nitrocarburizing/nitreg-technologies/gas-nitriding-nitreg/, DoA.11.09.2022.

[109] Radhika N., Subramaniam T. and Radhakrishnan J. (2019), ‘‘Development and Properties of Centrifugally Cast Silicon Nitride Reinforced Functionally Graded Copper Matrix Composite’’, *Springer – Silicon*, Vol. 11, No 14, pp. 2103-2116, DOI:10.1007/s12633-018-0030-y.

[110] Ambigai R. and Prabhu S. (2020), “Optimizing and characterization of aluminium based functionally graded silicon nitride composite”, *Proceedings of the Institution of Mechanical Engineers, Part C: Journal of Mechanical Engineering Science*, Vol. 235, No 18, pp. 3611-3623, DOI:10.1177/0954406220960784.

[111] Radhika N., Thirumalini S. and Jojith R. (2019), “Development and properties of centrifugally cast silicon nitride reinforced functionally graded copper matrix composite”, *Silicon*, Vol. 11, No 4, pp. 2103-2116, DOI:10.1007/s12633-018-0030-y.

[112] Zhang L., Chen F., Shen Q. and Yan F. (2008), ‘‘Fabrication of Silicon Nitride Ceramics with Pore Gradient Structure’’, *AIP Conference Proceedings*, Vol.973, No 3, pp. 1-5, DOI:10.1063/1.2896812.

[113] Fei C., Qiang S., Lianmeng Z., Paulino G. H., Pindera M., Dodds R. H. and Chen L. (2008), “Preparation of silicon nitride multilayer ceramic radome material and optimal design of the Wall Structure”, *AIP Conference Proceedings*, DOI:10.1063/1.2896899.

[114] Lee F. and Lahti L. E. (1972), “Solubility of urea in water-alcohol mixtures”, *Journal of Chemical & Engineering Data*, Vol. 17, No. 3, pp. 304-306, DOI:10,1021/je60054a020.

[115] Kardeşler Makina (2022), *30 Ton Uzun Hidrolik Pres*, https://kardeslermakina.net/hidrolik-presler/kollu-hidrolik-presler/30-ton-uzun-hidrolik-pres/, DoA.11.09.2022.

[116] MTI Corporation (2022), *Muffle Furnaces (400-2000^{o}C)*, https://www.mtixtl.com/muffle-furnaces.aspx, DoA.11.09.2022.

[117] Eskişehir Teknik Üniversitesi (Estekiz) (2022), *Spark Plasma Furnace*, https://estekiz.eskisehir.edu.tr/Login#, DoA.11.09.2022.

[118] Anti-corrosive muffle furnace with ceramic chamber, “Lab equipments and advanced crystal substrates”, *MTI Corp.*, https://www.mtixtl.com/KSL-1000X.aspx. DoA.11.09.2022

[119] Rigaku (2022), *XRD Products From Rigaku*, https://www.rigaku.com/pt-br/products/xrd/miniflex, DoA.11.09.2022.

[120] Hitachi (2022*), Schottky Field Emission Scanning Electron Microscope SU5000*, https://www.hitachi-hightech.com/eu/product_detail/?pn=em-su5000&version, DoA.11.09.2022.

[121] Saadatian-Elahi M., Teyssou R. and Vanhems P. (2008), ‘‘Staphylococcus aureus, the major pathogen in orthopaedic and Cardiac Surgical Site Infections: A literature review’’, *International Journal of Surgery*, Vol. 6, No 3, pp. 238-245, DOI:10,1016/j,ijsu,2007,05,001.

[122] Wikipedia (2022), *Staphylococcus aureus*, https://en,wikipedia,org/wiki/Staphylococcus_aureus, DoA.11.09.2022.

[123] Zivcová Z., Gregorová E. and Pabst W. (2008), ‘’Alumina ceramics prepared with new pore-forming agents’’, *Processing and Application of Ceramics*, Vol. 2 No 1, pp. 1-8, DOI: 10,2298/pac0801001z.

[124] Hulbert S.F., Young F. A., Mathews R. S., Klawitter J. J., Talbert C. D. and Stelling F. H. (1970), ‘‘Potential of ceramic materials as permanently implantable skeletal prostheses’’, *Journal of Biomedical Materials Research* , Vol. 4, No 3, pp. 433–456, DOI: 10.1002/jbm.820040309.

[125] Hayes J. S., Czekanska E. M. and Richards R. G. (2012), ‘‘Tissue Engineering III: Cell-Surface Interactions for Tissue Culture’’, *The Cell-Surface Interaction*, Vol. 126, pp. 1-31, DOI: 10.1007/978-3-642-28282-9.

[126] TÜBİTAK (2020), TÜBİTAK ARAŞTIRMA PROJESİ GELİŞME RAPORU (Bilimsel Rapor), *Silisyum nitrür esaslı süspansiyonların hazırlanması*, Ankara.